Characterization of Ethylene/1-Octene Copolymers with High-Temperature Thermal Gradient Interaction Chromatography (HT-TGIC)

by
Abdulaal Alkhazaal

A thesis
presented to the University of Waterloo
in fulfillment of the
thesis requirements for the degree of
Doctor of Philosophy
in
Chemical Engineering

Waterloo, Ontario, Canada, 2016

Author's Declaration

I hereby declare that I am the sole author of this thesis. This is a true copy of the thesis, including any required final revisions, as accepted by my examiners.

I understand that my thesis may be made electronically available to the public.

Abstract

Chemical composition distribution (CCD) of polyolefins is being measured by well established crystallization techniques, but they are limited to semi-crystalline polyolefins. High-temperature thermal gradient interaction chromatography (HT-TGIC) was recently developed for CCD determination of semi-crystalline and amorphous polyolefins, thus broadening the range of techniques available for the analysis of polyolefin chemical composition distributions. HT-TGIC fractionation relies on the interaction of polyolefin chains with a graphite surface upon a temperature change in an isocratic solvent based on the adsorption/desorption mechanism. The main objective of this research is to understand the fractionation mechanism of HT-TGIC and study factors controlling this mechanism using one series of ethylene/1-octene copolymers having similar molecular weight averages, but a distinct 1-octene fraction (Category I) and six series of ethylene/1-octene copolymers that in each series having a similar 1-octene mole fraction and a wider range of molecular weight averages (Category II).

It was found that due to the presence of short chain branches formed via 1-octene incorporation, the shape of the HT-TGIC profile and the position of the peak elution temperature shift to lower and become broader with increasing 1-octene mole fraction. Also, the peak elution temperature is gradually linearly related to comonomer content. 2^3 experimental factorial design were applied to three individual and blend samples of ethylene/1-octene copolymers (Category I) to regulate which operation parameters (cooling rate, heating rate, and heating flow rate) influence HT-TGIC peak temperatures and profiles. The cooling rate has no significant effect on the peak elution temperature and the broadness of the HT-TGIC chromatograms. On the other hand, the heating rate and the elution flow rate, as well as their interaction, substantially influence the HT-TGIC peak temperature and breadth.

Four individual samples and their blend of ethylene/1-octene copolymers having different comonomer fractions and approximately the same molecular weight averages were chosen to investigate how commercial Hypercarb columns with distinct lengths and average particle

sizes affected HT-TGIC fractionation. Neither average particle size nor column length plays an important role on the fractionation of polyolefins and their blends. Interestingly, the fraction of the component with high comonomer content in a binary blend could affect the peak position of the fraction with low comonomer content, perhaps because of co-desorption effects.

The joint effect of chain length and comonomer fraction on HT-TGIC chromatograms and the position of peak elution temperature were investigated using sets of ethylene/1-octene copolymer samples that each set had different chain length and similar 1-octene fraction (category II). The peak elution temperature decreased exponentially, and the profiles became increasingly broader below a critical number average chain length value that increased linearly with the fraction of comonomer in the copolymer.

Stockmayer distribution and Monte Carlo simulation estimating the distribution of average (AESD) and longest (LESD) ethylene sequences were used to explain the observed behavior of HT-TGIC profiles. It was found that no simple correlation exists between ethylene sequences in the copolymers and peak elution temperature, but there is a strong evidence that axial dispersion is responsible for symmetrical broadening of the HT-TGIC profiles. Also, the HT-TGIC of binary blends was studied, finding that components with similar 1-octene contents and dissimilar chain lengths tend to increase co-adsorption/co-desorption effects.

Acknowledgments

My most incompetent gratitude is to Allah, the Almighty, who have directed me to every component of this work and my life in his unlimited gifts, wisdom, and perception.

My continuous thanks go to my mother, Safeiyah Al-Khazal, my father, Zuhayr Al-Khazal, my daughters, Rayhana and Fatimah, and my sweetheart wife, Zahrah Al-Khazal, for their love, support, and incentive. They did their best to encourage me to finish this project.

I am extremely grateful and thankful to all of you who have enclosed me with their love and care. I thank my great brothers, Hussain, Yousef, and AbdulHamid, my lovely sisters, Jawaher, Khadijah, Bibi, and Zainab, and my best friends for their courage and patience to overcome all the problems blended with a new flavor in this short trip of our lives.

I am thankful to my supervisor Professor João Soares who gave me the opportunity to become one of his students. I thank him for giving me the chance to learn from him and use his laboratories. I would have never completed this work without his kind of support, continuous encouragement, and valuable guidance throughout this academic time.

I would like to express my sincere gratitude to my supervisory committee members: Professor Leonardo Simon, Professor Ali Elkhamel, Professor Xianshe Feng, Professor Jean Duhamel, and Professor Michael Cunningham

Many thanks go to my colleagues in the polyoefin laboratories in University of Waterloo and University of Alberta who have helped me by advising me and giving me some of their time to finish this project.

Finally, I would like to thank the Ministry of Education in Kingdom of Saudi Arabia for supporting my Ph.D. program financially and funding me during the program.

Dedication

To the Vicegerent of Allah and the Helper of his Truth

To the Proof of Allah and the Guide of his Intention

To whom fill the earth with justice and fairness

To my Master… To my Imam

Peace be upon you and your family

Please… accept my humble gift

Table of Contents

Author's Declaration ii
Abstract iii
Acknowledgments v
Dedication vi
Table of Contents vii
List of Figures x
List of Tables xv
Nomenclature xvii
Chapter 1. Introduction 1
1.1 Motivation 1
1.2 Research Objectives 2
1.3 Thesis Content 3
Chapter 2. Literature Review 4
2.1 Polyethylene Microstructure 4
2.2 Ethylene Polymerization with Coordination Catalysts 6
2.2.1 Metallocene Catalysts 7
2.2.2 Polymerization Mechanism 9
2.3 Polyethylene Microstructural Characterization 12
2.3.1 Crystallization-Based Techniques 12
2.3.2 High Performance Liquid Chromatography 20
2.3.3 Thermal Gradient Interaction Chromatography (HT-TGIC) 27
Chapter 3. Polyethylene Synthesis and Analysis 35
3.1 Polyethylene Synthesis 35
3.1.1 Materials 36
3.1.2 Polymerization Reactors 37
3.1.3 Polymerization Procedure 38
3.1.4 Copolymerization Conditions 39
3.2 Polyethylene Microstructural Analysis 44
3.2.1 HT-GPC Analysis 44

3.2.2 ^{13}C-NMR Analysis 48
3.2.3 FTIR Analysis 52
3.2.4 HT-TGIC Analysis 54
Chapter 4. Influence of Heating and Cooling Cycle Parameters on HT-TGIC Profiles 58
4.1 Introduction 58
4.2 Polymer Synthesis 58
4.3 Polymer Analysis 58
4.4 Results and Discussion 59
4.4.1 Composition Characterization by HT-TGIC 59
4.4.2 Influence of Operation Conditions on the Analysis of Individual Resins 62
4.4.3 Influence of Operation Conditions on the Analysis of Blends 67
4.5 Conclusions 73
Chapter 5. Effect of Column Type on Polyolefin Fractionation by HT-TGIC 75
5.1 Introduction 75
5.2 Results and Discussion 75
5.2.1 Effect of Blend Composition on HT-TGIC Profiles 75
5.2.2 Effect of Average Particle Size on HT-TGIC Profiles 78
5.2.3 Effect of Column Length on HT-TGIC Profiles 80
5.3 Conclusions 83
Chapter 6. Joint Effect of Polyolefin Chain Length and Comonomer Fraction on HT-TGIC 85
6.1 Introduction 85
6.2 Polyethylene Synthesis 85
6.3 polyethylene Analysis 86
6.4 Monte Carlo Simulation 86
6.5 Results and Discussion 88
6.5.1 Chain Length and 1-Octene Mole Fraction Effect on HT-TGIC of Individual Polymer Samples 93
6.5.2 Using Stockmayer Bivariate Distribution to Interpret HT-TGIC Profiles 104
6.5.3 Chain Length and 1-Octene Mole Fraction Effect on the HT-TGIC Analysis of Blends 109
6.6 Conclusions 116

Chapter 7. Conclusions and Recommendations 118
7.1 Conclusions 118
7.2 Recommendations and Future Work 121
Bibliography 123
Appendices 134
Appendix A -Mathematical Model for Average Chain Length Control 134
Appendix B - ^{13}C NMR Analysis 138
Appendix C - Effects of CR, HR and F_E on HT-TGIC Profiles of E/O-9.8 and E/O-23.2 Samples . 144
Appendix D - W_AES and W_LES Results 149

List of Figures

Figure 2-1. Commercial polyethylene types.[2] 4

Figure 2-2. Mechanism of short chain branch formation by coordination polymerization. The chains are shown growing on a titanium active site.[2] 6

Figure 2-3. General structure of methylaluminoxane (MAO) (red ball: oxygen; gray ball: aluminum and methyl group) [21] 8

Figure 2-4. Generalized structure of a metallocene catalyst; *M*: Transition metal; *X*: hydrocarbyl, alkylidene, halogen radicals; *R*: hydrogen, hydrocarbyl radicals; B-bridging group[6] 9

Figure 2-5. Some examples of metallocene catalysts: a) Cp_2ZrCl_2; b) rac-Et$(Ind)_2ZrCl_2$; c) Constrained geometry catalyst.[6] 9

Figure 2-6. Catalyst activation by reaction with cocatalyst; *A*: transition metal (most commonly, Ti, Zr or Hf), *L*: ligands, *X*: halogen atom (commonly, Cl), *R*: alkyl group (methyl or ethyl).[27] 10

Figure 2-7. Monomer initiation and propagation; *A*: transition metal (most commonly, Ti, Zr or Hf), *L*: ligands, *R*: alkyl group (methyl or ethyl), *n*: number of monomers, *Pol*: growing polymer chain.[27] .. 10

Figure 2-8. Chain transfer reactions; *A*: transition metal (most commonly, Ti, Zr or Hf), *L*: ligands, *R*: alkyl group (methyl or ethyl), *n*: number of monomers, *Pol*: growing polymer chain.[27] 11

Figure 2-9. TREF and CRYSTAF profiles of an ethylene/1-butene copolymer made with a heterogeneous Ziegler-Natta catalyst.[26] 13

Figure 2-10. Crystallization and elution steps in TREF and CEF.[38] 14

Figure 2-11. Effect of cooling rate on CEF co-crystallization. Continuous lines are the experimental profiles of blends of two components of ethylene/1-octene copolymers having different comonomer contents (50% of 1.51, and 50% of 3.51 mol%). Dashed lines represent the predicted profile for the same blends.[39] 17

Figure 2-12. The procedure used to generate a calibration curve for CEF. 18

Figure 2-13. CEF calibration curves for ethylene/1-olefin copolymers.[51] 19

Figure 2-14. HT-HPLC profile for separation of a blend of polyethylene and polypropylene. (Column: Nucleosil 500, mobile phase: EGMBE-TCB, T: 140°C, detector: ELSD). The dotted line is the solvent gradient profile.[61] 21

Figure 2-15. HT-HPLC profile for ethylene/propylene copolymers. (Column: Nucleosil 500, mobile phase: EGMBE-TCB, temperature: 140°C, detector: ELSD).[63] 21

Figure 2-16. HT-SGIC profile of blends of isotactic polypropylene (iPP), atactic polypropylene (aPP), syndiotactic polypropylene (sPP) and linear polyethylene (PE). (Column: Hypercarb, Solvent gradient: from 100% 1-decanol to 100% TCB, T: 160 °C)[66] 22

Figure 2-17. HT-SGIC profile of ethylene/4-methyl-1-pentene copolymers. (Column: Hypercarb, Solvent gradient: from 100% 1-decanol to 100% TCB, T: 160 °C)[67] 23

Figure 2-18. HT-SGIC profiles of isotactic polypropylene (iPP) with distinct M_w (a) and linear polyethylene (PE) with distinct M_w (b). (Column: Hypercarb, Solvent gradient: from 100% 1-decanol to 100% TCB, T: 160 °C).[68] 24

Figure 2-19. Schematic for HT 2D-LC.[72] 25

Figure 2-20. HT-TGIC profile of ethylene/1-octene copolymers. (Column: Hypercarb®, Temperature gradient range: (175 – 0) °C, Solvent: ODCB).[77] 28

Figure 2-21. HT-TGIC calibration curve for ethylene/1-octene copolymers.[77] 28

Figure 2-22. Effect of molar mass on the elution peak of HT-TGIC for polyethylene.[80] 29

Figure 2-23. Effect of cooling flow rate on HT-TGIC profile for the ethylene/1-octene copolymer. (Column: Hypercarb®, Temperature gradient: (155 –90) °C, Solvent: ODCB).[82] 29

Figure 2-24. Effect of cooling rate on HT-TGIC profile for the ethylene/1-octene copolymer. (Column: Hypercarb®, Temperature gradient: (155 –90) °C, Solvent: ODCB).[82] 30

Figure 2-25. Effect of cooling flow rate on HT-TGIC profile of Blend-2 (50% of 3.51 % and 50% of 1.16 mol % of 1-octene). (Column: Hypercarb®, Temperature gradient: (155 –90) °C, Solvent: ODCB).[82] 30

Figure 2-26. Effect of heating rate on HT-TGIC profile for the ethylene/1-octene copolymer. (Column: Hypercarb®, Temperature gradient: (155 –90) °C, Solvent: ODCB).[82] 31

Figure 2-27. Comparison between experimental and calculated profiles of Blend-2 (50% of 3.51 % and 50% of 1.16 mol % of 1-octene) using heating rates of 3 °C/min (A) and 1 °C/min (B). (Column: Hypercarb®, Temperature gradient: (155 –90) °C, Solvent: ODCB).[82] 31

Figure 2-28. Effect of solvent type on HT-TGIC profile for the ethylene/1-octene copolymer, containing 3.51% octene. (Column: Hypercarb®, Temperature gradient: (155 –90) °C, Solvent: ODCB, CN, and TCB).[81] 32

Figure 2-29. TH-TGIC profiles of ethylene/1-octene copolymer samples using Hypercarb column (above) and molybdenum sulfide column (bottom).[87] 33

Figure 2-30. Adsorption of polyethylene schematic on the atomic level flat surface (ALFS): A) no SCB, longer ethylene sequences, and B) with SCB, shorter ethylene sequences.[88] 34

Figure 3-1. Ethylene/1-octene copolymers investigated in this research: Category I includes samples with similar M_n and different 1-octene content; Category II comprises samples with similar 1-octene content and different M_n. (H = homopolymer, C = copolymer, number beside C corresponds to the mole fraction of 1-octene in the copolymer). 35

Figure 3-2. Reactor A: 600 mL autoclave polymerization reactor. 37

Figure 3-3. Reactor B: 300 mL autoclave polymerization reactor..... 37

Figure 3-4. Linear relation between the hydrogen amount (mmol) added to the reactor and the reciprocal of the number average chain length ($\tau = 1/r_n$). H = homopolymers; C = ethylene/1-octene copolymers. Numbers indicate the mol% of 1-octene incorporated in the copolymer. 41

Figure 3-5. ^{13}C-NMR spectrum of an ethylene/1-octene copolymer.[89] 49

Figure 3-6. FTIR calibration curve..... 54

Figure 3-7. Schematic diagram of CEF instrument (Polymer Char, Valencia, Spain) used for the HT-TGIC experiments. 55

Figure 3-8. Schematic of HT-TGIC experimental setup. T_S is the stabilization temperature, T_{C1} and T_{C2} are the first and last temperatures in the cooling cycle, CR is the cooling rate, F_C is the solvent flow rate during the cooling cycle, HR is the heating rate, F_E is the solvent flow rate during the heating cycle, T_E is the last temperature in the heating cycle, and F_{CL} is solvent flow rate during the cleaning. 57

Figure 4-1. MWDs of ethylene/1-octene copolymers with different comonomer fractions. 59

Figure 4-2. HT-TGIC profiles for ethylene/1-octence copolymers. (Operation conditions: F_C= 0.02 mL/min, CR= 5 °C/min, HR= 3 °C/min, F_E= 0.5 mL/min, temperature range in both cycles = 160-35 °C) 61

Figure 4-3. HT-TGIC Calibration curve for ethylene/1-octene copolymers of Category I 62

Figure 4-4. Cooling rate effect on HT-TGIC profiles of sample E/O-16.4. 65

Figure 4-5. Heating rate effect on HT-TGIC profile of sample E/O-16.4. 66

Figure 4-6. Effect of elution flow rate on HT-TGIC profile of sample E/O-16.4. 67

Figure 4-7. Experimental (continuous line) and predicted (dotted line) HT-TGIC profiles for a blend of 50% of E/O-9.8 and 50% of E/O-16.4 at different operation conditions. 70

Figure 4-8. Experimental (continuous line) and predicted (dotted line) HT-TGIC profile of Blend 2 (50% of E/O-9.8, 50% of E/O-16.4). (Operation conditions: CR = 5 °C/min, HR = 3 °C/min, F_E = 0.5 mL/min, temperature range in both cycles = 160-35 °C) 72

Figure 4-9. Experimental (continuous line) and predicted (dotted line) HT-TGIC profile of Blend3 (50% of E/O-16.4, 50% of E/O-23.2). (Operation conditions: CR = 5 °C/min, HR = 3 °C/min, F_E = 0.5 mL/min, temperature range in both cycles = 160-35 °C) 73

Figure 4-10. Experimental (continuous line) and predicted (dotted line) HT-TGIC profile of Blend3 (50% of E/O-13.2, 50% of E/O-21.3). (Operation conditions: CR = 5 °C/min, HR = 3 °C/min, F_E = 0.5 mL/min, temperature range in both cycles = 160-35 °C) 73

Figure 5-1. Experimental and predicted HT-TGIC profiles of five blends of E/O-5.6 and E/O-16.4 measured in Column 1. 77

Figure 5-2. HT-TGIC profiles of four ethylene/1-octene copolymers (E/O-5.6, E/O-9.8, E/O-16.4, and E/O-21.3) measured in three Hypercarb columns having packing with distinct average particle sizes. 79

Figure 5-3. HT-TGIC profiles of the blend of E/O-9.8 and E/O-16.4 (50/50 wt.%), analyzed in three Hypercarb columns having packing with distinct average particle sizes. 79

Figure 5-4. HT-TGIC profiles of the blend of E/O-5.6 and E/O-16.4 (50/50 wt.%), analyzed in three Hypercarb columns having packing with distinct average particle sizes. 80

Figure 5-5. HT-TGIC profiles of four ethylene/1-octene copolymers (E/O-5.6, E/O-9.8, E/O-16.4, and E/O-21.3) analyzed in two Hypercarb columns having different lengths: *L* = 250 mm (dotted line) and *L* = 100 mm (continuous line). 81

Figure 5-6. HT-TGIC profiles of four ethylene/1-octene copolymers (E/O-5.6, E/O-9.8, E/O-16.4, and E/O-21.3) analyzed in two Hypercarb columns having different lengths: *L* = 250 mm (dotted line) and *L* = 100 mm (continuous line). The profiles measured in the shorter column have been shifted to higher temperatures. 81

Figure 5-7. HT-TGIC profiles of Blend 1 (E/O-9.8 and E/O-23.2, 50/50 wt.%) and Blend 2 (E/O-9.8 and E/O-16.4, 50/50 wt.%) measured in two Hypercarb columns having different lengths: *L* = 250 mm (dotted line) and *L* = 100 mm (continuous line). 82

Figure 5-8. HT-TGIC profiles of Blend 1 (E/O-9.8 and E/O-23.2, 50/50 wt.%) and Blend 2 (E/O-9.8 and E/O-16.4, 50/50 wt.%) measured in two different Hypercarb columns having different lengths: *L* = 250 mm (dotted line) and *L* = 100 mm (continuous line). The profiles measured in the longer column have been shifted to lower temperatures. 83

Figure 6-1. Algorithm of Monte Carlo simulation program 87

Figure 6-2. An Example of AES and LES calculation in Monte Carlo simulation 88

Figure 6-3. Adsorption of polyethylene on an atomic level flat surface: A) without SCB, longer ethylene sequences, stronger interaction, and B) with SCB, shorter ethylene sequences, weaker interactions.[87] 89

Figure 6-4. HT-TGIC profiles of polyethylenes and ethylene/1-octene copolymers with different r_n. 94

Figure 6-5. Average ethylene sequences (AES) depend weakly on r_n for ethylene/1-octene copolymers with a high 1-octene fraction. 95

Figure 6-6. Average longest ethylene sequences (LES) depend more strongly on r_n for ethylene/1-octene copolymers. 96

Figure 6-7. Overall ethylene sequence distributions (left), and longest ethylene sequence distributions (right) of ethylene/1-octene copolymers become narrow, and shift towards lower averages as r_n decreases. 97

Figure 6-8. Elution peak temperature versus r_n for polyethylene and ethylene/1-octene copolymers, showing how the critical r_n ($\hat{r}_n$) gets higher when the fraction of 1-octene in the copolymer increases. 99

Figure 6-9. Relationship between the critical r_n ($\hat{r}_n$) and mole fraction of 1-octene in the copolymer. 100

Figure 6-10. Peak temperatures do not depend on AES for samples with higher 1-octene fractions (C7.8 and C13). 101

Figure 6-11. Peak temperatures do not depend on LES for all sets of ethylene/1-octene copolymers. 101

Figure 6-12. Elution peak temperatures versus $1/r_n$. 102

Figure 6-13. Elution peak temperatures versus 1/LES. 103

Figure 6-14. Slope of the curves shown in Figure 6-12 and Figure 6-13 versus 1-octene content in the copolymer. 103

Figure 6-15. Joint effect of 1-octene mol% and r_n on HT-TGIC peak temperature. 104

Figure 6-16. HT-TGIC calibration curve. 106

Figure 6-17. Comparison experimental (continuous line) and predicted (dotted line) HT-TGIC profiles. 107

Figure 6-18. Relation between (σ_T/σ_S) and F_E for the samples in Figure 17. 108

Figure 6-19. Comparison of HT-TGIC profiles and broadened Stockmayer distributions. 109

Figure 6-20. Nomenclature for the dual-resin blends. 110

Figure 6-21. Experimental and predicted HT-TGIC profiles of Group-A blends. 111

Figure 6-22. Experimental and predicted HT-TGIC profiles of Group-B blends. 112

Figure 6-23. Experimental and predicted HT-TGIC profiles of Blend-C2, Blend-D2, Blend-E2, and Blend-F2. 113

Figure 6-24. Relation between co-adsorption index and AES ratio of all blends. 114

Figure 6-25. Relation between the co-adsorption index and LES ratio of all blends. 114

Figure 6-26. 3D plot showing how the co-desorption index (CDI) varies with CC ratio and LES ratio. 115

Figure 6-27. 3D plot showing how the co-desorption index (CDI) varies with CC ratio and r_n ratio. 116

List of Tables

Table 2-1. Common physical and mechanical properties of LDPE, HDPE, and LLDPE. 4

Table 2-2. Example of commercial catalysts and their general characteristics 7

Table 2-3. Main characteristics of TREF, CRYSTAF and CEF. 14

Table 3-1. Materials used to synthesize ethylene/1-octene copolymers. 36

Table 3-2. Definitions of symbols in Figure 3-1 and 3-2. 38

Table 3-3. Copolymerization conditions for copolymers in Category I. 40

Table 3-4. Ethylene homopolymerization conditions (Category II). 41

Table 3-5. Polymerization conditions for ethylene/1-octene copolymers with 1.0 mol % of 1-octene (Category II). 42

Table 3-6. Polymerization conditions for ethylene/1-octene copolymers with 2.6 mol % of 1-octene (Category II). 42

Table 3-7. Polymerization conditions for ethylene/1-octene copolymers with 3.7 mol % of 1-octene (Category II). 43

Table 3-8. Polymerization conditions for ethylene/1-octene copolymers with 7.8 mol % of 1-octene (Category II). 43

Table 3-9. Polymerization conditions for ethylene/1-octene copolymers with 12.9 mol % of 1-octene (Category II). 44

Table 3-10. Properties of ethylene/1-octene copolymers in Category I (similar M_n). 45

Table 3-11. Properties of ethylene homopolymer (Category II). 46

Table 3-12. Properties of ethylene/1-octene copolymers with 1.0 mol % of 1-octene (Category II).. 46

Table 3-13. Properties of ethylene/1-octene copolymers with 2.6 mol % of 1-octene (Category II).. 47

Table 3-14. Properties of ethylene/1-octene copolymers with 3.7 mol % of 1-octene (Category II).. 47

Table 3-15. Properties of ethylene/1-octene copolymers with 7.8 mol % of 1-octene (Category II).. 48

Table 3-16. Properties of ethylene/1-octene copolymers with 12.9 mol % of 1-octene (Category II). 48

Table 3-17. Integration limits for ^{13}C NMR spectrum of ethylene/1-octene copolymer 50

Table 3-18. Integration limits of 13C NMR spectra of the samples of Category I 51

Table 3-19. Integration limits of 13C NMR spectra of the samples of Category I 52

Table 3-20. Properties of Hypercarb columns. 55

Table 4-1. HT-TGIC data for ethylene/1-octene copolymer samples of Category I 60

Table 4-2. Factor levels used in the 2^3 factorial design. 62

Table 4-3. Output values for the 2^3 factorial design. 63

Table 4-4. ANOVA table for the elution peak temperatures for sample E/O-16.4. 64

Table 4-5. ANOVA table for the standard deviation of HT-TGIC profiles for sample E/O-16.4. 64

Table 4-6. Output values of 2^3 factorial design for Blend 1. 69

Table 4-7. ANOVA TABLE for the co-desorption index of Blend1 presented in Table 4-6 71

Table 4-8. Additional blends used to study the effect of operation conditions on the co-desorption index. 72

Table 5-1. Co-desorption index of five copolymer blends. 76

Table 5-2. Average values for HT-TGIC analysis of four samples using three different Hypercarb columns. 78

Table 6-1. HT-GPC and HT-TGIC data for ethylene homopolymers. 90

Table 6-2. HT-GPC and HT-TGIC data for ethylene/1-octene copolymers with 1.0 mol % of 1-octene. 90

Table 6-3. HT-GPC and HT-TGIC data for ethylene/1-octene copolymers with 2.6 mol % of 1-octene. 91

Table 6-4. HT-GPC and HT-TGIC data for ethylene/1-octene copolymers with 3.7 mol % of 1-octene. 91

Table 6-5. HT-GPC and HT-TGIC data for ethylene/1-octene copolymers with 7.8 mol % of 1-octene. 92

Table 6-6. HT-GPC and HT-TGIC data for ethylene/1-octene copolymers with 12.9 mol % of 1-octene. 92

Table 6-7. Stockmayer parameters and HT-TGIC-measured CCDs. 106

Table 6-8. Co-desorption index of the two major group blends. 110

Table 6-9. Additional blends used to study the effect of M_n on the co-desorption index. 112

Nomenclature

Symbols

A	Transition metal (most commonly, Ti, Zr, or Hf)
AlR_3	Alkylaluminum cocatalyst
A_{CH3}	Absorbance at 1378 cm^{-1} that represents the methyl branches
$Area_{CH2}$	The area of the methylene combination band at 2019 cm^{-1}
Cm-n	Ethylene/1-octene copolymer samples where *m* is 1-octene mole fraction and *n* is number average molecular weight
C_P	Cyclopentadienyl
E/O-m	Ethylene/1-octene copolymers where m is the 1-octene mole faction in copolymer
F_E	Ethylene mole fraction in the copolymer
F_O	1-Octene mole fraction in the copolymer
H-n	Polyethylene samples where n is the number average molecular weight
L	Ligands
M_n	Number average molecular weight
M_w	Weight average molecular weight
MW_E	Ethylene molecular weight
MWo	1-Octene molecular weight
n	Number of monomers.
N	SCB/1000 C - Number of short chain branches per 1000 carbons
Pol	Growing polymer chain
R	Alkyl group
r_n	Number average chain length for branched copolymer
T_p	Peak elution temperature
τ	Reciprocal of the number average chain length ($1/r_n$)

X	Halogen atom (commonly Cl)

Acronyms

AES	Average ethylene sequence length
ALFS	Atomic level flat support surfaces
BN	Boron nitride
CCD	Chemical composition distribution
CDI	Co-desorption index
CEF	Crystallization elution fractionation
CGC	Constrained geometry catalyst
CN	Chloronaphthalene
CR	Cooling rate
CRYSTAF	Crystallization elution fractionation
^{13}C NMR	Carbon-13 nuclear magnetic resonance spectroscopy
EGMBE	Ethylene glycol monobutylether
ELSD	Evaporate light scattering detector
ES	Ethylene sequence
EVA	Ethylene-vinyl acetate
F_E	Elution flow rate
FTIR	Fourier transform infrared spectroscopy
HDPE	High-density polyethylene
HR	Heating rate
HT-GPC	High-temperature gel permeation chromatography
HT-SGIC	High-temperature solvent gradient interaction chromatography
HT-TGIC	High-temperature thermal gradient interaction chromatography
HT 2D-LC	High temperature two-dimensional liquid chromatography
HPLC	High performance liquid chromatography
LES	Average longest ethylene sequence length

LESD	Longest ethylene sequence distribution
LDPE	Low-density polyethylene
LCBs	Long chain branches
LLDPE	Linear low-density polyethylene
MAO	Methylaluminoxane
MoS_2	Molybdenum sulfide
MW	Molecular weight
MWD	Molecular weight distribution
ODCB	O-dichlorobenzene
OESD	Overall ethylene sequence distribution
PDI	Polydispersity index
PGC	Porous graphitic carbon
SCBs	Short chain branches
TCB	1,2,4-trichlorobenzene
TCE	1,1,2,2-terachloroethane
TREF	Temperature rising elution fractionation
TMA	Trimethylaluminum
WS_2	Tungsten sulfide

Chapter 1. Introduction

1.1 Motivation

Polyolefins, which include polyethylene and polypropylene, are the most important class of synthetic polymers today. It is impressive that polyolefins, made from simple monomers containing only carbon and hydrogen, can be used in a wide variety of applications in the information technology, energy industry, transportation, packaging, health care, and different blow-molded objects such as bottles. The large impact of polyolefins in the market is due mainly to their low production cost, reduced environmental impact, and their flexible and tunable physical and mechanical properties.

The microstructure of polyolefin chains, composed of only carbon and hydrogen atoms, is the key to understanding their physical and mechanical properties. The major fundamental structural parameters affecting resin properties include their distributions of molecular weight (MWD), chemical composition (CCD), and long chain branching (LCBD). Several analytical techniques are used to measure these distributions.

High-temperature gel permeation chromatography (HT-GPC) is widely used to measure the MWD of polyolefins. Temperature rising elution fractionation (TREF), crystallization analysis fractionation (CRYSTAF), and crystallization elution fractionation (CEF) are crystallization-based techniques used to measure the CCD of polyolefins. TREF, CRYSTAF, and CEF are limited to semi-crystalline polyolefins. Recently, high performance liquid chromatography (HPLC) has been developed to quantify the CCD of semi-crystalline *and* amorphous polyolefins based on an adsorption-desorption mechanism, thus broadening the range of crystallization-based CCD analytical techniques. These techniques include high-temperature solvent gradient interaction chromatography (HT-SGIC) and high-temperature thermal gradient interaction chromatography (HT-TGIC). The fractionation mechanism is achieved by the interaction of polyolefin chains with a porous graphitic carbon packing upon either solvent change at high temperature (HT-SGIC) or temperature change in an isocratic solvent (HT-

TGIC). HT-SGIC is limited to evaporative light scattering detectors because solvent composition varies during analysis. On the other hand, all commercially available detectors can be used with HT-TGIC. HT-TGIC has the potential to revolutionize polyolefin analysis because it can measure the CCD of resins with a wider range of comonomer fractions than TREF, CRYSTAF, or CEF and eliminate the detector limitation of HT-SGIC.

1.2 Research Objectives

The main objective of this thesis is to investigate and understand the separation mechanism of HT-TGIC for polyolefin fractionation using series of homogeneous ethylene/1-octene copolymers synthesized with a single-site catalyst. Two major copolymer series were considered: 1) polymers having similar molecular weight averages but different 1-octene molar fractions and 2) polymers with the same average 1-octene content, but different molecular weight averages. These samples were used to study the joint effect of molecular weight (or chain length) and chemical composition on HT-TGIC fractionation of individual and binary blends of ethylene/1-octene copolymers.

It is also important to understand how operating factor affects polyolefin separation by HT-TGIC. Therefore, a systematic study of the different HT-TGIC operation analytical parameters was performed to study the impact on the chromatograms of HT-TGIC and find conditions that optimize peak resolution and minimize analysis time for individual samples and their binary blends.

Hypercarb columns, made of porous graphitic carbon, are considered to be among the best choices for polyolefin fractionation based on the adsorption-desorption mechanism. However, the effect of the length and average particle size of Hypercarb has never been investigated before. In this thesis, four different Hypercarb columns were compared to evaluate if these parameters had a significant effect on polyolefin fractionation.

1.3 Thesis Content

Chapter 2 briefly reviews the literature on ethylene polymerization with metallocene catalysts, and provides a detailed overview of several microstructural characterization techniques used to measure the CCD of polyolefins. Chapter 3 describes the polymerization procedure used to synthesize ethylene/1-octene copolymers, and the analytical methods used to determine their microstructures, notably MWD and CCD. Chapter 4 discusses the influence of different HT-TGIC analytical parameters for individual ethylene/1-octene samples and their binary blends. Chapter 5 compares different Hypercarb columns used to fractionate individual copolymer samples and their blends. Chapter 6 analyzes the joint effect of the chain length and 1-octene content on the fractionation mechanism of HT-TGIC for individual copolymers and their binary blends, and proposes a fundamental interpretation of the experimental results using Monte Carlo simulation and Stockmayer distribution. Finally, Chapter 7 summarizes the conclusions of the entire work done in this thesis, and suggests recommendations for future investigations.

Chapter 2. Literature Review

2.1 Polyethylene Microstructure

Polyethylene is the most important commercial polyolefin. Figure 2-1 illustrates typical microstructures of the three major types of commercial polyethylenes: low-density polyethylene (LDPE) – made by free-radical polymerization – linear low-density polyethylene (LLDPE) and high-density polyethylene (HDPE) – made by coordination polymerization.[1,2] Table 2-1 compares a few mechanical and physical properties of these polyethylene types.

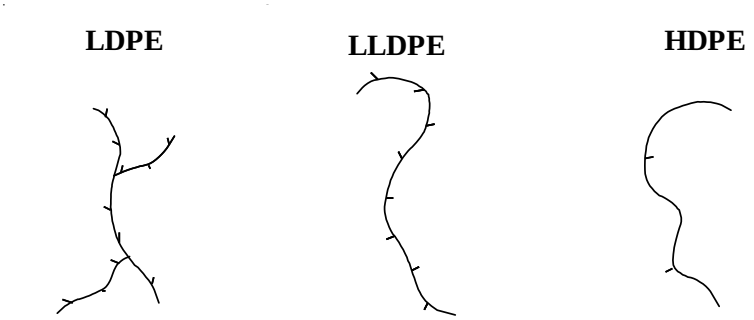

Figure 2-1. Commercial polyethylene types.[2]

Table 2-1. Common physical and mechanical properties of LDPE, HDPE, and LLDPE.

Property	LDPE	HDPE	LLDPE
Degree of branching 1000/C	20-40	0	15-30
Density (g/cm^3)	0.915-0.935	0.945-0.975	0.915-0.940
Degree of Crystallinity %	40-60	70-90	55-75
Melting point (°C)	100-120	133-138	120-130
Strength	Low	High	Medium

LDPE is an ethylene homopolymer made by free radical bulk polymerization in a high-pressure (120-300 MPa) and high-temperature (140-325 $^{\circ}$C) process in either autoclave or tubular reactors. LDPE has different lengths of short chain (SCB) formed via backbiting reactions, and long chain branches (LCB) made by transfer to polymer reactions. Long chain branches have lengths comparable to that of the polymer backbone, allowing easier processing of high molecular weight materials, and making the resin especially useful for extrusion coating. The SCB in LDPE decreases the degree of crystallinity and, therefore, the density of polyethylene.[3–5]

HDPE was discovered two decades later by Karl Ziegler and Giulio Natta using coordination polymerization catalysts.[6–8] This type of polyethylene has linear chains with no, or very few, SCBs, being more rigid and stiff than LDPE. The degree of crystallinity in HDPE may be as high as 90%, resulting in a high density polymer (0.94-0.975 g/cm^3). LLDPE has higher SCB frequency, combining the toughness of LDPE with the rigidity of HDPE. The presence of SCBs plays a major role in decreasing the degree of crystallinity (55-65%) and density of the polymer. HDPE and LLDPE may be made with single-site catalysts, such as metallocenes, or multiple-site catalysts, such as Ziegler-Natta and Philips catalysts. HDPE and LLDPE are made by copolymerizing ethylene and 1-olefins such as 1-butene, 1-hexene, and 1-octene. A short chain branch is formed in the polymer backbone when a 1-olefin is copolymerized with ethylene, as shown in Figure 2-2. The physical properties of LLDPE depend upon structural characteristics of the copolymer chains such as MWD and CCD. However, for the same comonomer molar fraction, the density and melting points of an ethylene/1-olefin copolymer decrease generally with increasing SCB length (Methyl>Ethyl>Butyl>Hexyl).[9–12]

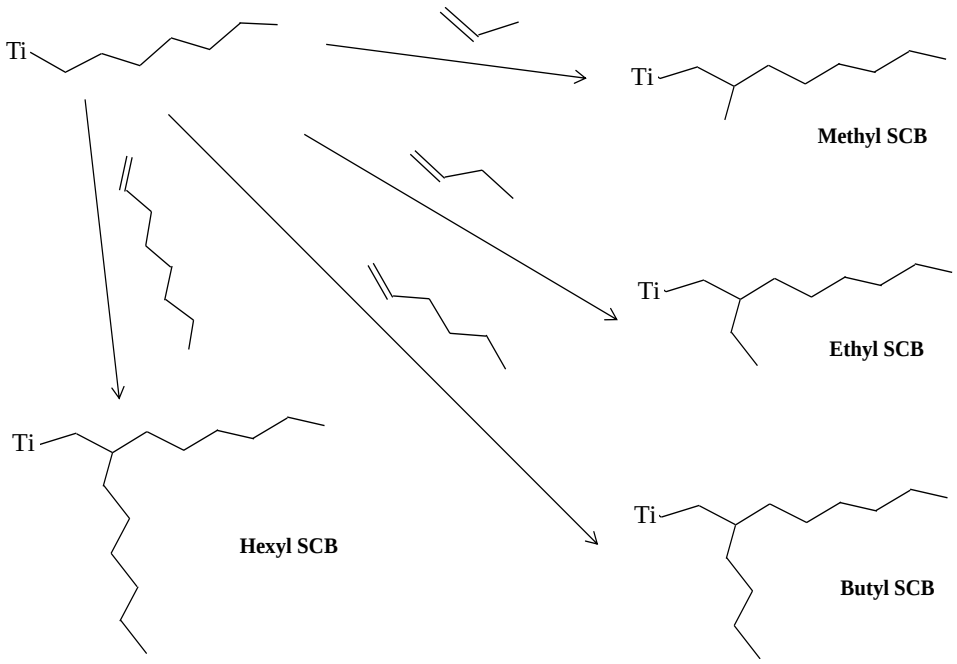

Figure 2-2. Mechanism of short chain branch formation by coordination polymerization. The chains are shown growing on a titanium active site.[2]

2.2 Ethylene Polymerization with Coordination Catalysts

Polyethylenes (HDPE and LLDPE) are produced by coordination polymerization using Ziegler-Natta catalysts, chromium oxide (Philips) catalysts or, more recently, metallocene and late transition metal catalysts (post-metallocenes). Table 2-2 illustrates the main commercial catalyst types used to make HDPE and LLDPE. Multiple-site catalysts, including Ziegler-Natta and Phillips, make polymers with non-uniform microstructures, characterized by broad and sometimes bimodal MWDs and CCDs, while single-site catalysts (metallocene and post-metallocenes) produce polyolefins with narrow and uniform microstructural distributions.[6,13–16]

The investigations described in this thesis used ethylene/1-olefin copolymers with narrow MWD and CCD to investigate HT-TGIC fractionation because these are well-defined materials that are ideally used as standards; therefore, multiple-site catalysts will not be covered any further in this chapter.

Table 2-2. Example of commercial catalysts and their general characteristics

Catalyst	Transition Metal	Characteristics
Metallocene	Zr, Ti, Hf	• Methylaluminoxane or borate/borane cocatalyst • Narrow polymer molecular weight distribution (*PDI*≈2)* • Hydrogen as chain transfer agent
Ziegler-Natta	Ti	• Aluminum alkyl cocatalyst • Broad polymer molecular weight distribution (*PDI*=4-6) • Hydrogen as chain transfer agent
Philips	Cr	• No cocatalyst • Very broad polymer molecular weight distribution (*PDI*>6) • Thermal treatment and support type are used to control polymer molecular weight

* *PDI* is polydispersity index for MWD

2.2.1 Metallocene Catalysts

Metallocene catalysts are as old as Ziegler-Natta catalysts, but they had very low activities when activated with trimethylaluminum (commonly used to activate Zeigler-Natta catalysts).[8,17,18] In the early 1980s, Kaminsky and others[13,19–21] discovered serendipitously that metallocenes became very active for olefin polymerization when they were activated with methylaluminoxane (MAO). MAO (Figure 2-3) is produced by the controlled hydrolysis of trimethylaluminum.[21] Metallocenes started to be commercially important soon after Kaminsky's discovery because polymerization processes that used Ziegler-Natta catalysts could be adapted to work with metallocenes without too many modifications. Since these catalysts have only one type of active site, they make polyolefins with a degree of microstructural control that is not possible with conventional heterogeneous multiple-site catalysts. For instance, metallocenes polyolefins have narrow MWD (polydispersity index close to the theoretical minimum value of 2.0) and high strength.[14, 19,22]

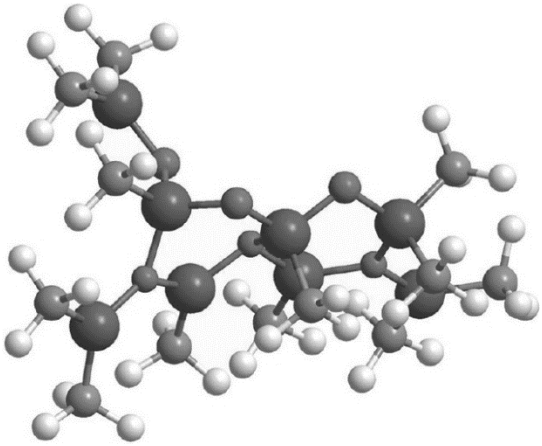

Figure 2-3. General structure of methylaluminoxane (MAO)[21]

Metallocene catalysts are organometallic compounds composed of a transition metal, typically Ti, Zr, or Hf, attached to one or more cyclopentadienyl rings (C_P) (or C_P derivatives) via π-bonds, as indicated in Figure 2-4.[6] Figure 2-5 show a few examples of metallocene catalysts.[6, 13,19] Many factors that regulate the catalytic behavior of the metallocenes towards olefin polymerization, such as the nature and type of transition metal, number and type of the cyclopentadienyl rings, cocatalyst/catalyst ratio, and polymerization conditions.[23–25] These factors determine catalyst activity, comonomer reactivity ratios, response to transfer agents, stereo- and regioselectivity.

A constrained geometry catalyst (CGC) is a type of metallocene with only one cyclopentadienyl ring and a nitrogen substituent coordinated to the metal center, as shown in Figure 2-5-c. CGCs, also called half-sandwich catalysts, have high reactivity ratios towards 1-olefin incorporation because of steric and electronic reasons. Copolymers made with CGCs have been claimed to have a better balance of physical properties and processability than LDPE and other metallocene LLDPE.[2, 4, 14,24]

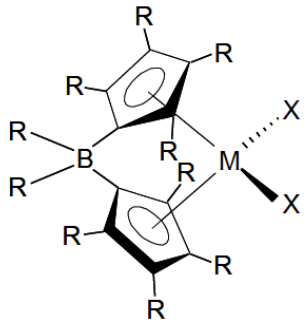

Figure 2-4. Generalized structure of a metallocene catalyst; *M*: Transition metal; *X*: hydrocarbyl, alkylidene, halogen radicals; *R*: hydrogen, hydrocarbyl radicals; B-bridging group[6]

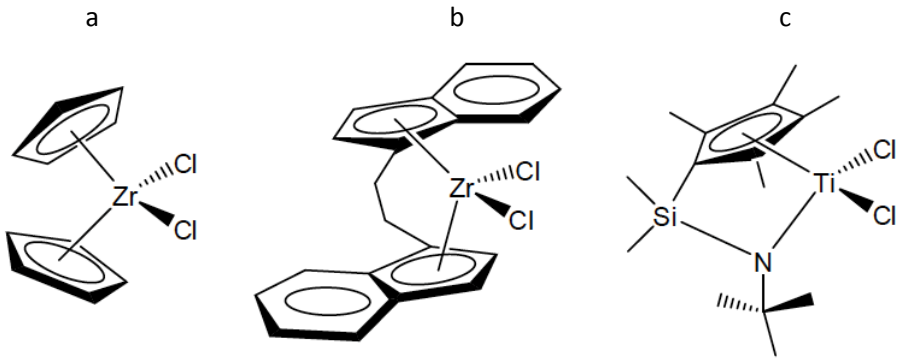

Figure 2-5. Some examples of metallocene catalysts: a) Cp_2ZrCl_2; b) rac-$Et(Ind)_2ZrCl_2$; c) Constrained geometry catalyst.[6]

2.2.2 Polymerization Mechanism

The first step in coordination polymerization is the formation of the active site in the catalyst. Active sites are formed by the reaction of a pre-catalyst (or catalyst precursor) and an activator or cocatalyst (AlR_3). The cocatalyst alkylates the pre-catalyst after extracting two halogen atom to form a cationic active site and a non-coordinating anion for catalyst stabilization. Since the cocatalyst works as a Lewis acid (electron acceptor), it also scavenges polar impurities (electron donors such as moisture) from the reactor that poison the active site. Figure 2-6 shows

a simplified chemical equation for the activation mechanism and its correspondent chemical equation.[2,26]

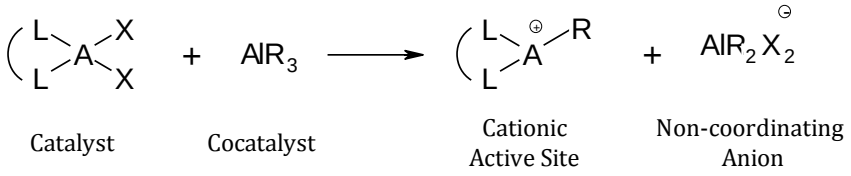

Figure 2-6. Catalyst activation by reaction with cocatalyst; *A*: transition metal (most commonly, Ti, Zr or Hf), *L*: ligands, *X*: halogen atom (commonly, Cl), *R*: alkyl group (methyl or ethyl).[27]

After the catalyst activation, the polymerization proceeds through two main steps: monomer (ethylene) coordination to the active site (chain initiation) and insertion into the living polymer chain, as described in Figure 2-7. First, an incoming ethylene monomer coordinates to the vacancy of the transition metal via its carbon double bond to form a four-member ring structure among the active site, alkyl group, and ethylene carbon-carbon double bond. Then, the monomer molecule is inserted between the carbon-metal bond. Once the insertion of the first monomer has been completed, a new free coordination site is generated at the metal vacant position to begin new insertion that lengthens the growing polymer chain.[10, 18,28]

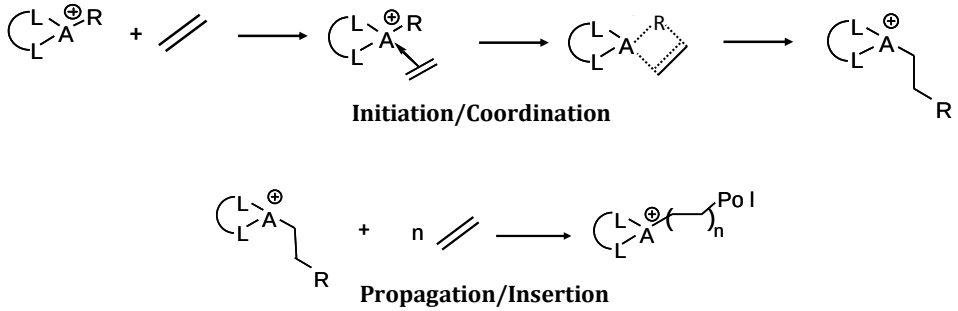

Figure 2-7. Monomer initiation and propagation; *A*: transition metal (most commonly, Ti, Zr or Hf), *L*: ligands, *R*: alkyl group (methyl or ethyl), *n*: number of monomers, *Pol*: growing polymer chain.[27]

During propagation, the length of the growing polymer chain increases via repeated monomer insertions until a chain transfer reaction stops the growth of the polymer chain, resulting in a dead polymer chain and a polymer-free active site that can make another polymer chain. Figure

2-8 displays several chain transfer reactions that are possible in coordination polymerization.[2,10] The type of chain transfer step determines the nature of the chemical group bound to the chain end. β-Hydride elimination, and transfer to ethylene made dead chains capped with a vinyl group (unsaturated ends). Transfer to hydrogen or cocatalyst, on the other hand, generate dead polymers with saturated chain ends. Although most chain transfer steps may occur during polymerization, chain transfer to hydrogen is the most common way to control polyolefin molecular weight in the laboratory and industrial reactors.[27,29]

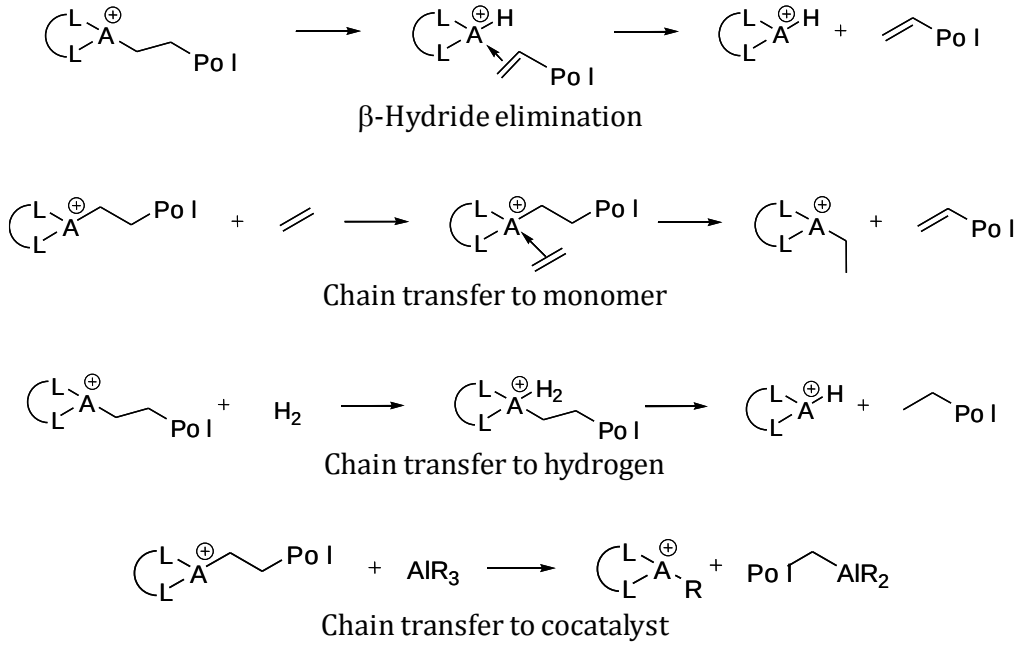

Figure 2-8. Chain transfer reactions; *A*: transition metal (most commonly, Ti, Zr or Hf), *L*: ligands, *R*: alkyl group (methyl or ethyl), *n*: number of monomers, *Pol*: growing polymer chain.[27]

The steps for ethylene homopolymerization described above are valid also for ethylene/1-olefin copolymerization. For a given catalyst/cocatalyst system, both propagation and chain transfer rates during copolymerization are affected by the type of monomers coordinated to the active site and inserted into the growing polymer chain due to the competition of two monomers.[27,28]

2.3 Polyethylene Microstructural Characterization

The microstructure of polyolefins is defined by their molecular weight distribution (MWD), chemical composition distribution (CCD), and long chain branching distribution (LCBD). These distributions determine the end-use properties of polyethylenes. Characterization techniques developed to measure CCD, including crystallization-based techniques and interactive-based techniques will be discussed in the following sections.

2.3.1 Crystallization-Based Techniques

TREF, CRYSTAF and CEF have been used extensively to measure the CCD of polyethylenes in the last three decades. These techniques rely on the fact that chains with higher 1-olefin fraction have lower crystallization temperatures than chains with lower comonomer content. Differences in crystallizability are then transformed in differences in comonomer content using a calibration curve. The fractionation takes place by slowly decreasing the temperature of a dilute polymer solution, either in a stirred vessel (CRYSTAF) or in a packed column (TREF, CEF).[26]

TREF uses two temperature cycles, crystallization and elution. First, the sample is dissolved in a solvent at high temperature and then the polymer solution is introduced into a column containing an inert support, such as glass beads. In the crystallization step, the column temperature is decreased gradually to room temperature at a very slow cooling rate (typically 2 ºC/h) for enhanced resolution. Polymer chains with higher crystallizabilities (low comonomer fraction) precipitate first, followed by polymer chains with lower crystallizabilities (high comonomer fraction). TREF requires a second temperature cycle (elution step) to separate those fractions physically. The elution cycle is done by flowing solvent through the column at increasing temperatures to remove the polymer chains in the reverse order they were precipitated. Fractions of increasing crystallinities are dissolved from the column as the temperature rises. TREF provides good peak resolution but requires long analysis times.[30–32]

In 1991, CRYSTAF was introduced by Monrabal[33,34] as a new analytical technique to speed up the CCD analysis of polyolefins. It shares with TREF the same separation mechanism based on crystallizability. However, fractionation is achieved only in the crystallization step (no elution cycle), decreasing analysis time. In CRYSTAF, the analysis takes place inside a stirred crystallization vessel without the use of supports. An in-line mass detector measures the polymer concentration in the solution as the polymer solution temperature decreases. The measured cumulative distribution is transformed into the CCD (differential distribution) by taking its first derivative with respect to the crystallization temperature. CRYSTAF and TREF profiles have similar shapes, as shown in Figure 2-9. However, CRYSTAF curves are shifted towards lower temperatures because TREF profiles are measured during dissolution and CRYSTAF curves are measured during crystallization. [33,35–37]

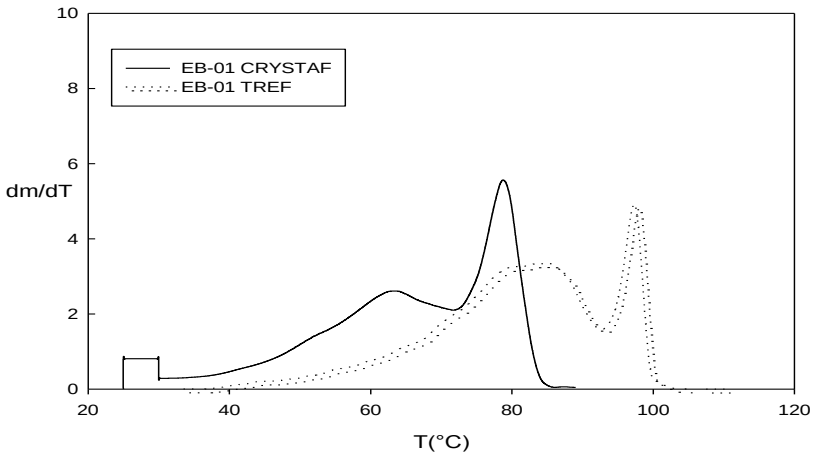

Figure 2-9. TREF and CRYSTAF profiles of an ethylene/1-butene copolymer made with a heterogeneous Ziegler-Natta catalyst.[26]

In 2006, Monrabal[38] introduced CEF as a faster fractionation technique. Differently from TREF, where the polymer solution crystallizes without solvent flow, the solvent is flown through the CEF column during the crystallization step, as illustrated in Figure 2-10. TREF uses short columns, typically 10-15 cm long, while CEF needs longer columns, usually 100-200 cm long. In the CEF crystallization cycle, once the crystallization temperature of a fraction is reached, it is precipitated on the support while the other fractions are still soluble in the

solvent and keep moving along the column until their crystallization temperatures are reached. Thus, CEF reduces co-crystallization by segregating fractions of different crystallizabilities in the column. Because co-crystallization is substantially reduced, CEF can be operated at much faster cooling rates than TREF and CRYSTAF.[38–40] Table 2-3 summarizes the main characteristics of TREF, CRYSTAF and CEF.

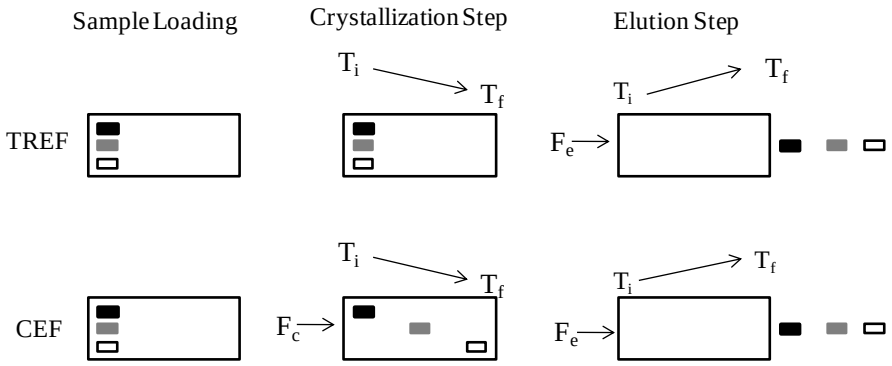

Figure 2-10. Crystallization and elution steps in TREF and CEF.[38]

Table 2-3. Main characteristics of TREF, CRYSTAF and CEF.

Technique	Characteristics
TREF	• Column fractionation technique • No flow during the crystallization step • Detection during the elution step • Long analysis times
CRYSTAF	• Batch technique • Detection during the crystallization step • No elution step • Shorter analysis times than TREF
CEF	• Column fractionation technique • Flow during the crystallization step • Detection during the elution step • Short analysis times

Molecular weight and comonomer mole fraction are the main key factors affecting the crystallizability of polymer molecules. Wild *et al*.[32] indicated that the molecular weight might not affect the position of peak temperature in TREF. They studied a series of linear polyethylene samples made with a single site catalyst and investigated that the peak elution temperature was independent of molecular weight for polyethylenes with a number average molecular weight (M_n) greater than 10,000 g/mol. Nieto *et al*.[35] established the same conclusion for CRYSTAF peak temperature that molecular weight for samples with M_n greater than 5,000 g/mol did not change the crystallization temperature. Anantawaraskul *et al*.[41] realized that although both molecular weight and comonomer content significantly affect the broadness of CCD of these techniques, comonomer mole fraction is the main determining factor affects the position of CCD peak for most samples with a variation of molecular weights. Since molecular weights of most industrial linear polyethylene are high, TREF and CRYSTAF profiles are relatively insensitive to the molecular weights of those resins.

The operating conditions used in TREF, CRYSTAF and CEF affect the profiles measured by these techniques.[30,42–46] The crystallization step is of great importance for all these three techniques since the polymer molecules get firstly separated from the bulk polymer during this step. Therefore, the cooling rate (CR) is the key parameter in these techniques. CCD profiles shift to higher peak temperatures when slower cooling rates are used, likely due to the formation of larger crystallites. Anantawarskul *et al*.[30,43] used the average temperature lag in the steady-state regime to correct the CRYSTAF profiles and they found an experimental linear relationship between the average temperature lag and the cooling rate. On the other hand, they demonstrated that decreasing heating and solvent flow rates in TREF shift the profiles to higher peak temperatures due to increased residence time in the column. CCDs also become broader at higher heating rates, as a given volume of solvent will elute the polymer over a wider range of crystallinities. Alghyamah *et al*.[39,42] concluded similar observation for CEF profiles that are strongly affected by the cooling rate and the solvent flow rate using a series of ethylene/1-octene copolymer samples. Aust *et al*.[44] optimized the operating parameters of TREF using the aid of a factorial design experiments which leads to a remarkable increase in resolution of

TREF profile of ethylene/propylene copolymer. Chokputtanawuttilerd *et al*.[45] developed a mathematical model of CEF based on population balance with the crystallization kinetic and the axial dispersion models to describe the experimental CEF at various operating conditions. They demonstrated that the model parameters estimated were found to be in good agreement with those obtained from other crystallization based techniques.

Co-crystallization is one of the main limitations of crystallization-based techniques and the most important factor reducing their resolution.[36, 40,42–47] Anantawaraskul *et al*.[43,47] investigated whether co-crystallization effect on CCDs measured by TREF and CRYSTAF is correlated to the value of cooling rate by studying blends of ethylene/1-hexene copolymer samples. They noticed that slow cooling rates reduce, but do not completely eliminate co-crystallization in blends with components of similar crystallizabilities. The degree of co-crystallization can be calculated by comparing predicted and measured blend profiles. Alghyamah *et al*.[39,42] applied this method to study the effect of several operation parameters on co-crystallization in the CEF profiles of blends of ethylene/1-octene copolymers. Figure 2-11 shows that the degree of co-crystallization in CEF was considerably reduced as the cooling rate decreased. However, blend components having very close elution peak temperatures remain affected by co-crystallization, even when impractically low cooling rates (from 0.5 °C/min to 0.09 °C/min) were used.[39,42]

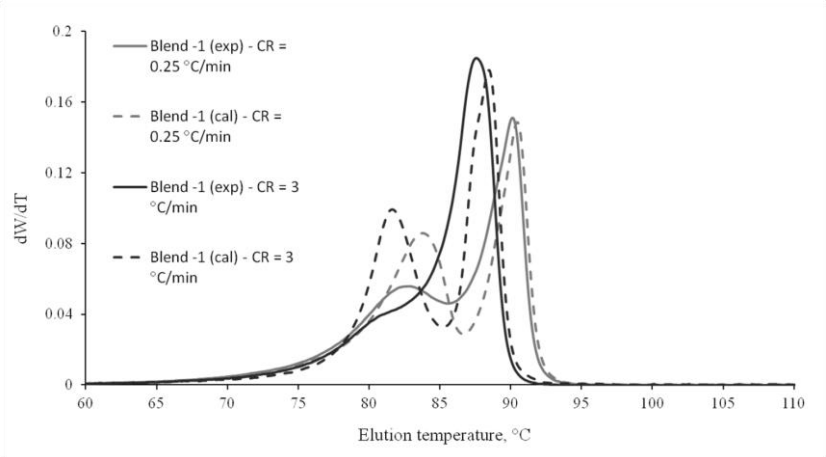

Figure 2-11. Effect of cooling rate on CEF co-crystallization. Continuous lines are the experimental profiles of blends of two components of ethylene/1-octene copolymers having different comonomer contents (50% of 1.51, and 50% of 3.51 mol%). Dashed lines represent the predicted profile for the same blends.[39]

TREF, CRYSTAF, and CEF can be calibrated to obtain CCDs from their elution or crystallization curves. Ethylene/1-olefin copolymers synthesized by single-site metallocene catalysts are useful calibration standards for these techniques as they have narrow CCDs and cover a broad range of comonomer incorporation. Figure 2-12 shows how to obtain a calibration curve for CEF. A similar procedure can be used to establish a calibration curve for CRYSTAF and TREF.[10, 36,48–50]

Sample	Comonomer Mole%
1	1.04
2	1.60
3	2.15
4	2.66
5	4.54
6	5.65
7	6.46

1) Comonomer fraction analysis using ^{13}C NMR

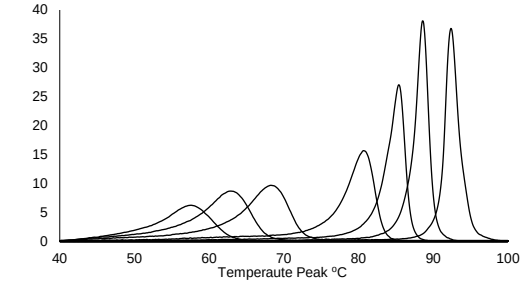

2) CEF peak temperature measurement

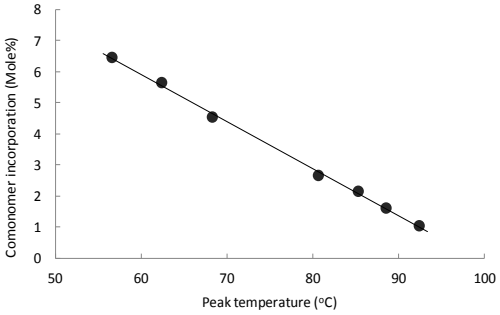

3) Plot of CEF peak temperature versus comonomer fraction (calibration curve)

Figure 2-12. The procedure used to generate a calibration curve for CEF.

Several TREF and CRYSTAF calibration curves have been reported in the literature.[31, 36,49,50] Figure 2-13 shows CEF calibration curves for ethylene/1-hexene, ethylene/1-octene and ethylene/1-dodecene copolymers.[51] Linear relationships between comonomer mole fraction and peak temperatures are generally observed for TREF, CRYSTAF, and CEF. The slope of calibration curve obtained with ethylene/1-olefin copolymers with shorter branches (butyl) is higher than those for ethylene/1-olefin copolymers with longer branches (hexyl or decyl). It indicates that butyl branches are less effective in disrupting the crystallizability of the copolymer chains than hexyl or decyl branches, perhaps because butyl branches can be partially incorporated into the crystal lattice. On the other hand, after a certain limit, the length

of the SCB stops having an effect on the calibration curve. Figure 2-13 demonstrates that the calibration curves for ethylene/1-octene and ethylene/1-dodecene copolymers are the same.[51]

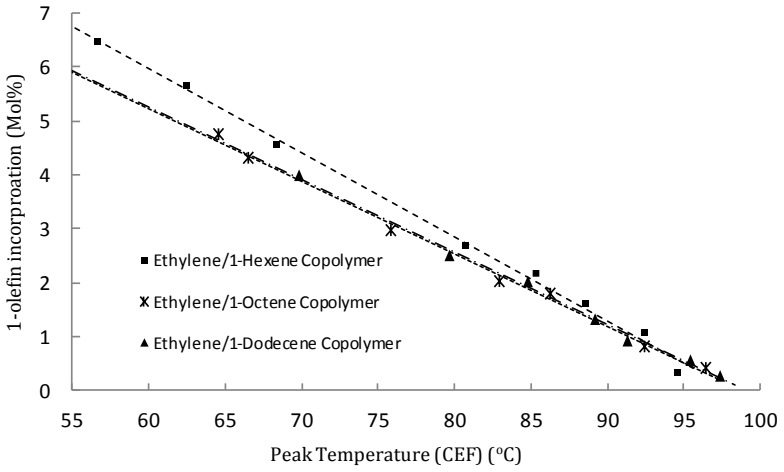

Figure 2-13. CEF calibration curves for ethylene/1-olefin copolymers.[51]

A microstructural model, such as Stockmayer bivariate distribution and Monte Carlo simulation was applied to obtain a more detailed picture of the polyethylene microstructures and compared the information provided by TREF and CRYSTAF.[52–55] Soares *et al*.[31] used Stockmayer bivariate distribution to model the ideal fractionation of polyolefins by TREF. Also, Soares *et al*.[36,55] used this modeling to fit the CRYSTAF-measured CCDs of several ethylene/1-octene copolymer samples made with a single site catalyst. They noticed that although a good agreement was obtained between CRYSTAF-measured profiles and predicted Stockmayer distribution, CRYSTAF curves tended to be skewed to lower crystallization temperatures. CRYSTAF profiles were broader than the theoretical prediction by Stockmayer distribution due to peak instrumental broadening.

Beigzadeh *et al*.[52–54] proposed the first Monte Carlo model for simulating the fractionation process in CRYSTAF and the profiles by calculating the average longest ethylene sequence (LES) of the polymer chain and plotting the distribution of longest ethylene sequence (LESD) for five ethylene/1-octene copolymer samples synthesized with a single-site catalyst. They proposed that the LES per chain governs the crystallization process in CRYSTAF and a good

agreement between experimental and simulation results were observed. However, Anantawaraskul *et al*.[30,41] used Monte Carlo simulation to propose that using the distribution of overall ethylene sequence (OESD), instead of LESD, represents a better modeling approach for CRYSTAF profile for a wider range of ethylene/1-octene copolymers.

2.3.2 High Performance Liquid Chromatography

High performance liquid chromatography (HPLC) is a fractionation technique used to characterize polymers according to their chemical composition. Because previous applications of HPLC were limited to temperatures up to about 80 °C, their applicability to polyolefin analysis was restricted.[56,57] In 2003, however, Macko *et al*.[56–60] separated isotactic polypropylene from linear polyethylene using ethylene glycol monobutylether (EGMBE) as eluent in an HPLC column packed with silica gel chemically modified with oligo(dimethylsiloxane) by the precipitation/re-dissolution mechanism. Because covalent bonds between the oligo(dimethylsiloxane) layer and silica gel are stable up to 380 °C, this packing can be used to fractionate polyolefins at high temperature.[61] Separation in this system is possible because EGMBE is a good solvent for isotactic polypropylene, but a non-solvent for polyethylene.[62] The recovery of polyethylene, however, decreased as its molecular weight increased. Therefore, the fraction of polyethylene with this method was limited by the solubility of polyethylene in the mobile phase, and suffered from poor resolution.[56–60]

Heinz *et al*.[61] used a gradient of TCB/EGMBE to fractionate polyethylene and polypropylene blends (Figure 2-14). TCB is a good solvent for both polyethylene and polypropylene, while EGMBE is a good solvent only for polypropylene. The polymer blend was first dissolved in a good solvent (1-decanol), and then injected into the mobile phase composed of 100% EGMBE. After a few minutes, polyethylene begins to precipitate onto the column (Silica gel-Nucleosil 500), while polypropylene elutes from the column (precipitation step). In the re-dissolution step, the volume fraction of TCB is increased gradually up to 100% to re-dissolve the precipitated polyethylene into the mobile phase. Ethylene/propylene copolymers were fractionated by composition using a TCB/EGMBE gradient in a HPLC column packed with

silica gel (Nucleosil 500) using the same method. The column outlet was connected to an evaporative light scattering detector (ELSD, model PL-ELS 1000).[63] As illustrated in Figure 2-15, propylene-rich chains are eluted at low TCB/EGMBE ratios and ethylene-rich fractions at high TCB/EGMBE ratios.[61,63]

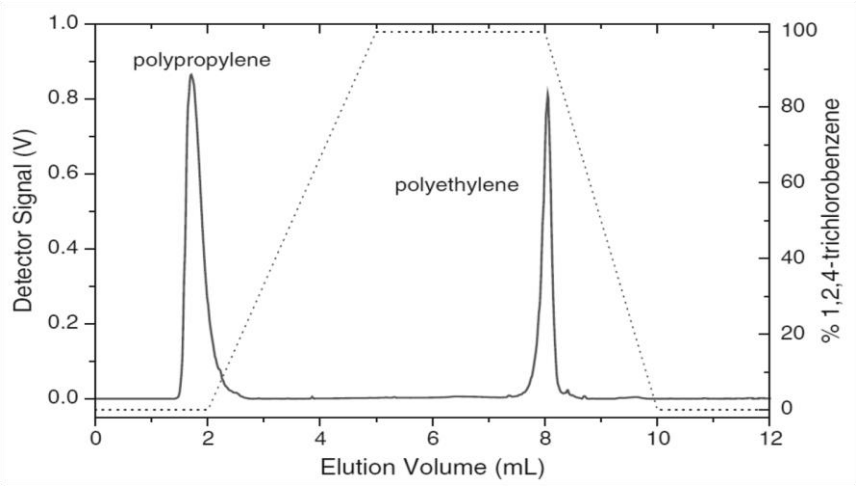

Figure 2-14. HT-HPLC profile for separation of a blend of polyethylene and polypropylene. (Column: Nucleosil 500, mobile phase: EGMBE-TCB, T: 140°C, detector: ELSD). The dotted line is the solvent gradient profile.[61]

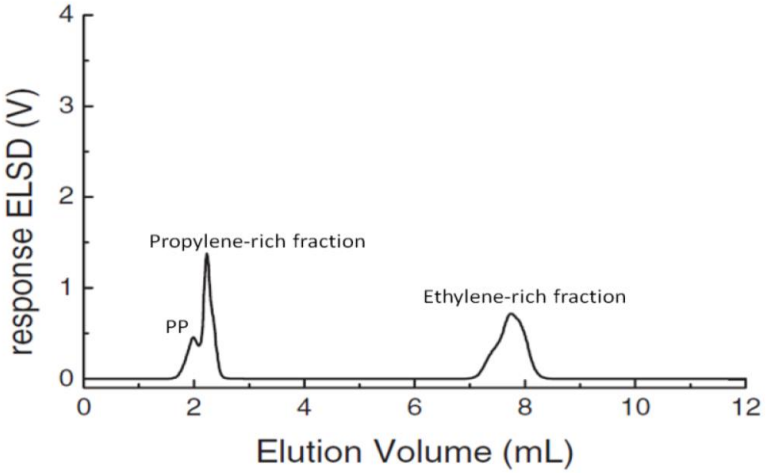

Figure 2-15. HT-HPLC profile for ethylene/propylene copolymers. (Column: Nucleosil 500, mobile phase: EGMBE-TCB, temperature: 140°C, detector: ELSD).[63]

Macko *et al*.[64] studied the adsorption of isotactic polypropylene in a chromatographic column filled with an Ultra Stable faujasite zeolite CBV-780. Isotactic polypropylene can fully or

partially adsorb onto the column packing, but the retained polymer could not be desorbed from the zeolite support.

Macko and Pasch[65–70] used a Hypercarb porous graphitic carbon (PGC) column instead of zeolites to fractionate polyolefins. The use of PGC supports was the key to fractionate polyolefin based on the adsorption-desorption mechanism. They demonstrated that polyethylene, atactic polypropylene, and syndiotactic polypropylene were fully adsorbed onto PGC columns at 160 °C as shown in Figure 2-16. The sample was first dissolved in 1-decanol and injected to the column at the same temperature. The retained polymers were desorbed and eluted from the column using a solvent gradient (from 100% 1-decanol to 100% TCB). This technique is called high-temperature solvent gradient interaction chromatography (HT-SGIC) and has become very successful for polyolefin fractionation since then.

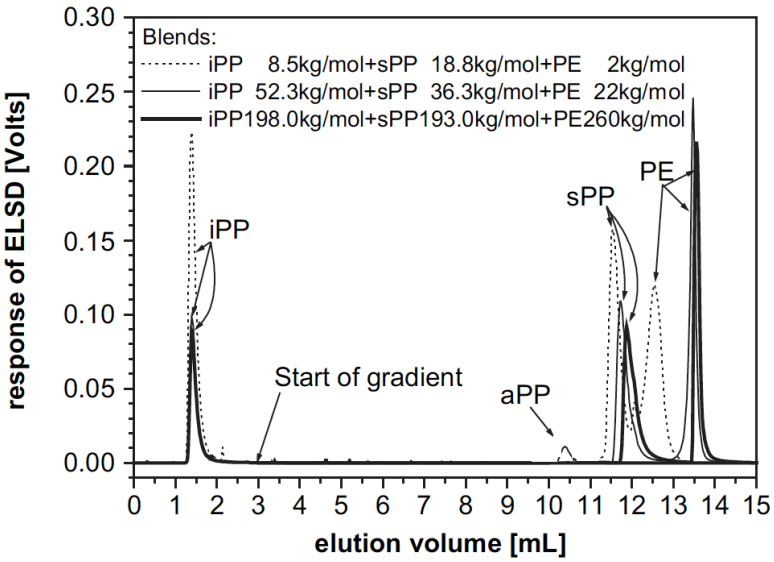

Figure 2-16. HT-SGIC profile of blends of isotactic polypropylene (iPP), atactic polypropylene (aPP), syndiotactic polypropylene (sPP) and linear polyethylene (PE). (Column: Hypercarb, Solvent gradient: from 100% 1-decanol to 100% TCB, T: 160 °C)[66]

Macko *et al.*[66–68] used the same adsorption/desorption-based HPLC technique (HT-SGIC) with 1-decanol/TCB/Hypercarb column system to fractionate ethylene/1-olefin copolymers with a large variety of comonomer units, ethylene/4-methyl-1-pentene copolymers, and

ethylene/norbornene copolymers. They found that only the samples copolymerized with 4-methyl-1-pentene were partially adsorbed from 1-decanol on the PGC column (Figure 2-17), but all other samples were fully desorbed after TCB was added into the mobile phase. The elution volumes of copolymers decreased with the increase of the concentration of the branching in these samples except for the samples copolymerized with cyclic comonomer (norbornene). They demonstrated that the presence of short chain branches (SCBs) in the polyethylene chain shortens the length of continuous methylene sequences and thus decreases the probability of orientation of the macromolecule in a flat conformation on the graphite surface. Also, they indicated that there is, in general, a linear correlation between the elution volumes and the average chemical composition of ethylene/1-olefin copolymers.

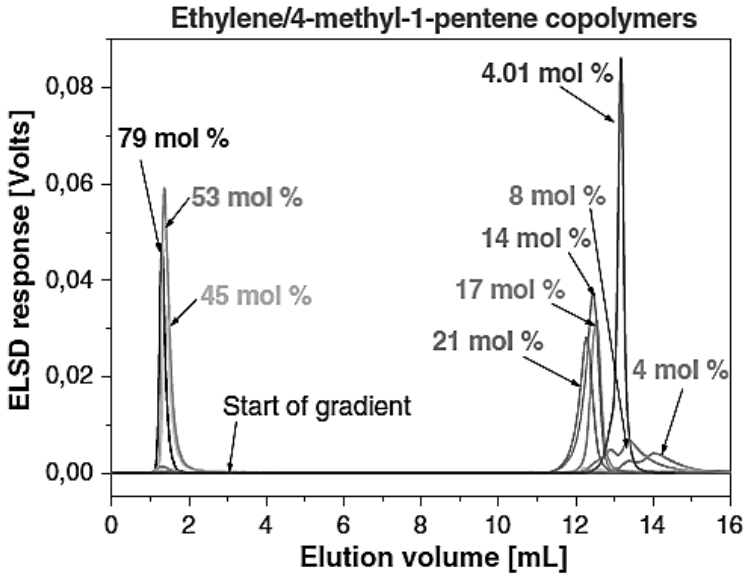

Figure 2-17. HT-SGIC profile of ethylene/4-methyl-1-pentene copolymers. (Column: Hypercarb, Solvent gradient: from 100% 1-decanol to 100% TCB, T: 160 °C)[67]

Macko *et al*.[67,68] studied the influence of the molecular weight on the fractionation of isotactic polypropylene and on the separation of polyethylene using HT-SGIC as shown in Figure 2-18. They demonstrated that molecular weight did not significantly affect the peak position of the elution volume of isotactic polypropylene samples since the elution takes place before the start of the solvent gradient. The elution volumes of ethylene/1-olefin copolymers with weight

average molecular weight greater than 15-20 kg/mol were not affected by their molecular weight.

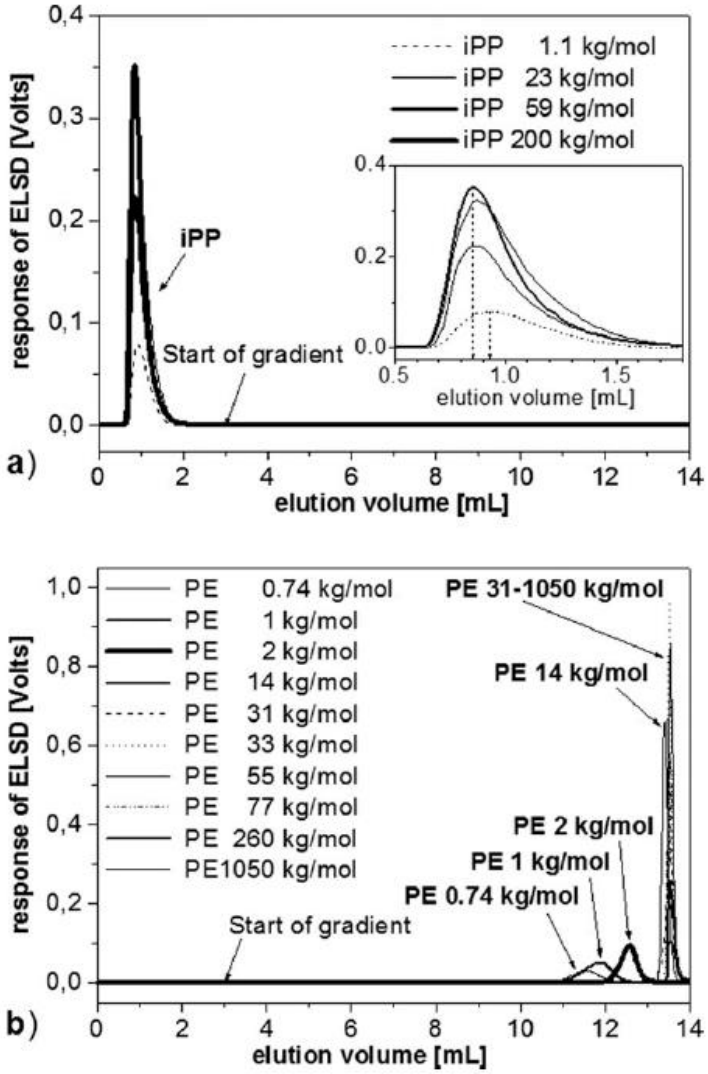

Figure 2-18. HT-SGIC profiles of isotactic polypropylene (iPP) with distinct M_w (a) and linear polyethylene (PE) with distinct M_w (b). (Column: Hypercarb, Solvent gradient: from 100% 1-decanol to 100% TCB, T: 160 °C).[68]

Chitta *et al*.[65,71] used three different types of the column (Hypercarb, Zirchrom-CARB, and activated carbon-TA95) and different solvent (mainly 1-decanol, 2-ethyl-1-hexanol and TCB) to study the influence of carbon packing on the fractionation of linear polyethylene and polypropylene with different tacticities using HT-SGIC with different solvent/sorbent system.

They found that fractionation of polyethylene and polypropylene could be achieved in different sorbent/solvent systems. Polyethylene can be fractionated using all tested sorbent/solvent systems. However, polypropylene samples could not be separated according to their tacticity when 2-ethyl-1-hexanol/TCB/ ZirChrom-CARB system was used.

High temperature two-dimensional liquid chromatography (HT 2D-LC), as shown in Figure 2-19, is a powerful technique to investigate the microstructure of polyolefins. In this technique, polymers are first fractionated by HT-SGIC (first dimension); then, each HT-SGIC fraction is analyzed by HT-GPC (second dimension), providing a comprehensive picture of the joint MWD×CCD of the semi and non-crystalline polyolefin.

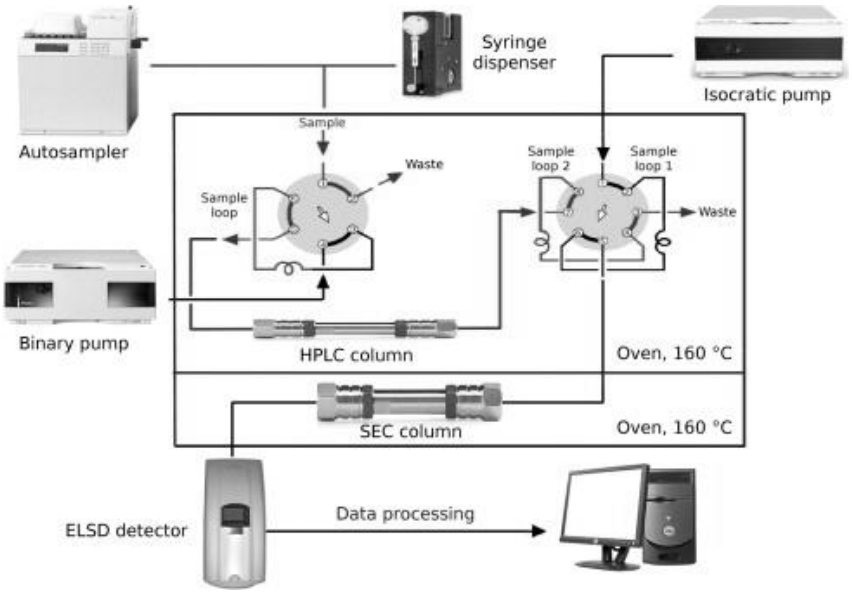

Figure 2-19. Schematic for HT 2D-LC.[72]

Ginsburg *et al.*[72–74] were able to fractionate a blend of linear polyethylene and polypropylenes with different tacticities, and a blend of ethylene-vinyl acetate (EVA) copolymers with different comonomer contents including amorphous samples using HT 2D-LC. They applied a new approach to determine the void and dwell volume of the developed HT 2D-LC instrument by calibrating both dimensions, HPLC and GPC. They showed, for the first time,

that the elution of isotactic polypropylene in the gradient HPLC depends on molecular weight. Roy *et al.*[75] used the same HT 2D-LC system to study the influence of different catalyst types (Ziegler-Natta and metallocene) on the microstructure of ethylene/1-octene copolymers. They showed that polyolefins made with different catalysts had different molecular weights, compositions, and number of resolved populations in their respective HT 2D-LC chromatograms as a function of catalyst type.

The poor detector response due to the dilution in the second dimension (GPC) is a common issue in HT 2D-LC. This problem cannot be solved by using higher sample concentrations or increasing the sample loops because of increasing viscosities and shifting in elution volume due to concentration effects. Mekap *et al.*[76] enhanced the detector response in HT 2D-LD using multiple injections of a sample and then starting the desorption step in the first dimension to avoid these issues without changing the elution volume or overloading of the stationary phase on the column.

Interestingly, adsorption/desorption-based HPLC techniques can be used to fractionate amorphous polyolefins with 1-olefin contents up to 100%, since they do not depend on polymer crystallization as TREF, CRYSTAF, and CEF.[77–79] Unfortunately, because solvent composition varies during solvent gradient HPLC analysis, most common detectors cannot be used with this technique. For instance, infrared detectors that are commonly used with other polyolefin analytical techniques are not easily applicable to solvent gradient HPLC because of the variation in the solvent composition reduces detector sensitivity. Instead, an evaporative light scattering detector (ELSD) is often used, which creates a problem for the quantification of this analysis, since the detector signal is non-linear with respect to concentration and solvent composition.[77] This limitation can be eliminated with the use of high-temperature thermal gradient interaction chromatography, which is discussed in the next section.

2.3.3 Thermal Gradient Interaction Chromatography (HT-TGIC)

HT-TGIC was invented by Dow Chemical to fractionate polyolefins based on the adsorption/desorption mechanism.[77] HT-TGIC overcomes the challenges encountered in the solvent gradient HPLC methods. In HT-TGIC, a PGC column is also used as a stationary phase; however, instead of relying on a solvent gradient, a temperature gradient is used to promote the fractionation in an isocratic solvent such as ODCB or TCB. Therefore, all commercially available detectors used with other polyolefin characterization techniques can be used. Also, as for HT-SGIC, HT-TGIC is free of co-crystallization effects that usually reduce the resolution of crystallization-based techniques. However, HT-TGIC profiles might be affected by co-adsorption/co-desorption phenomena, reducing the CCD resolution. Co-adsorption/co-desorption causes peak broadening when polymer chain fractions of different comonomer contents adsorb or desorb together.[77–79]

In a typical HT-TGIC experiment, the sample is dissolved in a solvent and injected into a PGC column at high temperature. Then, two temperature cycles are imposed: a cooling cycle for adsorption of the polymer chains and a heating cycle for desorption of retained polymer chains. During the cooling cycle, the column temperature is continuously decreased with or without solvent flow. While the column temperature is reduced gradually, the polymer chain fraction with the lowest comonomer content is adsorbed first at the highest temperature, while the other fractions remain in the solvent phase until their adsorption temperatures are reached. In the heating cycle, the retained polymer chains are desorbed and eluted in the solvent at increasing temperatures.

Cong *et al.*[77] used HT-TGIC to fractionate a series of ethylene/1-octene copolymers (Figure 2-20) and found that the peak temperatures of HT-TGIC chromatograms depended linearly on the 1-octene content (up to 50 mol %), as illustrated in Figure 2-21. Monrabal *et al.*[80] reported that the HT-TGIC elution peak positions did not depend on polymer molar mass, provided it was higher than 25 kg/mol, as illustrated in Figure **2-22**. HT-TGIC was also combined with TREF and CEF to analyze a blend of ethylene/1-octene copolymers (0.3% and 1.3% of 1-

octene) by adding a TREF or CEF column to the exit of the HT-TGIC column. This cross-fractionation approach observed significant improvements in resolution.[80]

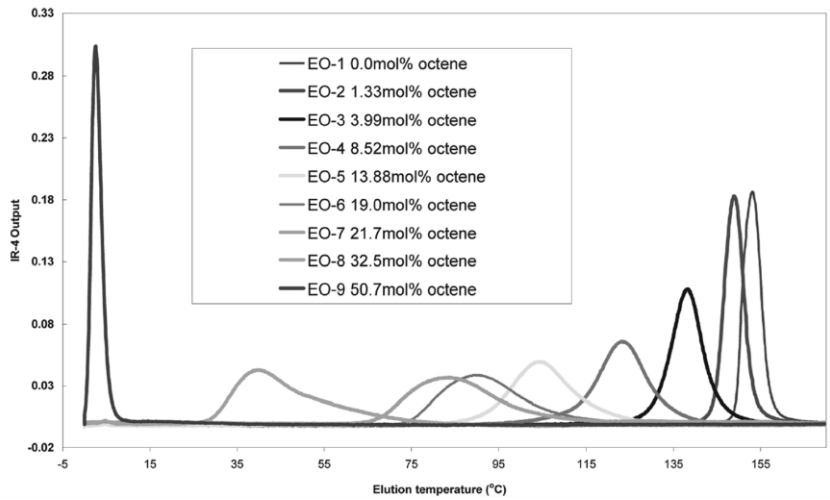

Figure 2-20. HT-TGIC profile of ethylene/1-octene copolymers. (Column: Hypercarb®, Temperature gradient range: (175 – 0) °C, Solvent: ODCB).[77]

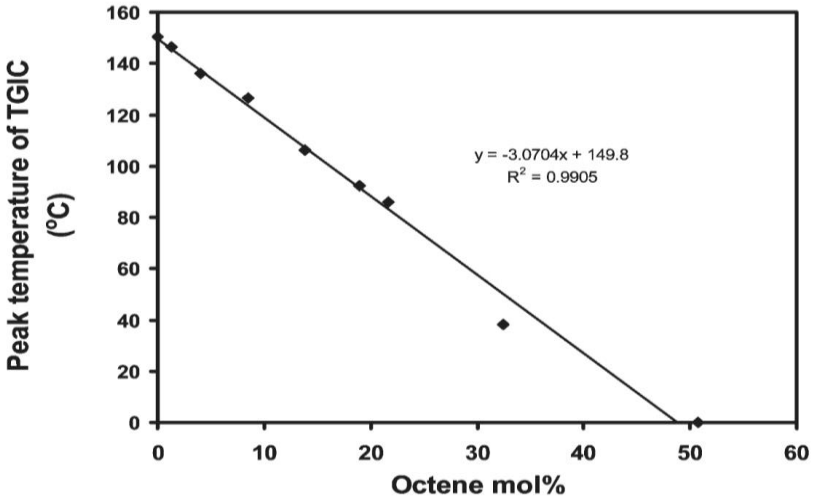

Figure 2-21. HT-TGIC calibration curve for ethylene/1-octene copolymers.[77]

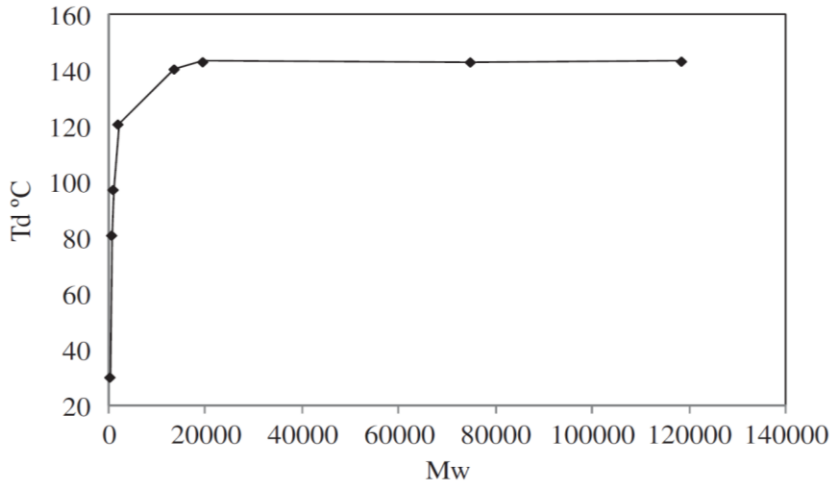

Figure 2-22. Effect of molar mass on the elution peak of HT-TGIC for polyethylene.[80]

Alghyamah *et al.*[39,81,82] studied various factors that might influence HT-TGIC profiles. A set of ethylene/1-octene copolymers with comonomer molar fractions up to 3.5% was used to investigate the effect of cooling and heating cycle parameters, sample volume solvent type (o-dichlorobenzene, ODCB; 1,2,4-trichlorobenzene, TCB; and chloronaphthalene, CN), and sample volume on individual resins. Figure 2-23, Figure 2-24, and Figure 2-25 show that cooling rate and cooling flow rate have little influence on HT-TGIC profiles of both individual resins and their blend.

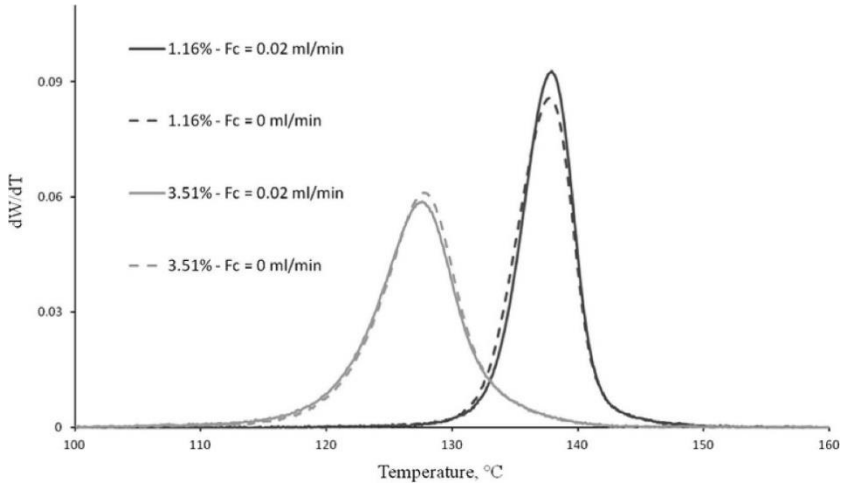

Figure 2-23. Effect of cooling flow rate on HT-TGIC profile for the ethylene/1-octene copolymer. (Column: Hypercarb®, Temperature gradient: (155 –90) °C, Solvent: ODCB).[82]

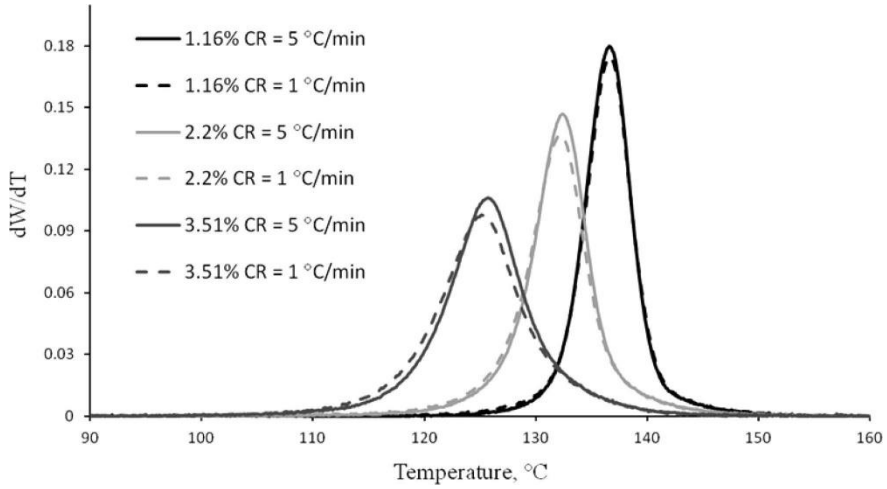

Figure 2-24. Effect of cooling rate on HT-TGIC profile for the ethylene/1-octene copolymer. (Column: Hypercarb®, Temperature gradient: (155 –90) °C, Solvent: ODCB).[82]

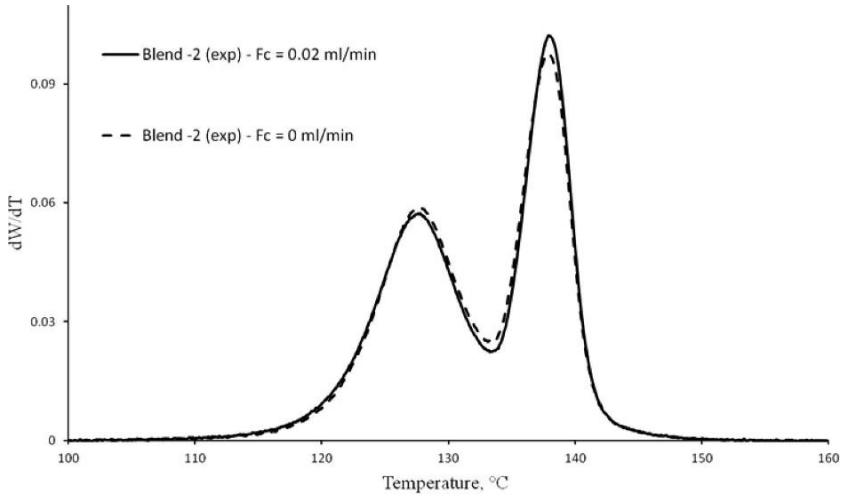

Figure 2-25. Effect of cooling flow rate on HT-TGIC profile of Blend-2 (50% of 3.51 % and 50% of 1.16 mol % of 1-octene). (Column: Hypercarb®, Temperature gradient: (155 –90) °C, Solvent: ODCB).[82]

On the other hand, the heating rate has a major influence on HT-TGIC profiles. Figure 2-26 shows that fast heating rates broaden and shift the HT-TGIC profiles to higher peak temperatures. Figure 2-27 indicate that using a slow heating rate increases peak resolution slightly, perhaps by minimizing co-desorption effects.[81]

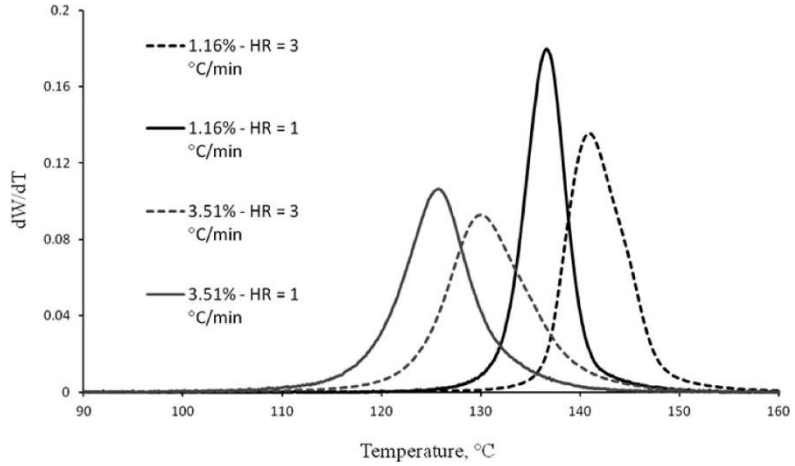

Figure 2-26. Effect of heating rate on HT-TGIC profile for the ethylene/1-octene copolymer. (Column: Hypercarb®, Temperature gradient: (155 –90) °C, Solvent: ODCB).[82]

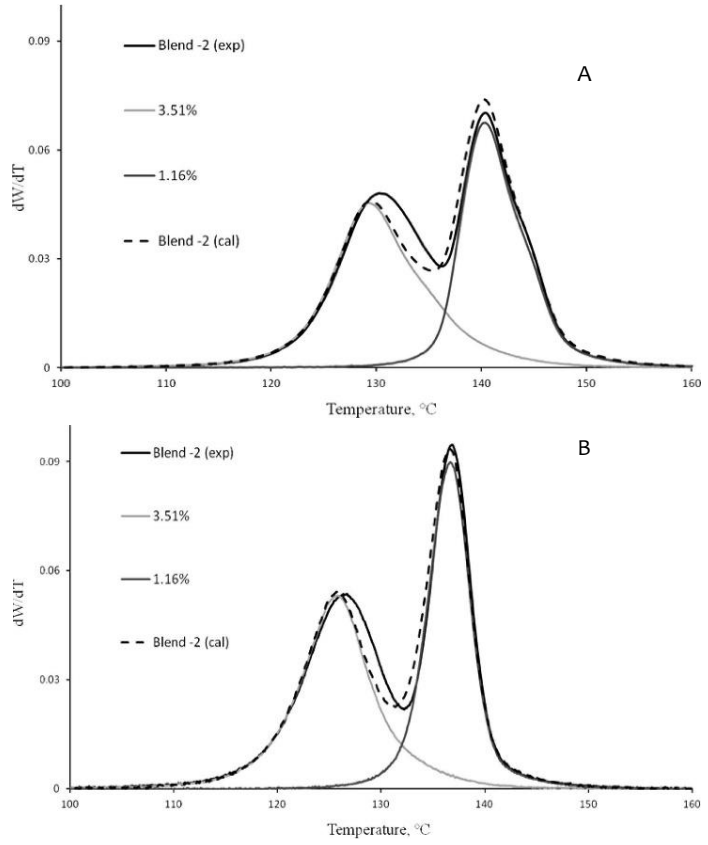

Figure 2-27. Comparison between experimental and calculated profiles of Blend-2 (50% of 3.51 % and 50% of 1.16 mol % of 1-octene) using heating rates of 3 °C/min (A) and 1 °C/min (B). (Column: Hypercarb®, Temperature gradient: (155 –90) °C, Solvent: ODCB).[82]

The elution peak temperatures of individual resins using ODCB are significantly higher than those measured with TCB and CN, as illustrated in Figure 2-28. ODCD was a better solvent for the separation of the blend samples than the two other solvents investigated by Alghyamah.[81] In addition, ODCB minimized co-adsorption effects. Small sample volumes (less than 100 μL) also seems to reduce co-adsorption.[81,82] Mekap *et al*.[83,84] used a series of ethylene/1-octene copolymers to evaluate binary solvent mixtures containing alkanes and aliphatic alcohols as components of the mobile phase using an ELSD in HT-TGIC. They showed that 40/60 (v/v) 1-decanol/TCB and 30/70 (v/v) 1-decanol/TCB were optimized binary solvent mixtures that enhanced the resolution of HT-TGIC fractionation of individual samples and blends of ethylene/1-octene copolymers.

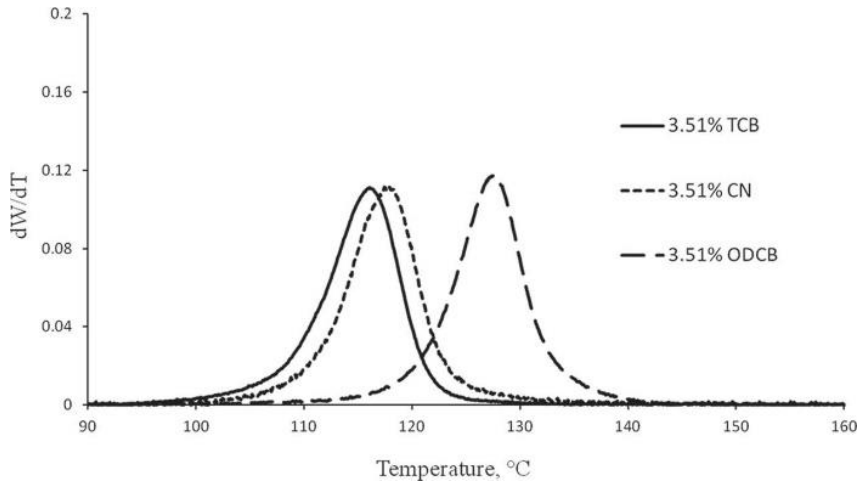

Figure 2-28. Effect of solvent type on HT-TGIC profile for the ethylene/1-octene copolymer, containing 3.51% octene. (Column: Hypercarb®, Temperature gradient: (155 –90) °C, Solvent: ODCB, CN, and TCB).[81]

Inwong *et al*.[85,86] developed a mathematical model for HT-TGIC fractionation based on population balances assuming a non-equilibrium, multi-stage adsorption-desorption mechanism. Their model fitted well experimental results of individual ethylene/1-octene samples and their binary blends measured under several operating conditions.

Monrabal *et al.*[87] compared different types of packing supports, including molybdenum sulfide (MoS_2), boron nitride (BN), and tungsten sulfide (WS_2), with equivalent graphitized carbon packing for the HT-TGIC analysis of polyolefins. Despite having different chemical structures, these supports could all be considered to be flat at the atomic level (atomic level flat surfaces - ALFS). They proposed that HT-TGIC profiles obtained with the MoS_2 column were broader due to a significantly higher Eddy diffusion, as the particle shape and size of MoS_2 material used were less uniform than Hypercarb columns, as shown in Figure 2-29. They demonstrated that regardless of the type of packing, the desorption temperature depended linearly on the comonomer mole fraction in the copolymer.

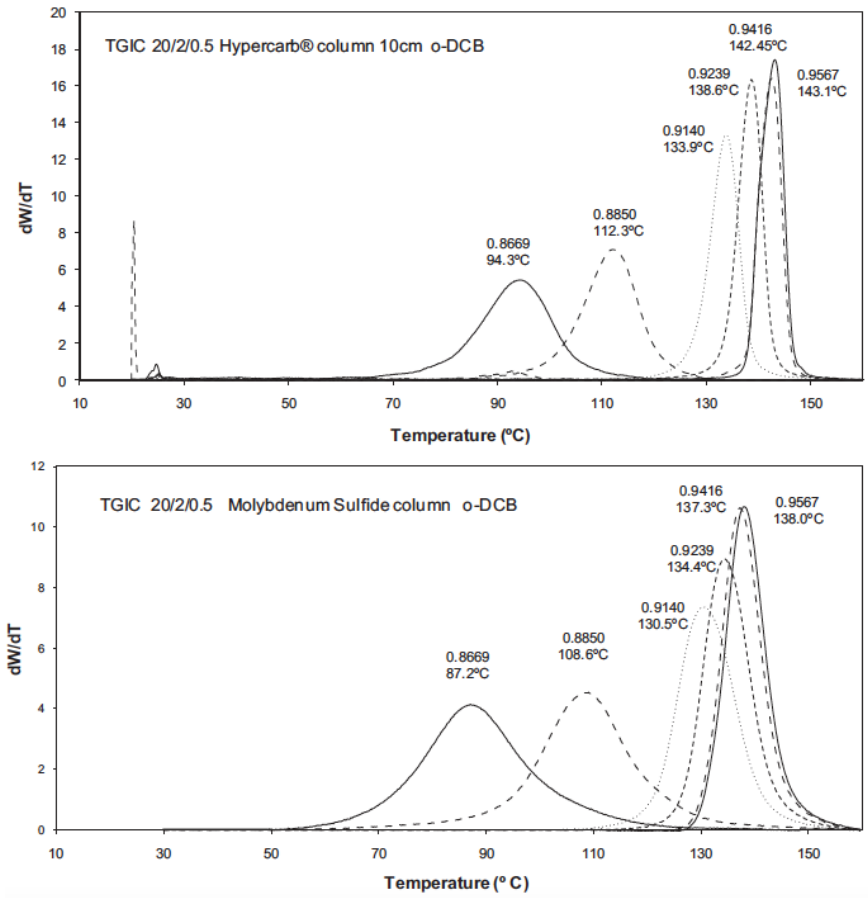

Figure 2-29. TH-TGIC profiles of ethylene/1-octene copolymer samples using Hypercarb column (above) and molybdenum sulfide column (bottom).[87]

Based on these findings, Monrabal *et al.*[87,88] proposed that the adsorption strength of ethylene/1-olefin copolymers on ALFS supports was related to the available contact surface area of the copolymer chain and the support surface, which depends on the short chain branching frequency of the copolymer, as displayed in Figure 2-30. A sample chain with no or few short chain branches has longer ethylene (or methylene) sequences, resulting in a larger contact surface area and stronger interactions with the support. Such a sample adsorbs on (or desorbs from) the surface at higher temperatures than a sample having many SCBs (shorter ethylene sequences).

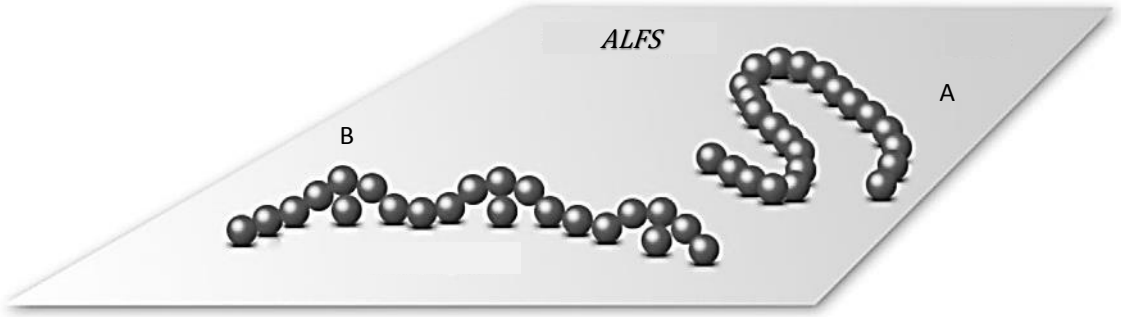

Figure 2-30. Adsorption of polyethylene schematic on the atomic level flat surface (ALFS): A) no SCB, longer ethylene sequences, and B) with SCB, shorter ethylene sequences.[88]

Chapter 3. Polyethylene Synthesis and Analysis

3.1 Polyethylene Synthesis

Two main categories of homogeneous ethylene/1-octene copolymers were synthesized in a stainless steel autoclave reactor operated in semi-batch mode. Category I comprised a series of ethylene/1-octene copolymers having a similar number average molecular weights (M_n) but different average 1-octene fractions to study the effect of operating parameters and column type on HT-TGIC chromatograms. Category II comprised six series of ethylene/1-octene copolymers; polymers in each series had similar 1-octene content (0-13 mol%) but different M_n to study the joint effect of molecular weight and 1-octene content on HT-TGIC fractionation. Figure 3-1 summarizes the M_n and 1-octene mol % for all samples.

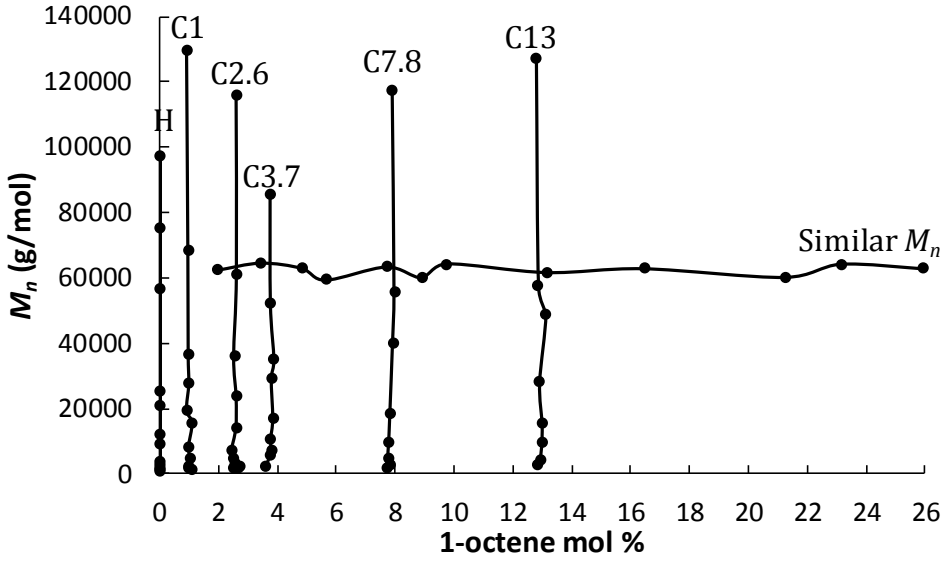

Figure 3-1. Ethylene/1-octene copolymers investigated in this research: Category I includes samples with similar M_n and different 1-octene content; Category II comprises samples with similar 1-octene content and different M_n. (H = homopolymer, C = copolymer, number beside C corresponds to the mole fraction of 1-octene in the copolymer).

3.1.1 Materials

All materials used in the polymerizations are listed in Table 3-1. Toluene was distilled over butyl lithium and metallic sodium to remove polar impurities and residual moisture. Ethylene and nitrogen were flown through molecular sieves and CuO/Al_2O_3 beds to remove oxygen and water traces. A continuous flow of nitrogen was bubbled through the comonomer for 6 hours before storage to displace any absorbed volatile contaminants. Methylaluminoxane (MAO) was used as received from either Sigma-Aldrich or Albemarle. Constrained geometry catalyst (CGC) was prepared at a concentration of 0.05 μmol/g in toluene.

For the copolymers in Category I, the polymerizations were done with 2.0-3.0 g (0.1-0.15 μmol) of the diluted catalyst and 2 g (1.33 mmol) of MAO, resulting in an Al/CGC ratio of about 20,000. For Category II, polymerizations were done with 1.0-16.0 g (0.05-0.8 μmol) of the diluted catalyst and 2 g (1.33 mmol) of MAO. Hydrogen was used as chain transfer agent to decrease polymer molecular weight of the copolymers in Category II.

Table 3-1. Materials used to synthesize ethylene/1-octene copolymers.

Material	Formula	Supplier	Grade
Ethylene	$CH_2=CH_2$	PRAXAIR	Polymer (5.0 PL-G)
1-Octene	$CH_2=CH(CH_2)_5\ CH_3$	SIGMA-ALDRICH	98%
Nitrogen	N_2	PRAXAIR	5.0 UHP
Hydrogen	H_2	PRAXAIR	5.0 UHP
Toluene	$C_6H_5\text{-}CH_3$	SIGMA-ALDRICH	HPLC, 99.9%
Methylaluminoxane (MAO)	$C_3H_9Al_3O_3X_2$	SIGMA-ALDRICH Albemarle	10 wt% in Toluene
Constrained Geometry Catalyst	CGC*	STREM-CHEMICALS	

*CGC: Methyl(6-t-butoxyhexyl)sily(η^5-tetramethylcyclopentadienyl)(*t*-butylamido)titanium dichloride.

3.1.2 Polymerization Reactors

The polyethylenes and ethylene/1-octene copolymers were made in two autoclave reactors operated in semi-batch mode: A) 600 mL Parr autoclave reactor equipped with a heating/cooling jacket, and B) 300 mL Parr autoclave reactor equipped with a cooling coil and a heating mantle. Figure 3-2 and Figure 3-3 show the system diagram of both polymerization reactors, and Table 3-2 identifies the symbols used in these figures.

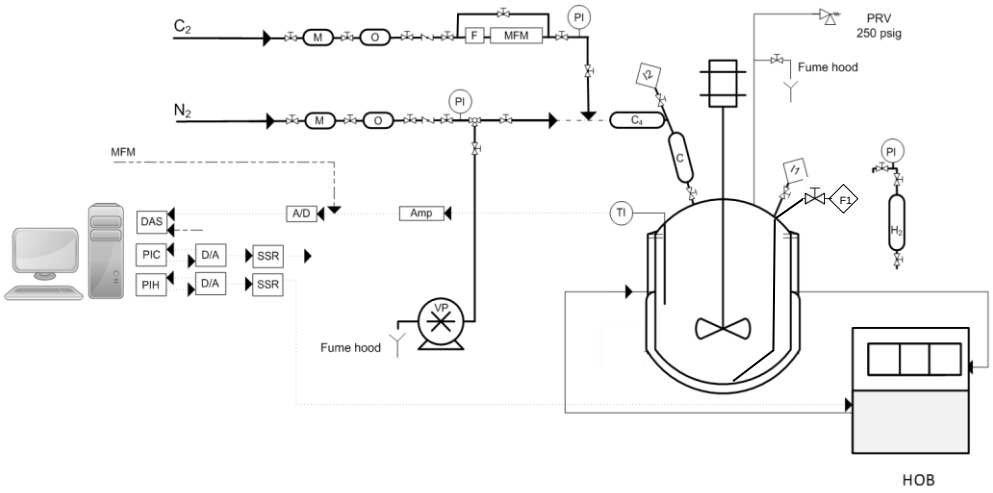

Figure 3-2. Reactor A: 600 mL autoclave polymerization reactor.

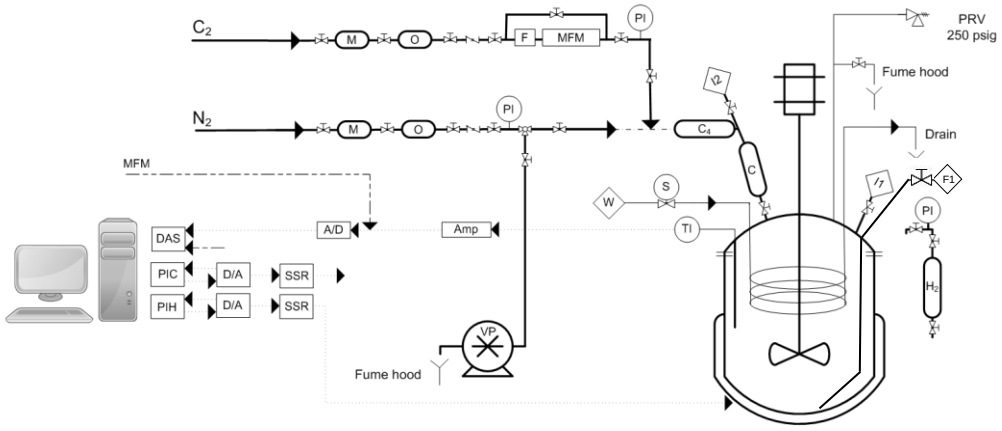

Figure 3-3. Reactor B: 300 mL autoclave polymerization reactor.

Table 3-2. Definitions of symbols in Figure 3-1 and 3-2.

Symbol	Identification	Symbol	Identification
C_2	Ethylene supply from manifold	PI	Pressure gauge
N_2	Nitrogen supply from manifold	TI	J-type thermocouple
C_4	1-butene bomb	Amp	Signal amplifier
C	Catalyst bomb	A/D	Analog to digital conversion board
H_2	Hydrogen bomb	D/A	Digital to analog conversion board
M	Molecular sieves-de moisturizing	DAS	Data acquisition system
O	Deoxygenation bed (CuO on alumina)	PIC	Proportional-Integral loop for cooling
F	7 μm inlet filter	PIH	Proportional-Integral loop for heating
MFM	Mass flow meter	SSR	Solid state relay
I1	Injection port 1	PRV	Pressure release valve
I2	Injection port 2	VP	Vacuum pump
F1	Flashing port 1	Drain	Open drain for spent cooling water
S	Solenoid valve	Fume	Vent to fume hood
W	Cold water supply	HOB	Heating oil bath

3.1.3 Polymerization Procedure

After the reactor had been assembled, its temperature was raised up to 125 ^{o}C. The reactor and the injection ports were purged with five alternating cycles of nitrogen flow (10 psi) and vacuum, and finally cooled down to 70 ^{o}C under a nitrogen atmosphere. The injection points were also purged for 3 minutes with nitrogen using a narrow cannula.

After cooling down the reactor, distilled toluene (200 mL in Reactor A and 150 mL in Reactor B) was used to transfer the required amounts of 1-octene and MAO into the reactor through injection port 2 using a cannula. 1-Octene, MAO and CGC solution were weighted in the glove

box in 20 mL vials individually, and sealed with Teflon-lined rubber septa. If hydrogen was required, an external bomb was filled with hydrogen to the required pressure, and then ethylene flow was used to transfer it to the reactor through injection port 2. Once the reactor temperature was increased to the polymerization temperature, toluene in the reactor was saturated with ethylene up to the required polymerization pressure under a stirring rate of 1500 rpm. CGC solution in a Teflon-lined sample cylinder (20 mL) was transferred via injection port 1 using an ethylene differential pressure of 20 psi to start the polymerization.

Once the polymerization started, a small exotherm was observed for about one minute, after which the temperature became approximately constant. After about 15 to 20 minutes of polymerization, the ethylene flow to the reactor was interrupted by closing the reactor feed (injection port 2) and the polymerization terminated. Then, injection port 1 was open to pressurize the reactor with nitrogen, and transfer the polymer solution from the reactor to a beaker filled with 300 mL of ethanol. After reducing the reactor temperature, toluene (200 mL or 150 mL) was transferred to the reactor via injection port 2, and the temperature was increased up to 120 ^{o}C. The reactor was kept at this temperature for 10 minutes under a stirring rate of 1500 rpm to dissolve the remaining of the polymer in the reactor. Finally, the purge toluene/polymer solution was flushed from the reactor under nitrogen pressure.

The polymer product, transferred to a beaker, was stirred for approximately six hours with a few drops of hydrogen chloride (to deactivate the catalyst). The product was filtered, and the resulting polymer was dried overnight in a vacuum oven.

3.1.4 Copolymerization Conditions

Copolymerization conditions are shown in Table 3-3 for all ethylene/1-octene copolymers in Category I (similar M_n). The copolymers were made in Reactor A. The two main factors changed during the polymerizations were temperature and 1-octene concentration to synthesize samples having similar number average molecular weight, but different 1-octene mole fractions (Appendix A). Samples in Category I were labeled according to the following

convention: the first letter identifies the monomer (E = ethylene), the second letter represents the comonomer (O = 1-octene), and the number indicates the mole percent of comonomer in the copolymer.

Table 3-3. Copolymerization conditions for copolymers in Category I.

Sample ID	Catalyst (CGC) μmol	Ethylene (psig)	1-Octene reactor concentration (mol/mL)	Temperature (°C)	Yield (g)
E/O-1.9	0.1	100	0.11	120	6.5
E/O-3.4	0.1	120	0.21	147.5	4.8
E/O-4.8	0.1	120	0.28	142	4.3
E/O-5.6	0.1	120	0.36	137	5.4
E/O-7.7	0.1	120	0.48	131	5.5
E/O-8.9	0.1	120	0.62	124	8.3
E/O-9.8	0.1	120	0.76	122	7.3
E/O-13.2	0.1	120	0.89	119	8.3
E/O-16.4	0.1	120	1.11	111	10.6
E/O-21.3	0.1	120	1.41	105	13.5
E/O-23.2	0.1	120	1.58	106.1	9.7
E/O-25.9	0.1	120	1.82	102.8	15.6

Reactor B was used to make the copolymers in Category II. Ethylene/1-octene ratio and copolymerization temperature were the same in each set of experiments. The major parameter changed during the copolymerization experiments was the amount of hydrogen added to the reactor. Figure 3-4 shows that the reciprocal of the number average chain length (τ=1/r_n) decreased linearly with the amount of hydrogen used in the polymerization, as theoretically expected. Since hydrogen reduces catalytic activity when ethylene/1-octene are copolymerized with CGC, we increased the catalyst concentration in the reactor to compensate for the drop in catalyst activity. Tables 3-4 to 3-9 summarize all polymerization conditions for the homopolymers and copolymers of Category II. The samples in these tables are labeled according to the following convention: H = homopolymerization, C = copolymerization, the

number following C is the mol% of 1-octene in the copolymer, and the number after the dash is the M_n of the sample in kg/mol.

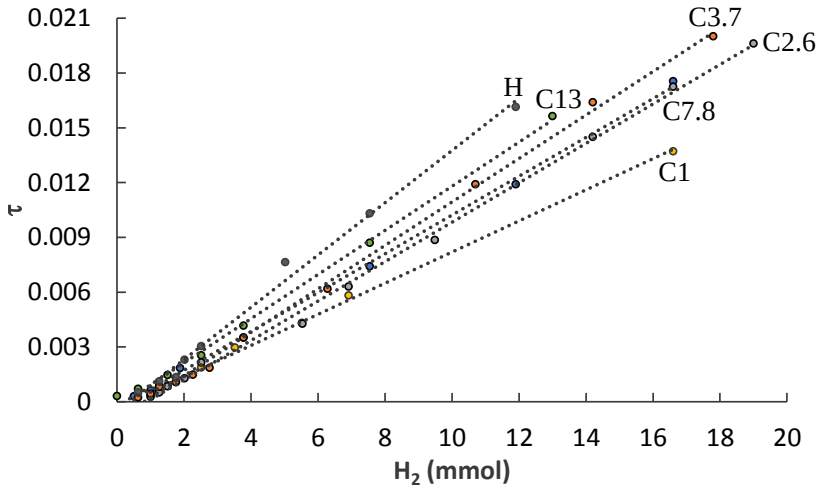

Figure 3-4. Linear relation between the hydrogen amount (mmol) added to the reactor and the reciprocal of the number average chain length ($\tau = 1/r_n$). H = homopolymers; C = ethylene/1-octene copolymers. Numbers indicate the mol% of 1-octene incorporated in the copolymer.

Table 3-4. Ethylene homopolymerization conditions (Category II).

Sample ID	Catalyst (CGC) μmol	Ethylene (psig)	Temperature (°C)	Hydrogen (mmol)	Yield (g)
H-1.0	0.60	90	120	15.32	1.01
H-1.2	0.40	85	120	13.11	1.02
H-1.7	0.30	120	120	11.91	1.52
H-2.7	0.25	120	120	7.54	1.05
H-3.6	0.25	120	120	5.02	1.18
H-9.2	0.20	120	120	2.51	2.61
H-12.2	0.15	120	120	2.01	2.76
H-21.0	0.10	120	120	1.76	2.13
H-25.3	0.10	120	120	1.26	2.48
H-56.6	0.10	120	120	0.63	3.08
H-75.0	0.20	80	120	0	4.31
H-97.0	0.20	90	120	0	4.78

Table 3-5. Polymerization conditions for ethylene/1-octene copolymers with 1.0 mol % of 1-octene (Category II).

Sample ID	Catalyst (CGC) μmol	Ethylene (psig)	1-Octene reactor concentration (mol/mL)	Temperature (°C)	Hydrogen (mmol)	Yield (g)
C1-1.4	0.65	150	0.061	110	17.8	2.41
C1-1.7	0.55	150	0.061	110	14.2	2.01
C1-2.4	0.45	150	0.061	110	10.7	3.91
C1-4.6	0.35	150	0.061	110	6.28	3.05
C1-8.2	0.35	150	0.061	110	3.77	3.52
C1-15.6	0.25	150	0.061	110	2.76	1.81
C1-19.5	0.25	150	0.061	110	2.26	3.91
C1-27.1	0.20	150	0.061	110	1.76	5.51
C1-36.3	0.20	150	0.061	110	1.26	5.81
C1-68.1	0.15	150	0.061	110	1.00	4.61
C1-129.4	0.15	150	0.061	110	0.628	6.01

Table 3-6. Polymerization conditions for ethylene/1-octene copolymers with 2.6 mol % of 1-octene (Category II).

Sample ID	Catalyst (CGC) μmol	Ethylene (psig)	1-Octene reactor concentration (mol/mL)	Temperature (°C)	Hydrogen (mmol)	Yield (g)
C2.6-1.5	0.80	160	0.178	110	19.0	1.28
C2.6-1.7	0.75	160	0.178	110	16.6	2.51
C2.6-2.0	0.65	160	0.178	110	14.2	3.22
C2.6-3.4	0.55	160	0.178	110	9.49	3.15
C2.6-4.8	0.50	160	0.178	110	6.91	3.43
C2.6-7.0	0.50	160	0.178	110	5.53	4.82
C2.6-14.1	0.30	160	0.178	110	2.51	2.41
C2.6-23.6	0.20	160	0.178	110	2.01	1.92
C2.6-36.0	0.15	160	0.178	110	1.51	1.43
C2.6-61.1	0.10	160	0.178	110	1.26	2.02
C2.6-115.7	0.10	160	0.178	110	1.00	1.75

Table 3-7. Polymerization conditions for ethylene/1-octene copolymers with 3.7 mol % of 1-octene (Category II).

Sample ID	Catalyst (CGC) μmol	Ethylene (psig)	1-Octene reactor concentration (mol/mL)	Temperature (°C)	Hydrogen (mmol)	Yield (g)
C3.7-2.3	0.50	170	0.296	105	16.6	2.76
C3.7-5.4	0.45	170	0.296	105	6.91	3.11
C3.7-7.2	0.40	170	0.296	105	5.52	4.85
C3.7-10.6	0.35	170	0.296	105	3.52	4.51
C3.7-16.8	0.25	170	0.296	105	2.51	2.81
C3.7-29.2	0.20	170	0.296	105	1.76	3.21
C3.7-34.8	0.20	170	0.296	105	1.51	3.51
C3.7-52.2	0.15	170	0.296	105	1.26	3.01
C3.7-85.2	0.15	170	0.296	105	1.00	3.18

Table 3-8. Polymerization conditions for ethylene/1-octene copolymers with 7.8 mol % of 1-octene (Category II).

Sample ID	Catalyst (CGC) μmol	Ethylene (psig)	1-Octene reactor concentration (mol/mL)	Temperature (°C)	Hydrogen (mmol)	Yield (g)
C7.8-1.9	0.75	130	0.475	95	16.6	3.92
C7.8-2.9	0.65	130	0.475	95	11.9	3.52
C7.8-4.6	0.65	130	0.475	95	7.54	5.81
C7.8-9.7	0.50	130	0.475	95	3.77	6.54
C7.8-18.5	0.35	130	0.475	95	1.88	4.11
C7.8-40.1	0.30	130	0.475	95	1.26	5.61
C7.8-55.7	0.25	130	0.475	95	1.00	5.69
C7.8-117.0	0.20	130	0.475	95	0.51	1.53

Table 3-9. Polymerization conditions for ethylene/1-octene copolymers with 12.9 mol % of 1-octene (Category II).

Sample ID	Catalyst (CGC) μmol	Ethylene (psig)	1-Octene reactor concentration (mol/mL)	Temperature (°C)	Hydrogen (mmol)	Yield (g)
C13-2.5	0.80	120	0.831	90	13.1	1.31
C13-4.5	0.75	120	0.831	90	7.54	3.52
C13-9.4	0.70	120	0.831	90	3.77	3.85
C13-15.4	0.60	120	0.831	90	2.51	4.52
C13-28.0	0.45	120	0.831	90	1.51	2.82
C13-48.8	0.40	120	0.831	90	1.26	8.16
C13-57.3	0.25	120	0.831	90	0.63	3.58
C13-127.0	0.25	120	0.831	90	0.00	4.05

3.2 Polyethylene Microstructural Analysis

Gel permeation chromatography (GPC) was used to determine the MWDs of all samples, and carbon-13 nuclear magnetic resonance (^{13}C NMR) was used to measure the average 1-octene content in the copolymers in Category I. This data was used to generate a calibration curve for Fourier Transform Infrared Spectroscopy (FTIR), which was subsequently used to estimate the molar fraction of 1-octene for the copolymers in Category II. Peak elution temperatures and CCDs of the samples were measured using HT-TGIC.

3.2.1 HT-GPC Analysis

High-temperature gel permeation chromatography is a powerful technique used to determine the molecular weight distribution (MWDs) for polyolefins. HT-GPC (Polymer Char, Valencia, Spain) was used to measure MWD for each copolymer samples in Category I and Category II using three linear columns (PLgel Olexis, 13 μm gel particles, and 300 mm × 7.5 mm) at 145 °C. Narrow-MWD polystyrene standards used to calibrate the columns. A volume of 200 μL polymer solution was injected into the columns at a flow rate of 1.0 mL/min of TCB. The HT-GPC chromatographer was equipped with an infrared detector, used as a mass detector to

determine the concentrations of polymer and a viscometer to measure the intrinsic viscosity on line. MWDs of all samples were determined using the universal calibration curve and Polymer Char software package following standard procedures.

The molecular weight averages and polydispersity for all homo- and copolymers in Categories I and II are presented in Table 3-10 to 3-16. The samples have polydispersities close to 2.0, which is theoretically expected for polymers made with single-site metallocenes. However, samples with very low M_n had polydispersities lower than 2.0, likely because the peaks for the very low M_n polymers partially superimposed with the solvent peak, making it difficult clearly to define the baseline and the lower molecular weight integration limit.

Table 3-10. Properties of ethylene/1-octene copolymers in Category I (similar M_n).

Sample ID	HT-GPC		NMR		FTIR
	M_n (g/mol)	PDI	1-octene mol%	SCB/1000C	$A_{CH3}/Area_{CH2}$
E/O-1.9	62 200	2.45	1.93	9.1	0.217
E/O-3.4	64 300	2.50	3.43	15.6	0.401
E/O-4.8	62 800	2.46	4.83	21.1	0.495
E/O-5.6	56 400	2.38	5.64	24.1	0.531
E/O-7.7	63 200	2.26	7.71	31.3	0.664
E/O-8.9	60 100	2.28	8.91	34.4	0.751
E/O-9.8	67 100	2.34	9.75	37.7	0.805
E/O-13.2	61 600	2.42	13.15	45.1	0.983
E/O-16.4	62 700	2.32	16.45	54.8	1.148
E/O-21.3	60 200	2.29	21.25	60.9	-
E/O-23.2	64 000	2.48	23.15	64.1	-
E/O-25.9	62 700	2.43	25.92	68.1	-

Table 3-11. Properties of ethylene homopolymer (Category II).

Sample ID	HT-GPC	
	M_n (g/mol)	PDI
H-1.0	970	1.79
H-1.2	1 200	1.82
H-1.7	1 700	2.33
H-2.7	2 700	2.09
H-3.6	3 600	2.24
H-9.2	9 200	2.01
H-12.2	12 200	2.01
H-21.0	21 000	2.16
H-25.3	25 300	2.13
H-56.6	56 600	2.11
H-75.0	75 000	2.23
H-97.0	97 000	2.12

Table 3-12. Properties of ethylene/1-octene copolymers with 1.0 mol % of 1-octene (Category II).

Sample ID	HT-GPC		FTIR			
	M_n (g/mol)	PDI	$A_{CH3}/Area_{CH2}$	SCB/1000C	*wt%*	*mol%*
C1-1.4	1 400	1.79	0.159	5.1	4.11	1.06
C1-1.7	1 700	1.82	0.152	4.7	3.83	0.98
C1-2.4	2 400	2.33	0.151	4.7	3.79	0.97
C1-4.6	4 600	2.09	0.157	5.0	4.03	1.04
C1-8.2	8 200	2.24	0.153	4.8	3.87	0.99
C1-15.6	15 600	2.01	0.163	5.3	4.27	1.10
C1-19.5	19 500	2.01	0.147	4.5	3.63	0.93
C1-27.1	27 800	2.16	0.154	4.9	3.91	1.00
C1-36.3	36 300	2.13	0.152	4.8	3.83	0.98
C1-68.1	68 100	2.23	0.151	4.7	3.79	0.97
C1-129.4	129400	2.12	0.147	4.5	3.63	0.93

Table 3-13. Properties of ethylene/1-octene copolymers with 2.6 mol % of 1-octene (Category II).

Sample ID	HT-GPC		FTIR			
	M_n (g/mol)	PDI	$A_{CH3}/Area_{CH2}$	SCB/1000C	*wt%*	*mol%*
C2.6-1.5	1 500	1.66	0.287	11.5	9.22	2.47
C2.6-1.7	1 700	1.78	0.305	12.4	9.94	2.68
C2.6-2.0	2 000	1.79	0.306	12.5	9.98	2.69
C2.6-3.4	3 400	2.01	0.296	12.0	9.58	2.57
C2.6-4.8	4 800	1.97	0.290	11.7	9.34	2.50
C2.6-7.0	7 000	2.18	0.285	11.4	9.14	2.45
C2.6-14.1	14 100	2.06	0.298	12.1	9.66	2.60
C2.6-23.6	23 600	2.15	0.299	12.1	9.70	2.61
C2.6-36.0	36 000	2.24	0.292	11.8	9.42	2.53
C2.6-61.1	61 100	2.22	0.300	12.2	9.74	2.62
C2.6-115.7	115 700	2.23	0.299	12.1	9.70	2.61

Table 3-14. Properties of ethylene/1-octene copolymers with 3.7 mol % of 1-octene (Category II).

Sample ID	HT-GPC		FTIR			
	M_n (g/mol)	PDI	$A_{CH3}/Area_{CH2}$	SCB/1000C	*wt%*	*mol%*
C3.7-2.3	2 300	1.88	0.383	16.3	13.05	3.61
C3.7-5.4	5 400	2.06	0.394	16.8	13.49	3.74
C3.7-7.2	7 200	2.04	0.397	17.0	13.61	3.78
C3.7-10.6	10 600	2.07	0.396	16.9	13.57	3.77
C3.7-16.8	16 800	1.97	0.402	17.2	13.81	3.84
C3.7-29.2	29 200	2.12	0.398	17.0	13.65	3.79
C3.7-34.8	34 800	2.23	0.405	17.4	13.93	3.88
C3.7-52.1	52 200	2.11	0.395	16.9	13.53	3.76
C3.7-85.2	85 200	2.11	0.386	16.4	13.17	3.65

Table 3-15. Properties of ethylene/1-octene copolymers with 7.8 mol % of 1-octene (Category II).

Sample ID	HT-GPC		FTIR			
	M_n (g/mol)	PDI	$A_{CH3}/Area_{CH2}$	SCB/1000C	*wt%*	*mol%*
C7.8-1.9	1 900	1.54	0.683	31.2	25.02	7.69
C7.8-2.9	2 900	1.83	0.692	31.7	25.38	7.82
C7.8-4.6	4 600	2.01	0.687	31.4	25.18	7.75
C7.8-9.7	9 700	2.13	0.689	31.5	25.26	7.78
C7.8-18.5	18 500	2.12	0.692	31.7	25.38	7.82
C7.8-40.1	40 100	2.1	0.698	32.0	25.62	7.91
C7.8-55.7	55 700	2.15	0.701	32.1	25.74	7.96
C7.8-117.0	117 000	2.09	0.697	31.9	25.58	7.90

Table 3-16. Properties of ethylene/1-octene copolymers with 12.9 mol % of 1-octene (Category II).

Sample ID	HT-GPC		FTIR			
	M_n (g/mol)	PDI	$A_{CH3}/Area_{CH2}$	SCB/1000C	*wt%*	*mol%*
C13-2.5	2 500	1.51	0.986	46.3	37.11	12.83
C13-4.4	4 400	1.99	0.990	46.5	37.27	12.91
C13-9.4	9 400	1.93	0.993	46.7	37.39	12.97
C13-15.4	15 400	1.92	0.994	46.7	37.43	12.98
C13-28.0	28 000	2.19	0.989	46.5	37.23	12.89
C13-48.8	48 800	2.1	1.001	47.1	37.71	13.12
C13-57.3	57 300	2.17	0.987	46.4	37.15	12.85
C13-127.0	127 000	2.06	0.983	46.2	36.99	12.77

3.2.2 ^{13}C-NMR Analysis

^{13}C NMR is a powerful analytical approach to quantify chain end structures, short chain branching, and the sequence of comonomer units in the ethylene/1-olefin copolymer chains without using a calibration curve. A Bruker 500 MHz high-resolution ^{13}C NMR spectrometer

was used to measure the mole fraction of 1-octene in the copolymers displayed in Table 3-10 (Category I). A mass of 100 mg of each sample was dissolved in 1,1,2,2-terachloroethane (TCE) in a 10 mL NMR tube and homogenized by heating the tube in a heating block at 120 ^{o}C for about 10 hours before the test. Typical operation conditions were: pulse angle 90^{o}, 4000 scannings per sample, the acquisition time of about 6 seconds, the spin-lattice relaxation time of 10 seconds, and the spectrometer reference frequency of 125 MHz. The operation temperature for the ^{13}C NMR analysis was 120 ^{o}C.

The mole fractions of 1-octene in the samples of Category I were defined according to ASTM-D5017-96.[89,90] All peaks in the ^{13}C NMR spectra, such as the one shown in Figure **3-5** for an ethylene/1-octene copolymer, were integrated. An accurate full-scale integral is recorded from 10 to 45 ppm (the isolated methylene resonance is assigned to 30.0 ppm). Table 3-17 indicates the integration limits for a spectrum of ethylene/1-octene copolymer sample.

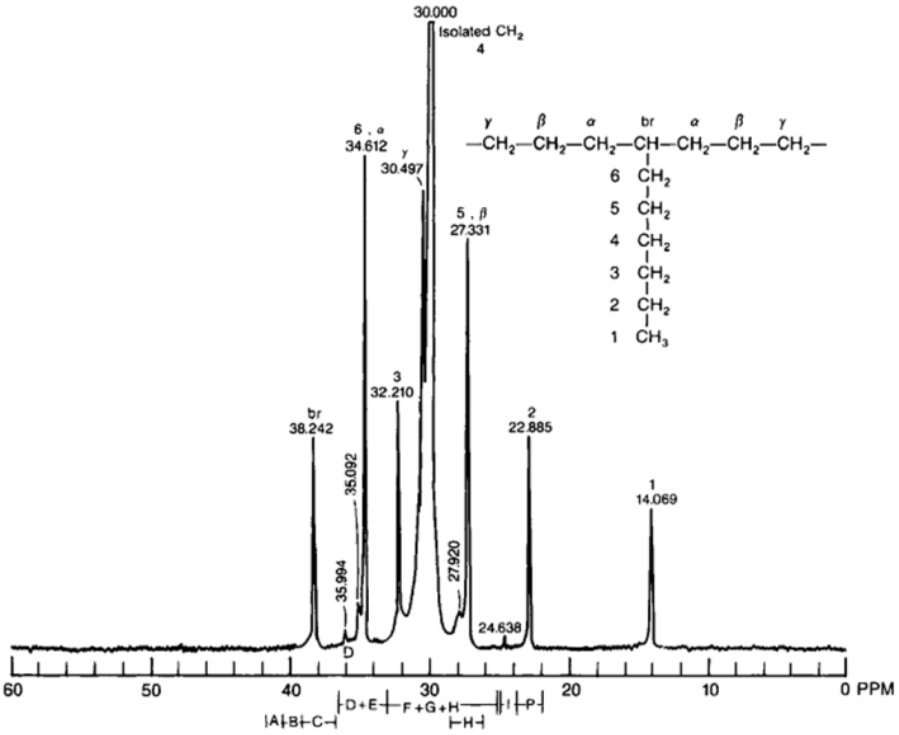

Figure 3-5. ^{13}C-NMR spectrum of an ethylene/1-octene copolymer.[89]

Table 3-17. Integration limits for ^{13}C NMR spectrum of ethylene/1-octene copolymer

Area	Region (ppm)
A	41.5 to 40.5
B	40.5 to 39.5
C	39.5 to 37.0
D	Peak at 35.8
D+E	36.8 to 33.2
F+G+H	33.2 to 25.5
H	28.5 to 26.5
I	25.0 to 24.0
P	24.0 to 22.0

After integrating the spectral regions, the mole fraction of 1-octene was estimated using the following equations:

$$O_1 = \frac{A + 2C + 2D}{2} \tag{3.1}$$

$$O_2 = \frac{1.5A + 2B + (C + D) - D}{3} \tag{3.2}$$

$$O' = \frac{O_1 + O_2}{2} \tag{3.3}$$

$$E' = \frac{(F + G + H) - (3A + 3B + H + P + I)}{2} + O' \tag{3.4}$$

$$F_o = \frac{O'}{O' + E'} \times 100 \tag{3.5}$$

where O_1 and O_2 are the carbon atoms located in *br* and α positions (Figure 3-5) in the backbone chain respectively, *E'* and *O'* are the mole average of ethylene and 1-octene in the copolymer respectively, and F_O is the percentage of 1-octene mole fraction.

In addition, Equation 3.6 was used to convert the mole fraction of 1-octene to the number of short chain branches per thousands of carbon atoms (SCB/1000 C).

$$SCB/1000\ C = \frac{1000 \times F_O}{2 \times (100 - F_O) + 8 \times F_O} \tag{3.6}$$

The ^{13}C NMR spectra of the ethylene/1-octene copolymers of Category I are shown in Appendix B. Table 3-18 and Table 3-19 showed the determinations of the molar fractions of these samples based on ASTM-D5017-96.[90]

Table 3-18. Integration limits of 13C NMR spectra of the samples of Category I

Area	Region ppm	E/O-1.9	E/O-3.4	E/O-4.8	E/O-5.6	E/O-7.7	E/O-8.9
A	41.5-40.5	0.000	0.000	0.000	0.000	0.000	0.000
B	40.5-39.5	0.000	0.000	0.000	0.000	0.000	0.000
C	39.5-37.0	1.000	1.000	1.000	1.000	0.930	1.000
D	Peak at 35.8	0.000	0.283	0.262	0.240	0.270	0.294
D+E	36.8-33.2	2.282	4.279	4.045	4.013	4.131	4.273
F+G+H	33.2-25.5	93.029	77.086	52.926	45.522	33.243	30.924
H	28.5-26.5	3.383	3.904	3.767	3.910	3.510	3.885
I	25.0-24.0	0.000	0.000	0.000	0.000	0.000	0.000
P	24.0-22.0	2.031	2.190	2.037	2.302	2.451	2.947
	O_1	1.000	1.283	1.262	1.240	1.200	1.294
	O_2	0.761	1.332	1.261	1.258	1.287	1.326
	O'	0.880	1.308	1.262	1.249	1.244	1.310
	E'	44.688	36.804	24.823	20.904	14.885	13.356
	Fo	1.93	3.43	4.84	5.64	7.71	8.91
	SCB/1000 C	9.1	15.3	20.7	23.5	30.4	34.1

Table 3-19. Integration limits of 13C NMR spectra of the samples of Category I

Area	Region ppm	E/O-9.8	E/O-13.2	E/O-16.4	E/O-21.3	E/O-23.2	E/O-25.9
A	41.5-40.5	0.000	0.000	0.171	1.000	1.000	1.000
B	40.5-39.5	0.000	0.000	0.257	1.068	0.877	0.647
C	39.5-37.0	1.000	1.000	1.000	3.699	2.899	2.134
D	Peak at 35.8	0.527	0.677	0.702	2.958	2.887	2.460
D+E	36.8-33.2	5.450	6.770	5.847	20.162	20.635	16.725
F+G+H	33.2-25.5	34.066	29.634	24.992	73.187	63.226	47.190
H	28.5-26.5	4.194	4.673	4.678	15.470	14.733	11.709
I	25.0-24.0	0.000	0.000	0.000	0.000	0.000	0.632
P	24.0-22.0	3.742	4.197	3.689	13.349	12.025	9.866
O_1		1.527	1.677	1.788	7.157	6.286	5.094
O_2		1.641	2.031	1.972	6.947	7.001	5.686
O'		1.584	1.854	1.880	7.052	6.643	5.390
E'		14.649	12.236	9.550	26.134	22.062	15.411
F_O		9.75	13.15	16.45	21.25	23.15	25.92
SCB/1000 C		36.4	45.1	52.2	60.9	63.9	67.9

3.2.3 FTIR Analysis

FTIR is a powerful tool to quantify the methyl group content that is proportional to the comonomer mole fraction in ethylene/1-olefin copolymers. Carry 600 Series FTIR Spectrometer (Agilent Technologies, USA) was used to measure the mole fraction of 1-octene in the copolymers of Category II. the FTIR spectrophotometer was calibrated with standards of known composition of the first category samples. The samples were prepared for FTIR spectroscopy by hot pressing about 1 g of copolymer. The thickness of each film was uniform and between 0.2 to 0.3 mm. Typically, 32 scans were used for spectral averaging, at a resolution of 4 cm^{-1} in the range between 400 cm^{-1} to 4000 cm^{-1}. Each spectrum was used to determine the ratio of the absorbance at 1378 cm^{-1} (A_{CH3}, representing methyl branches) and the area of the methylene combination band at 2019 cm^{-1} ($Area_{CH2}$), according to ASTM-D6645-1.[91]

The calibration curve shown in Figure 3-6 was created by plotting the ratio of the absorbance at 1378 cm^{-1} and the area of the methylene combination band at 2019 cm^{-1} (located in between 1980-2100 cm^{-1}) versus number of branches per 1000 carbons regulated by ^{13}C NMR spectroscopy for the samples in Category I. Once the standard calibration curve was established (Equation 3.7), the comonomer molar fraction in copolymer samples of Category II were calculated using Equation 3.9,

$$SCB/1000\,C = 49.336 \times \left(\frac{A_{CH_3}}{Area_{CH_2}}\right) - 2.415 \tag{3.7}$$

$$wt\% = 100 \times \left(\frac{N \times MW_O}{N \times MW_O + \frac{1000 - n \times N}{2} \times MW_E}\right) \tag{3.8}$$

$$mol\% = 100 \times \frac{\frac{wt\%}{MW_O}}{\frac{wt\%}{MW_O} + \frac{100 - wt\%}{MW_E}} \tag{3.9}$$

where *wt*% and *mol*% are the comonomer weight and mole percent, respectively, MW_E and MW_O are the molecular weight of ethylene and 1-octene respectively, *n* is the number of carbon atoms in the comonomer, and *N* is the number of short chain branches per 1000 carbons.

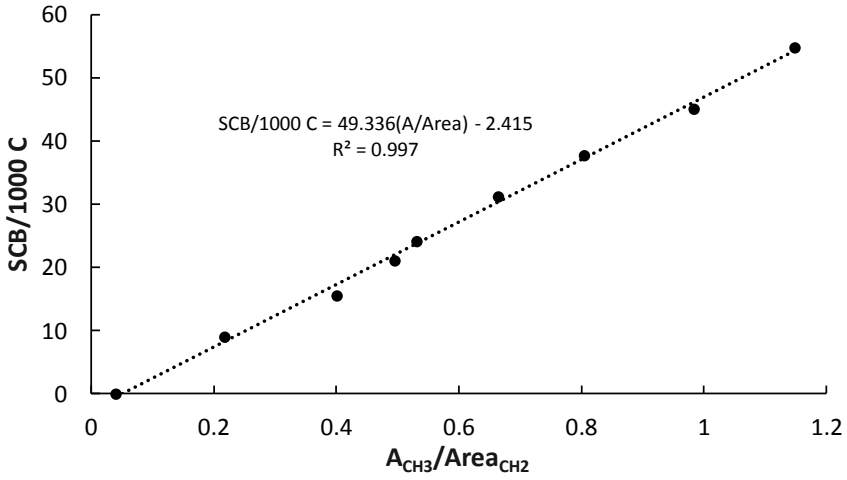

Figure 3-6. FTIR calibration curve

FTIR results of all ethylene/1-octene copolymer samples are shown in Table 3-10 to 3-16.

3.2.4 HT-TGIC Analysis

The polyethylene and ethylene/1-octene copolymers were analyzed by HT-TGIC to determine their CCDs. The HT-TGIC experiments were run with a Hypercarb column installed in a CEF oven (Polymer Char, Valencia, Spain). The instrument consists of four main parts: autosampler, adjustable temperature oven (main oven), top oven (where detectors are installed), and isocratic pump, as illustrated in Figure 3-7. The Hypercarb column was packed with porous graphitic carbon (PGC) received from Fisher Thermo Scientific.

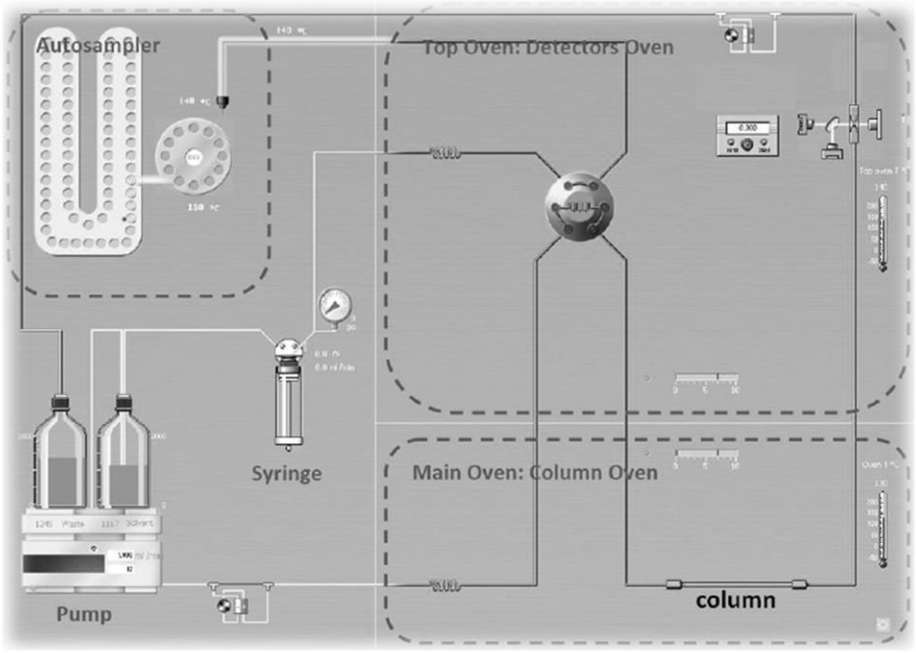

Figure 3-7. Schematic diagram of CEF instrument (Polymer Char, Valencia, Spain) used for the HT-TGIC experiments.

Four different Hypercarb columns were used in this research. They had the following common characteristics: 4.6 mm inside diameter, 120 m^2/g surface area, and 250 Å pore size. They differed in column length and average particle size, as shown in Table 3-20. O-dichlorobenzene (ODCB) and 1,2,4-trichlorobenzene (TCB) were used as a mobile phase for all HT-TGIC experiments. Antioxidant (Irganox 1010) was added to the solvents at a concentration of 0.2 g/L to prevent the thermal degradation of the copolymer samples during the analysis.

Table 3-20. Properties of Hypercarb columns.

	Column 1	**Column 2**	**Column 3**	**Column 4**
Column Length (mm)	100	100	100	250
Average Particle Size (μm)	5	3	7	5

The HT-TGIC analysis can be divided into five main steps: dissolution, injection, cooling cycle, heating cycle and cleaning. The sample was first dissolved in 8 mL of solvent inside 10-mL size vials. The dissolution was carried out at 160 ^{o}C in the instrument autosampler for one hour. The sample concentration was 1 mg/mL for both individual and blend samples. At the end of the dissolution period, a dispenser transferred the sample from the autosampler to the injection loop located in the top oven. The content of the loop (0.1 mL) was injected into the front of the PGC column using an isocratic pump at a temperature of 160 ^{o}C. The solution was kept for 10 minutes to stabilize its temperature (Ts = 160 ^{o}C). After the stabilization, the polymer sample was fractionated using two temperature cycles, as shown in Figure 3-8. In the cooling cycle, the column temperature was reduced to 35 ^{o}C gradually at a required cooling rate (CR = 3 or 5 $^{\circ}$C/min) to allow the polymer chains to adsorb onto the PGC column under a continuous solvent flow of F_C = 0.02 mL/min. The solvent flow rate is calculated from the cooling rate, column volume, and the difference between the first and the last temperatures in the cooling cycle. At the end of the cooling cycle, the column temperature was kept constant at 35 ^{o}C for 3 minutes. Then, the pump flow rate was increased to the elution flow rate and kept constant for 5 minutes to remove the polymer fraction that was not adsorbed onto the column at the final cooling temperature. After that, the column temperature was increased up to 160 ^{o}C at a pre-determined heating rate (HR=1 or 3 $^{\circ}$C/min) . As the temperature increased, the retained polymer fractions were desorbed and eluted using a continuous solvent flow (F_E= 0.1 or 0.5 mL/min) that allowed the fractions to move from the column to the infrared detector (IR4 detector, Polymer Char, Valencia, Spain). Finally, at the end of the heating cycle, the column was cleaned with fresh solvent at a high flow rate (F_{CL}=1 mL/min for 10 min) in order to be ready for the injection of the next sample.

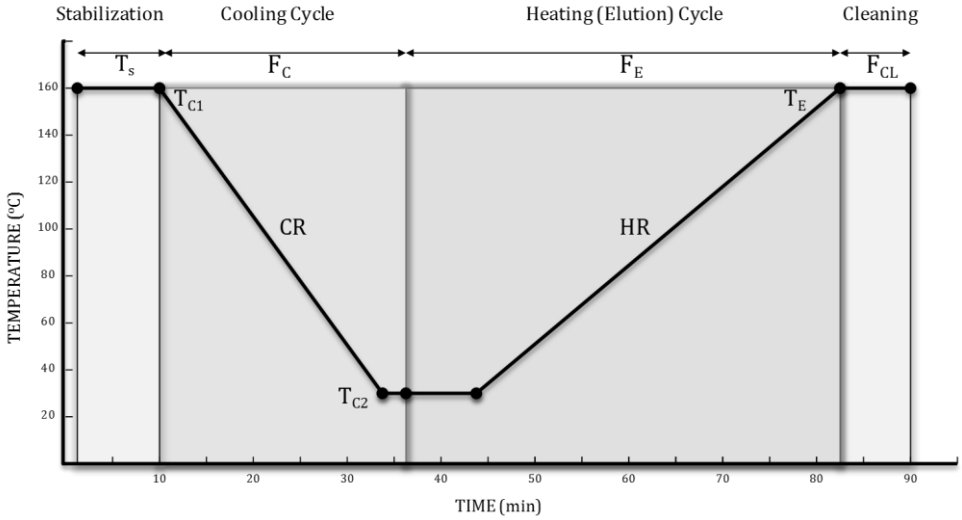

Figure 3-8. Schematic of HT-TGIC experimental setup. T_S is the stabilization temperature, T_{C1} and T_{C2} are the first and last temperatures in the cooling cycle, CR is the cooling rate, F_C is the solvent flow rate during the cooling cycle, HR is the heating rate, F_E is the solvent flow rate during the heating cycle, T_E is the last temperature in the heating cycle, and F_{CL} is solvent flow rate during the cleaning.

Chapter 4. Influence of Heating and Cooling Cycle Parameters on HT-TGIC Profiles [1]

4.1 Introduction

HT-TGIC fractionates polyolefins based on an adsorption/desorption mechanism that is influenced by several factors such as the analytical operation conditions. A set of homogenous ethylene/1-octene copolymers having different comonomer fractions (up to 25 mol% of 1-octene) and approximately the same molecular weight averages (Category I) were synthesized to investigate the separation mechanism of HT-TGIC. Their average chemical compositions were determined and then used to establish a calibration curve for HT-TGIC. Also, a 2^3 experimental factorial design was applied to three copolymer samples and their blends to study which operation parameters (cooling rate, heating rate, and elution flow rate) influence HT-TGIC peak shapes and positions to maximize the peak resolution and reduce the analysis time.

4.2 Polymer Synthesis

Section 3.1 in Chapter 3 explains the copolymerization procedures, copolymerization conditions, materials and 600 semi-batch autoclave reactor that were employed to synthesize the ethylene/1-octene copolymers of Category I used in this chapter.

4.3 Polymer Analysis

The characterization techniques used to analyze the copolymer samples of Category I were described in Section 3.2 in Chapter 3. HT-GPC determined the MWDs of all copolymer samples and ^{13}C NMR quantified the average 1-octene content in the copolymers. Peak elution temperatures and CCDs of the samples were measured using HT-TGIC with a Hypercarb

[1] The results discussed in this chapter have been published in (A. Z. Al-Khazaal, J. B. P. Soares, *Macromolecular Chemistry and Physics*, **2014**)[96]

column packed with porous graphite carbon (Column 1). The copolymer samples of Category I have very similar MWDs, as shown in Figure 4-1.

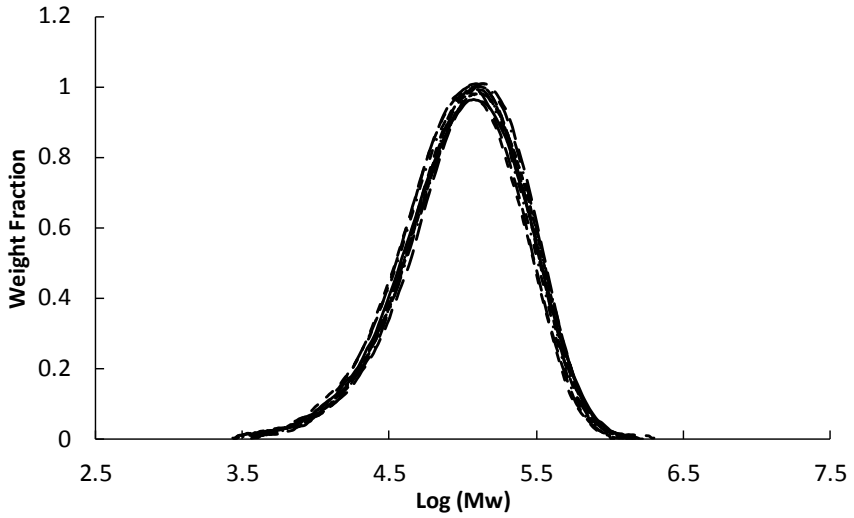

Figure 4-1. MWDs of ethylene/1-octene copolymers with different comonomer fractions.

4.4 Results and Discussion

4.4.1 Composition Characterization by HT-TGIC

The series of ethylene/1-octene copolymers of Category I was analyzed by HT-TGIC with Column 1. Table 4-1 shows the elution peak temperatures (T_p) for copolymers with different 1-octene mole fractions. The standard deviation of each chromatogram is also reported in Table 4-1 to quantify the broadness of HT-TGIC profiles. These values were calculated using Equations (4.1) to (4.3),

$$T_\mu = \int_{T_{E_1}}^{T_{E_2}} T \cdot f(T) \cdot dT \tag{4.1}$$

$$\sigma^2 = \int_{T_{E_1}}^{T_{E_2}} \left(T - T_\mu\right)^2 \cdot f(T) \cdot dT \tag{4.2}$$

$$\sigma = \sqrt{\sigma^2} \tag{4.3}$$

where, T_μ is the mean elution temperature in the interval T_{E1}-T_{E2} (35-160 °C), $f(T)$ is the normalized HT-TGIC profile, σ^2 is the variance, and σ is the standard deviation.

Table 4-1. HT-TGIC data for ethylene/1-octene copolymer samples of Category I

Sample ID	T_P (°C)	T_μ (°C)	σ	Weight fraction of non-adsorbed polymer
E/O-1.9	132.6	132.1	4.3	0.5
E/O-3.4	127.0	126.2	5.2	0.6
E/O-4.8	122.1	121.6	5.7	0.7
E/O-5.6	115.6	114.8	7.4	0.9
E/O-7.7	108.7	107.9	8.3	1.4
E/O-8.9	102.1	99.9	9.5	2.5
E/O-9.8	96.1	94.9	9.7	4.6
E/O-13.2	86.3	85.8	11.4	7.7
E/O-16.4	77.2	77.6	11.8	11.2
E/O-21.3	64.5	65.6	12.2	19.3
E/O-23.2	58.8	62.4	12.6	22.6
E/O-25.9	50.5	56.6	9.4	33.1

Figure 4-2 shows that the HT-TGIC profiles become broader as the 1-octene content increases (the standard deviation increases), except for the last samples with the highest 1-octene content. This apparent narrowing of the peaks is an artifact resulting from the fact that, as the 1-octene content increases, the fraction of polymer that is not adsorbed in the Hypercarb column also increases (Table 4-1). The fraction of polymer that is not adsorbed onto the column elutes as

sharp peak (purge peak) at the beginning of the analysis the purge peaks were omitted from Figure 4-2 since they do not add any additional information to the analyses.

The HT-TGIC chromatograms for the samples are narrow, as expected for copolymer samples made with a single-site catalyst. As the mole fraction of comonomer in the copolymer increases, the HT-TGIC profiles become broader and shift to lower temperatures. This behavior is expected since the presence of short chain branches (SCBs) in the polyethylene chains formed via comonomer incorporation decreases the length of the ethylene segments that are adsorbed onto the packing surface. Therefore, the incorporation of α-olefin hinders chain adsorption and reduces their desorption temperature. A relationship between the peak elution temperature and comonomer content is displayed in Figure 4-3.

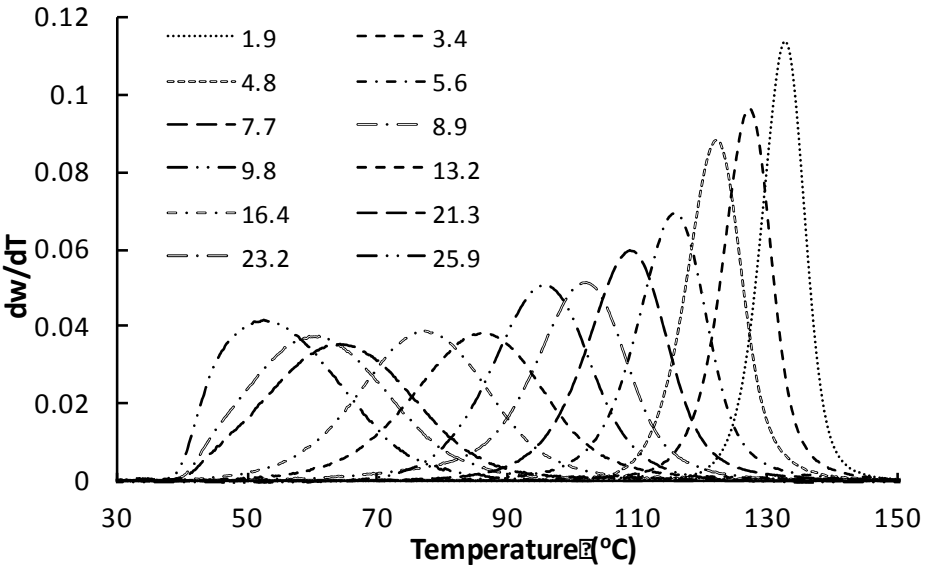

Figure 4-2. HT-TGIC profiles for ethylene/1-octence copolymers. (Operation conditions: F_C= 0.02 mL/min, CR= 5 °C/min, HR= 3 °C/min, F_E= 0.5 mL/min, temperature range in both cycles = 160-35 °C)

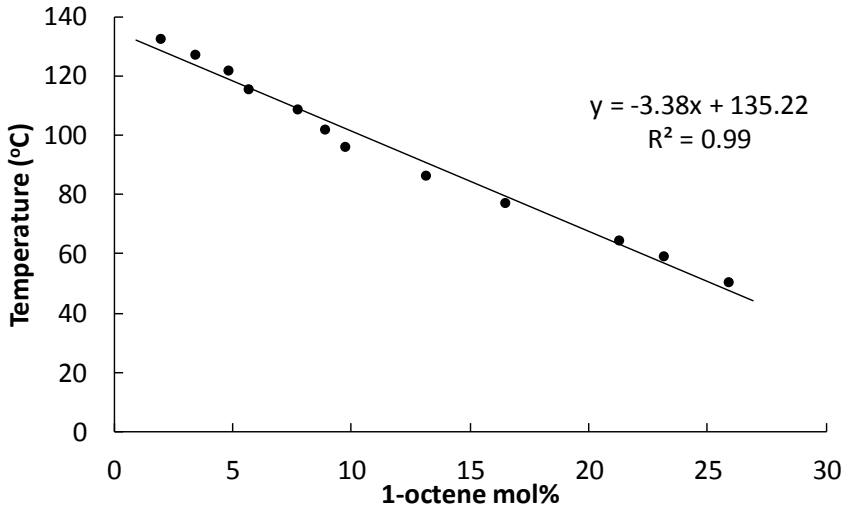

Figure 4-3. HT-TGIC Calibration curve for ethylene/1-octene copolymers of Category I

4.4.2 Influence of Operation Conditions on the Analysis of Individual Resins

A 2^3 experimental factorial design was applied to three samples (E/O-9.8, E/O-16.4, and E/O-23.2) and their blends to study the effect of operating conditions on HT-TGIC profiles. The three factors studied were the cooling rate (CR), heating rate (HR) and elution flow rate (F_E). The upper and lower values of these three factors are shown in Table 4-2. All other operating parameters were kept constant. The main effects and the interactions between these factors were computed using 95% confidence interval analysis of variance according to Montgomery.[92] The error terms were estimated based on three replicate experiments performed at the central conditions. Table 4-3 summarizes the results for this factorial experimental design.

Table 4-2. Factor levels used in the 2^3 factorial design.

	Coded value	(A) CR (°C/min)	(B) HR (°C/min)	(C) F_E (mL/min)
Upper level	+1	5	3	0.5
Lower level	-1	3	1	0.1
Central level	0	4	2	0.3

Table 4-3. Output values for the 2^3 factorial design.

Run	CR (°C/min)	HR (°C/min)	F_E (mL/min)	E/O-9.8		E/O-16.4		E/O-23.2		Time (min)
				σ	T_P (°C)	σ	T_P (°C)	σ	T_P (°C)	
1	(-)	(-)	(-)	10.2	95.1	10.8	77.9	9.2	61.7	200
2	(-)	(-)	(+)	11.1	91.3	11.5	73.8	13.1	59.1	200
3	(-)	(+)	(-)	12.6	103.1	13.6	85.8	12.6	69.9	110
4	(-)	(+)	(+)	9.5	95.7	10.5	77.8	10.8	61.3	110
5	(+)	(-)	(-)	9.1	95.0	10.9	76.1	9.2	59.6	180
6	(+)	(-)	(+)	8.8	91.1	11.6	72.7	11.6	56.7	180
7	(+)	(+)	(-)	12.5	106.3	13.4	85.2	12.4	69.9	90
8	(+)	(+)	(+)	9.7	95.1	11.6	77.2	11.8	59.3	90

The analysis of variance (ANOVA) tables for sample E/O-16.4, using 95 % confidence interval are shown in Table 4-4 for peak elution temperature and Table 4-5 for standard deviation. Similar tables for samples E/O-9.8 and E/O-23.2 are presented in Appendix C. According to F test results of these three samples, the cooling rate was found to have no significant effect on T_P and σ. On the other hand, heating rate and elution flow rate, as well as their interactions, had significant effects on both T_P and σ.

Table 4-4. ANOVA table for the elution peak temperatures for sample E/O-16.4.

Source of variance	Effect	Sum of Squares	Degree of Freedom	Mean Squares	$F_{observed}$	$F_{critical}$ F(1,2,0.05)
Main Factor						
A	-1.07	2.30	1	2.30	10.0	18.5
B	6.37	81.22	1	81.22	353.1*	
C	-5.89	69.44	1	69.44	301.9*	
Interaction						
AB	0.44	0.39	1	0.39	1.7	
AC	0.21	0.09	1	0.09	0.4	
BC	-2.11	8.88	1	8.88	38.6*	
ABC	-0.18	0.06	1	0.06	0.3	
ERROR		0.45	2	0.23		

Table 4-5. ANOVA table for the standard deviation of HT-TGIC profiles for sample E/O-16.4.

Source of variance	Effect	Sum of Squares	Degree of Freedom	Mean Squares	$F_{observed}$	$F_{critical}$ F(1,2,0.05)
Main Factor						
A	0.273	0.149	1	0.149	2.35	18.5
B	1.088	2.365	1	2.365	37.49*	
C	-0.903	1.629	1	1.629	25.82*	
Interaction						
AB	0.178	0.063	1	0.063	1.00	
AC	0.328	0.215	1	0.215	3.40	
BC	-1.538	4.728	1	4.728	74.93*	
ABC	0.323	0.208	1	0.208	3.30	
ERROR		0.126	2	0.063		

Figure 4-4 demonstrates that the value of the cooling rate does not significantly influence the elution peak temperature and shape of HT-TGIC profiles. Since HT-TGIC is not a crystallization-based technique, such as TREF, CRYSTAF or CEF, this is not an unexpected result. The fractionation phenomenon seems to be regulated by the interaction between the graphite surface and the ethylene sequences in the polymer chain. As indicated by the results in the tables above, this interaction is not strongly influenced by how fast the column is cooled. Since the cooling rate has a negligible effect on the HT-TGIC profiles, it is recommended that the fastest cooling rate (5 °C/min) be used to reduce analysis time.

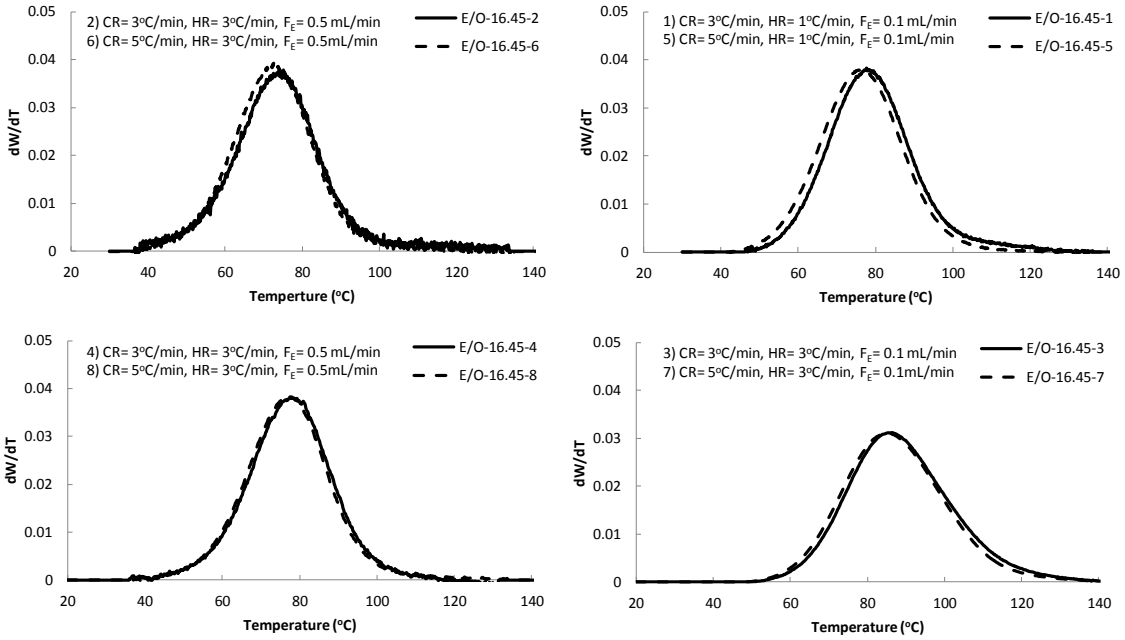

Figure 4-4. Cooling rate effect on HT-TGIC profiles of sample E/O-16.4.

On the other hand, the heating rate has a clear influence on the HT-TGIC profile as illustrated in Figure 4-5. When a fast heating rate was used, the CCD shifts to higher peak temperatures and becomes broader, especially at low elution flow rate (Runs 3 and 7). However, when the elution flow rate was high, heating rate affected the peak temperature positions without increasing the broadness (Runs 4 and 8) because the interaction between solvent flow rate and heating rate significantly influences the HT-TGIC profile, as shown in Table 4-5. HT-TGIC peaks shift to higher temperatures with increasing heating rate, since the desorption

temperature detected by the time that the solvent has reached the detector at the end of the column is higher when higher heating rates are applied.

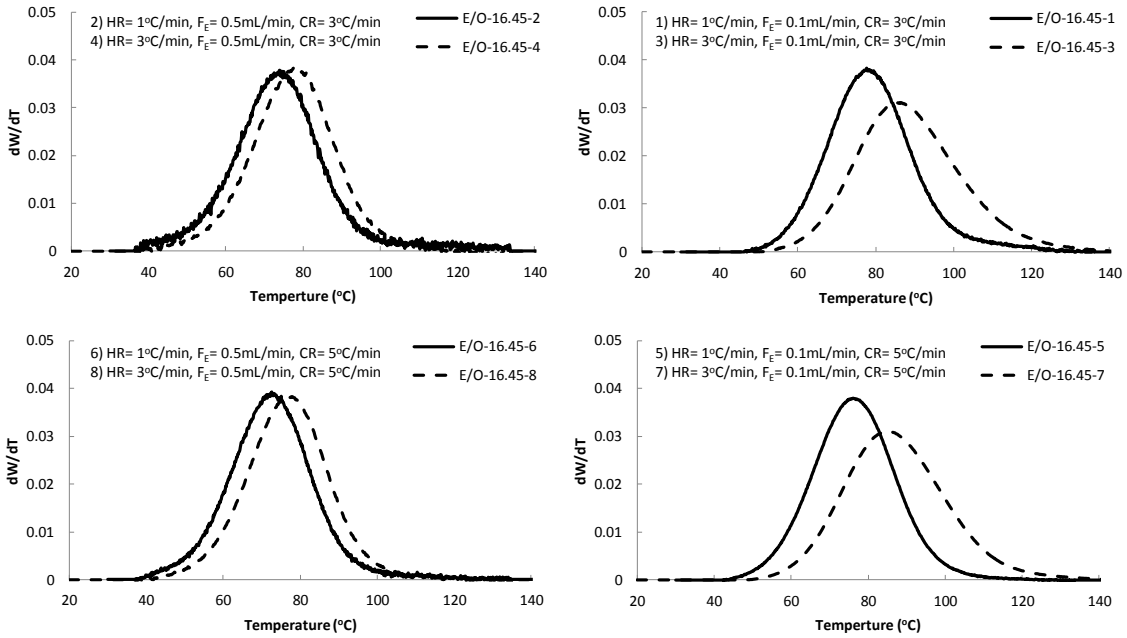

Figure 4-5. Heating rate effect on HT-TGIC profile of sample E/O-16.4.

Interestingly, Figure 4-6 shows that the elution flow rate has a significant effect on T_P and σ. When a slow elution flow rate was used, the peak temperature shifts to higher values. Since the solvent flow rate during the desorption step determines the residence time of the polymer solution in the column, slow elution flow rates broaden the HT-TGIC profile and shift its peak temperature to a higher value due to, most likely, an increase in residence time. Thus, it is essential to keep elution flow rate at 0.5 mL/min to minimize the residence time in the column after desorption. Similar conclusions can be reached for samples E/O-9.8 and E/O-23.2 (Appendix C).

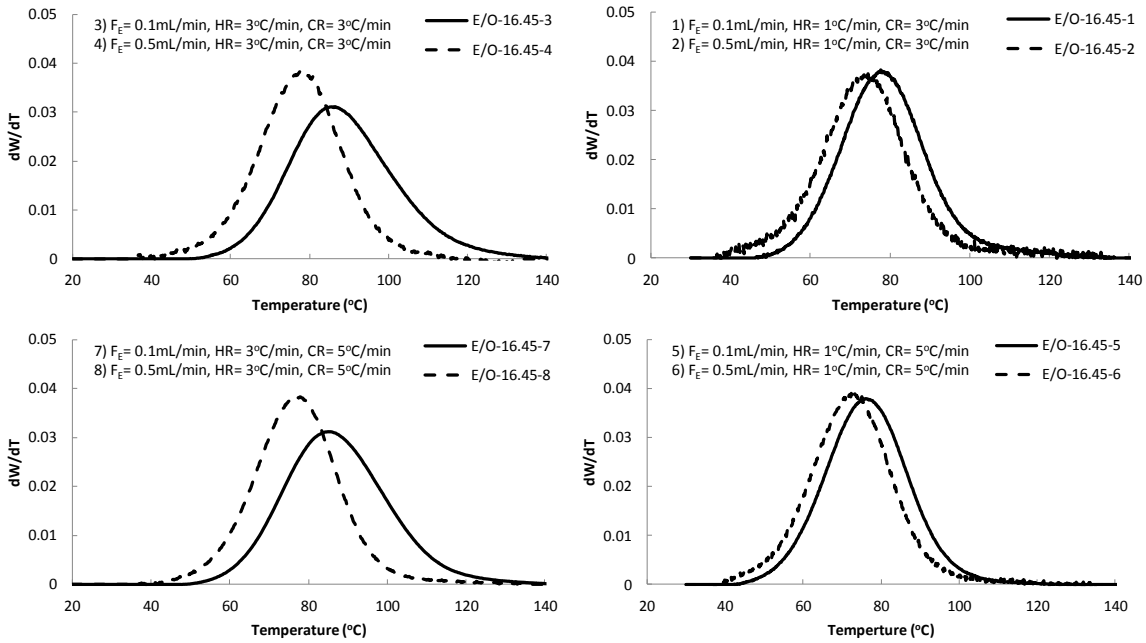

Figure 4-6. Effect of elution flow rate on HT-TGIC profile of sample E/O-16.4.

4.4.3 Influence of Operation Conditions on the Analysis of Blends

HT-TGIC can also be used to determine the chemical composition distribution of polyolefin blends. It has been observed[82] that the components of binary blends affect each other's HT-TGIC profile. This phenomenon has been attributed tentatively to co-adsorption or co-desorption effects of the two components in the polymer blend.

A 2^3 experimental factorial design was used to study the effect of operation conditions on the analysis of Blend 1, containing 50% of E/O-9.8 and 50% of E/O-23.2. Three factors (CR, HR and F_E) were studied to find out the operation conditions for "best" peak resolution. The upper and lower levels of each factor are listed in Table 4-2. The error term was estimated based on three replicate experiments performed at the central conditions. Equation (4.4) was used to define the co-desorption index (CDI) to quantify this effect on the blends,

$$CDI = 2 \times \int_{35\,℃}^{160\,℃} \left| \left(\frac{dw}{dT}\right)_{Exp} - \left(\frac{dw}{dT}\right)_{Pred} \right| dT \tag{4.4}$$

where $(dw/dT)_{Exp}$ is the height of the experimental HT-TGIC chromatogram and $(dw/dT)_{Pred}$ is the predicted height of the HT-TGIC profile. The predicted heights are estimated by adding the HT-TGIC profiles of each parent sample multiplied by their weight fractions in the blend, as shown in the expression below,

$$\left(\frac{dw}{dT}\right)_{pred} = m_1 \left(\frac{dw_1}{dT}\right)_{Exp} + (1 - m_1) \left(\frac{dw_2}{dT}\right)_{Exp} \tag{4.5}$$

where m_1 is the mass fraction of the first component in the blend and $(dw_1/dT)_{Exp}$ and $(dw_2/dT)_{Exp}$ are the heights of the experimental HT-TGIC chromatograms of each blend component (measured alone), respectively.

The index CDI is equal to zero if no co-desorption takes place and one if both blend components desorb from the column together. Therefore, it is a useful index to quantify how good is the agreement between the experimental and predicted profiles for the blend (0 = perfect agreement and no co-desorption, 1 = poor agreement and complete co-desorption).

The 8 Runs for Blend 1 were performed randomly. The output value (co-desorption index) for each run is presented in Table 4-6. Figure 4-7 shows the HT-TGIC profiles for these eight runs operating in different conditions.

Table 4-6. Output values of 2^3 factorial design for Blend 1.

Run	CR (°C/min)	HR (°C/min)	F_E (mL/min)	CDI
1	(-)	(-)	(-)	0.424
2	(-)	(-)	(+)	0.562
3	(-)	(+)	(-)	0.536
4	(-)	(+)	(+)	**0.148**
5	(+)	(-)	(-)	0.390
6	(+)	(-)	(+)	0.428
7	(+)	(+)	(-)	0.574
8	(+)	(+)	(+)	**0.110**

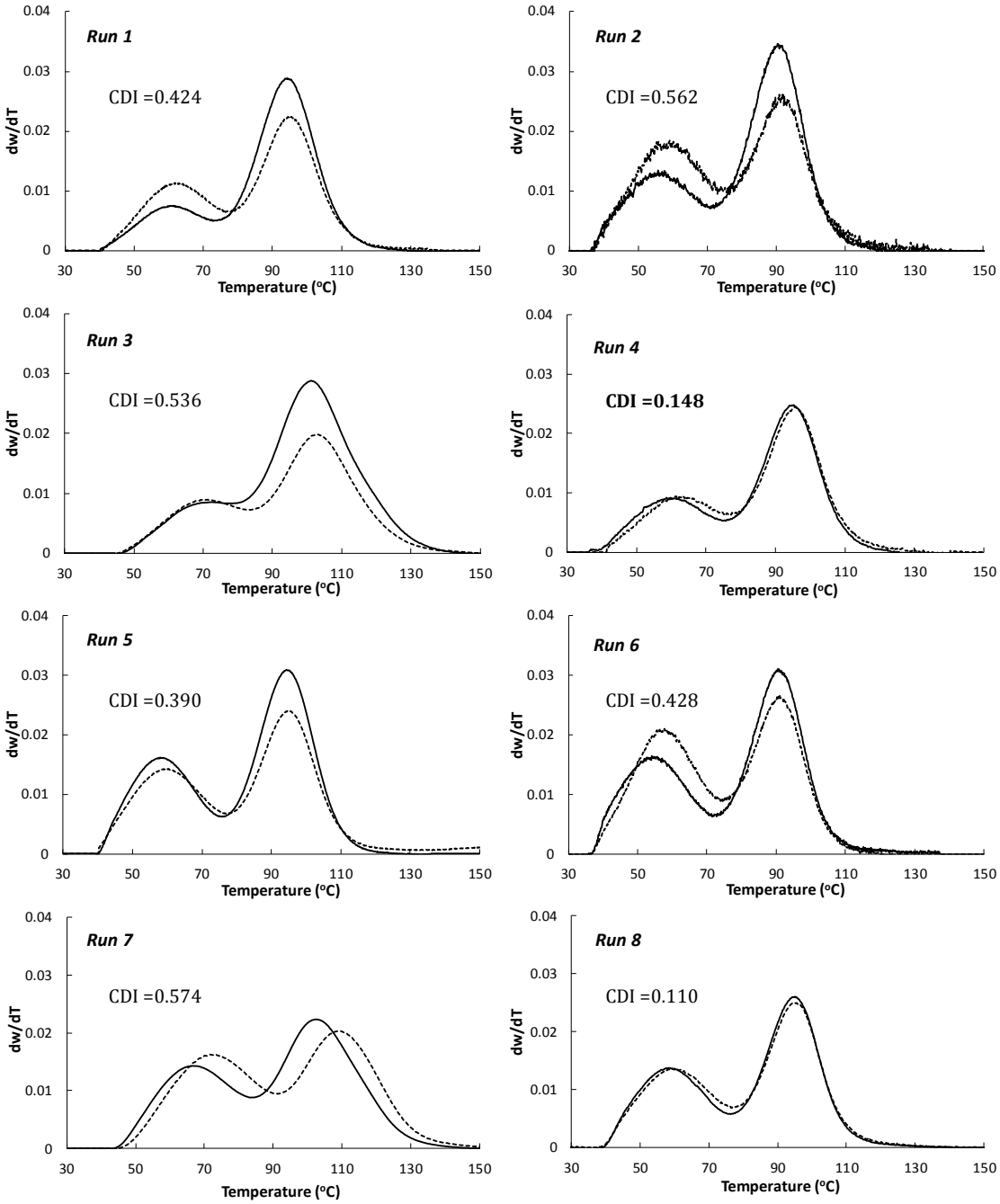

Figure 4-7. Experimental (continuous line) and predicted (dotted line) HT-TGIC profiles for a blend of 50% of E/O-9.8 and 50% of E/O-16.4 at different operation conditions.

The F test results calculated in the ANOVA table (Table 4-7) demonstrates that the cooling rate (CR) had no significant effect on the co-desorption index. However, heating rate and

elution flow rate (HR and F_E, respectively) and their interaction are significant factors influencing the co-desorption index.

Table 4-7. ANOVA TABLE for the co-desorption index of Blend1 presented in Table 4-6

Source of variance	Effect	Sum of Squares	Degree of freedom	Mean Squares	$F_{observed}$	$F_{critical}$ F(1,2,0.05)
Main Factor						
A	-0.20	0.08	1	0.08	5.17	18.5
B	-0.48	0.46	1	0.46	30.20*	
C	-0.56	0.63	1		41.91*	
Interaction						
AB	0.12	0.03	1		1.99	
AC	-0.20	0.08	1	0.08	5.43	
BC	-0.89	1.59	1	1.59	105.50*	
ABC	-0.01	0.00	1	0.00	0.02	
ERROR		0.04	2	0.02		

The operating conditions used in Runs 2, 3 and 7 led to the highest co-desorption index (0.562, 0.536, and 0.574 respectively) among all runs. The co-desorption index of Runs 4 and 8 are the lowest (0.148, and 0.11, respectively) and the experimental profiles matched the predicted profiles well, as shown in Figure 4-7. However, the low cooling rate in Run 4 increased the analysis time without enhancing peak resolution. Therefore, it is preferable to use the analytical conditions of Run 8 (CR=5 ^oC/min, HR= 3 ^oC/min, and F_E= 0.5 mL/min) to minimize the analysis time and reduce the co-desorption index (better resolution), at least for the samples covered in this investigation.

Moreover, three other different blends were chosen (Table 4-8) to investigate whether these analytical operation conditions were also adequate. Figure 4-8, Figure 4-9, and Figure 4-10 show that their predicted profiles match their experimental profiles well, indicating that those conditions are indeed appropriate to analyze polyolefin blends.

Table 4-8. Additional blends used to study the effect of operation conditions on the co-desorption index.

Sample	E/O-9.8	E/O-13.2	E/O-16.4	E/O-21.3	E/O-23.2	*CDI*
Blend 2	0.5	---	0.5	---	---	0.071
Blend 3	---	---	0.5	---	0.5	0.094
Blend 4	---	0.5	---	0.5	---	0.104

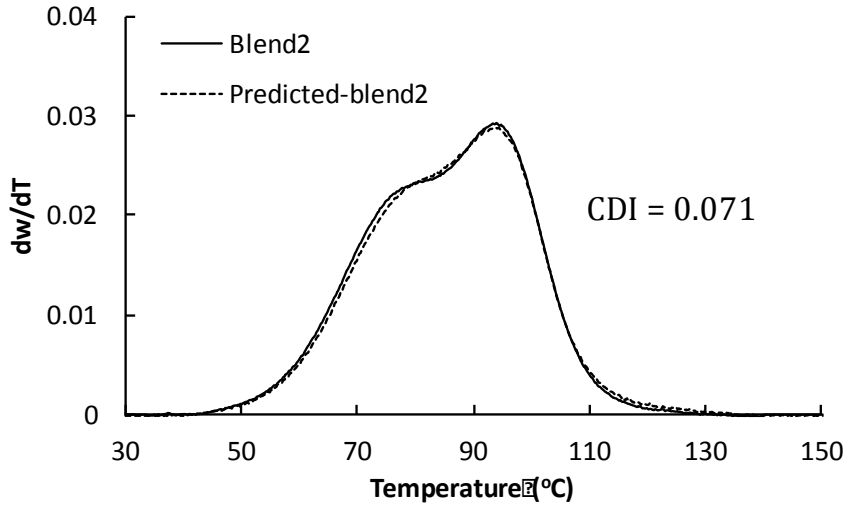

Figure 4-8. Experimental (continuous line) and predicted (dotted line) HT-TGIC profile of Blend 2 (50% of E/O-9.8, 50% of E/O-16.4). (Operation conditions: CR = 5 °C/min, HR = 3 °C/min, F_E = 0.5 mL/min, temperature range in both cycles = 160-35 °C)

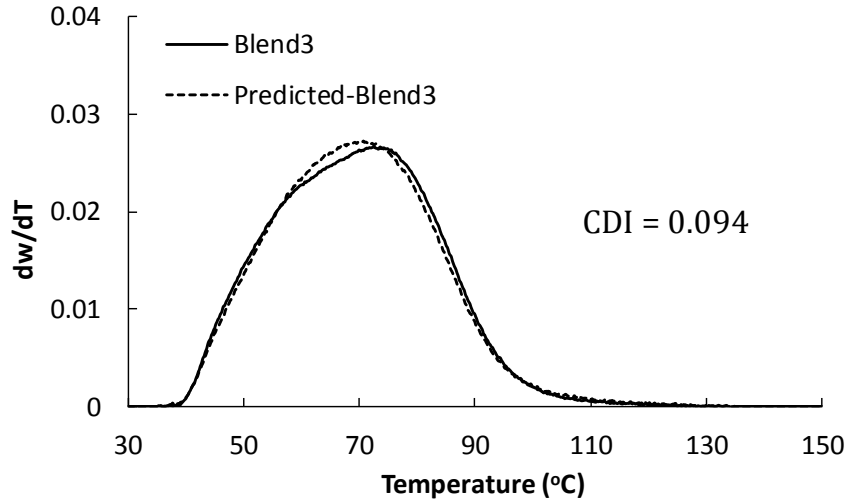

Figure 4-9. Experimental (continuous line) and predicted (dotted line) HT-TGIC profile of Blend3 (50% of E/O-16.4, 50% of E/O-23.2). (Operation conditions: CR = 5 °C/min, HR = 3 °C/min, F_E = 0.5 mL/min, temperature range in both cycles = 160-35 °C)

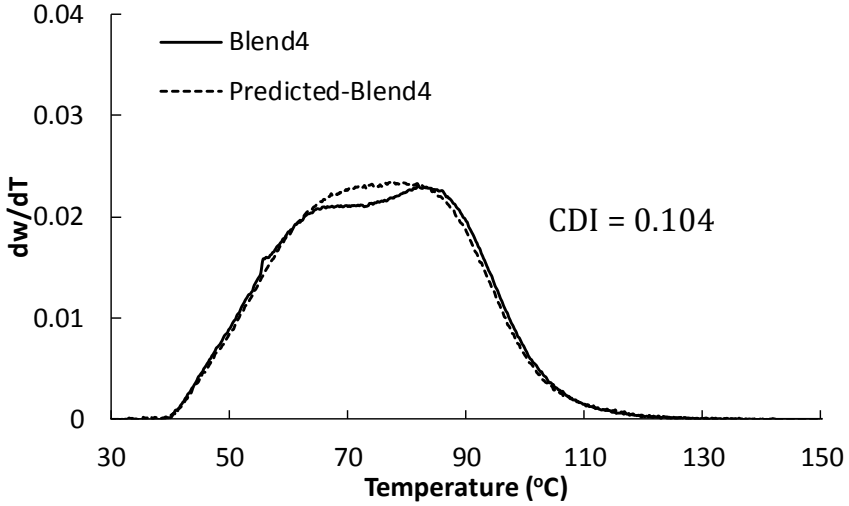

Figure 4-10. Experimental (continuous line) and predicted (dotted line) HT-TGIC profile of Blend3 (50% of E/O-13.2, 50% of E/O-21.3). (Operation conditions: CR = 5 °C/min, HR = 3 °C/min, F_E = 0.5 mL/min, temperature range in both cycles = 160-35 °C)

4.5 Conclusions

There are good indications that HT-TGIC is the next major step in a long sequence of polyolefin CCD-characterization techniques that started in the eighties with TREF. The main

objective of this chapter was to study the fractionation of ethylene/1-olefin copolymers systematically by HT-TGIC to better understand its mechanism and to propose conditions that maximize peak resolution while minimizing analysis time. One set of ethylene/1-octene copolymers having same molecular weight averages and different comonomer fractions were synthesized using a single-site catalyst and analyzed by HT-TGIC. The HT-TGIC chromatograms shift to lower elution temperatures and become broader when the comonomer content increased. As expected, the relationship between the desorption temperature and the comonomer mole fraction was linear.

HT-TGIC profiles of individual samples and binary blends are influenced by analytical operation conditions such as cooling rate (CR), heating rate (HR), and elution flow rate (F_E). The cooling rate had no significant effect on desorption temperature and broadness of the HT-TGIC chromatograms, indicating that interactions between the graphite surface and the ethylene sequences in the polymer chain are not strongly influenced by how fast the column is cooled. On the other hand, the heating rate and elution flow rate, as well as their interaction, had significant effects on both peak temperature and breadth. Increasing the heating rate shifts the HT-TGIC peaks to higher temperatures since the desorption temperature detected by the time that the solvent has reached the detector at the end of the column is higher. Furthermore, slow elution flow rates broaden the HT-TGIC profile and shift its peak temperature to a higher value due to, most likely, an increase in residence time of the polymer solution in the column.

Blend 1, containing 50% of E/O-9.8 and 50% of E/O-23.2, was studied to find the values of CR, HR, and F_E that led to the best peak resolution and minimum co-desorption. The cooling rates used did not influence the HT-TGIC profiles of this blend, but that the heating parameters and their interaction were significant. The preferred analytical conditions are CR=5 ^oC/min, HR= 3 ^oC/min, and F_E= 0.5 mL/min; these conditions reduce the co-desorption index (better resolution) and minimize the analysis time for the range of samples covered in this research.

Chapter 5. Effect of Column Type on Polyolefin Fractionation by HT-TGIC [2]

5.1 Introduction

Hypercarb columns packed with porous graphitic carbon are commonly used as the stationary phase in HT-TGIC fractionation even though other supports may be adequate. In this chapter, Hypercarb columns having distinct particle sizes and lengths were compared to investigate how the column type influences HT-TGIC fractionation for both individual samples and their binary blends. We used the same series of homogenous ethylene/1-octene copolymers of Category I, which was covered in Chapter 4, and experimentally and analytically discussed in Chapter 3, to extend the investigation of the factors affecting HT-TGIC. Also, binary copolymer blends were analyzed to study how different blend compositions affected HT-TGIC peak positions and shapes.

5.2 Results and Discussion

5.2.1 Effect of Blend Composition on HT-TGIC Profiles

In Chapter 4, we reported that the components of binary blends could affect the HT-TGIC profiles of each other due to the co-desorption of similar polymer chains present in the two components of the blend. Also, we established that the importance of this effect depended on the operation conditions used during HT-TGIC fractionation. The co-desorption index (CDI) was defined to quantify this effect that can be estimated using Equation 4.4. No co-desorption takes place when CDI is zero, and both blend components desorb from the column together when the value of CDI is 1.

[2] The results discussed in this chapter have been published in (A. Z. Al-Khazaal, J. B. P. Soares, Macromolecular symposia, **2015**)[97]

Five blends with different weight fractions of the components E/O-5.6 and E/O-16.4 were used to study the effect of blend composition on HT-TGIC profiles (Table 5-1). The CDI for these blends is shown in Table 5-1. The CDI increases for blends with more E/O-16.4. Therefore, we may conclude that increasing the fraction of the copolymer with higher comonomer content increases the co-desorption of the two components in the blends. This trend is apparent from inspection of the actual HT-TGIC profiles (measured and predicted) in Figure 5-1.

Table 5-1. Co-desorption index of five copolymer blends.

Sample ID	E/O-5.6 %	E/O-16.4 %	CDI
Blend A	85	15	0.13
Blend B	70	30	0.15
Blend C	50	50	0.17
Blend D	30	70	0.26
Blend E	15	85	0.31

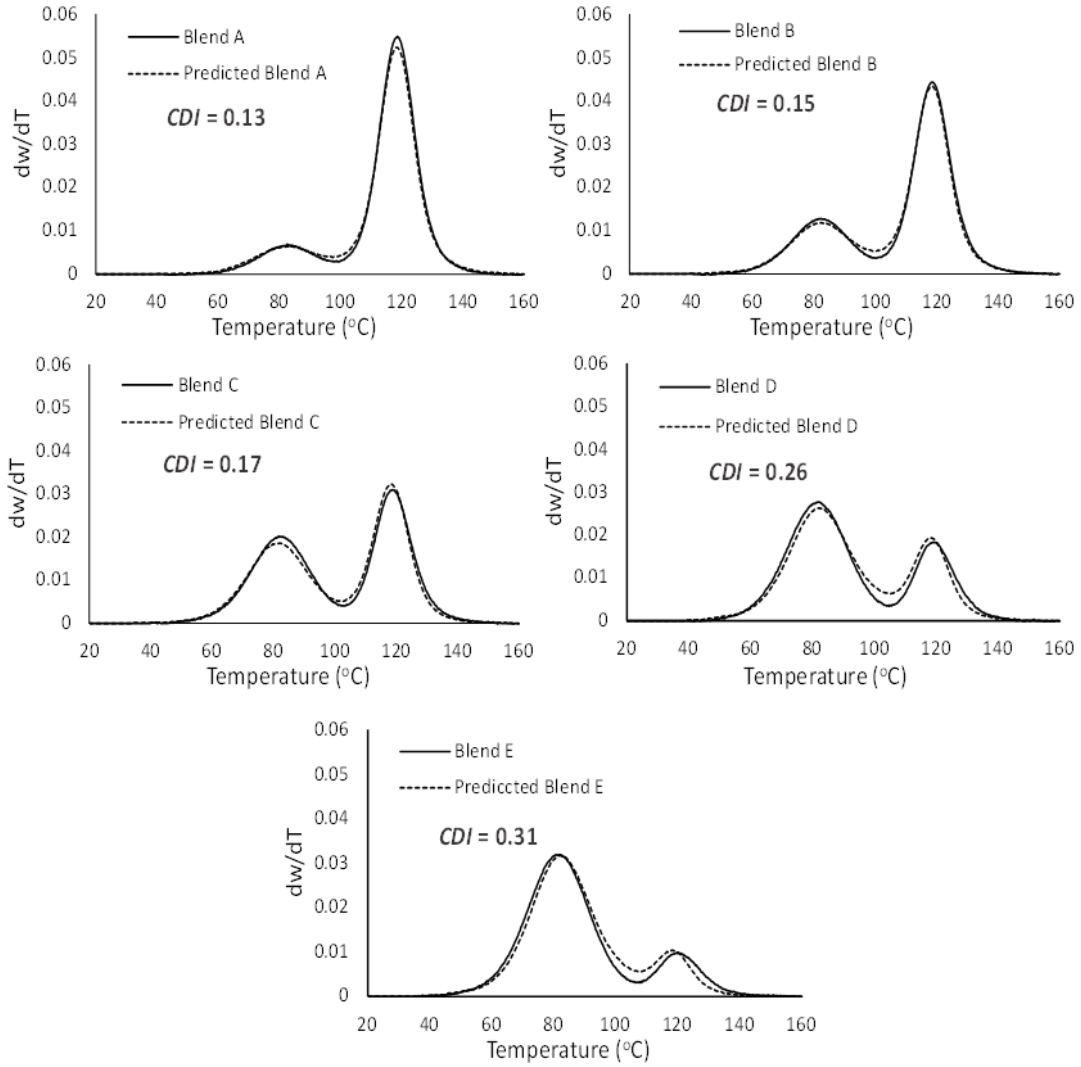

Figure 5-1. Experimental and predicted HT-TGIC profiles of five blends of E/O-5.6 and E/O-16.4 measured in Column 1.

This is an interesting observation, although it is not clear why increasing the fraction of the component with the highest comonomer content affects the HT-TGIC profiles in the way shown in Figure 5-1. Perhaps the presence of larger amounts of the copolymer with the lower adsorption temperature helps desorb the blend component with higher adsorption temperature (lower comonomer content). This is observed in Figure 5-1 as a shift of the high-temperature peak towards lower desorption temperatures as the amount of polymer under the low-temperature peak increases. Independently of its cause, it is important to account for this behavior when interpreting HT-TGIC peaks of polyolefin blends.

5.2.2 Effect of Average Particle Size on HT-TGIC Profiles

Four ethylene/1-octene copolymers from Category I were chosen to study the effect of the average particle size and column length on the temperature peak position and shape of HT-TGIC profiles. Elution peak temperatures (T_p), average elution temperatures (T_μ) and standard deviations (σ) of these samples are listed in Table 5-2.

Table 5-2. Average values for HT-TGIC analysis of four samples using three different Hypercarb columns.

Sample ID	Column 1 d_p = 5μm L = 100 mm			Column 2 d_p = 3μm L = 100 mm			Column 3 d_p=7μm L=100 mm			Column 4 d_p = 5μm L = 250 mm		
	T_P	T_μ	σ	T_P	T_μ	σ	T_P	T_μ	σ	T_P	T_μ	σ
E/O-5.6	118.9	119.2	10.0	118.2	120.9	9.6	119.2	119.5	10.1	127.3	126.7	10.6
E/O-9.8	99.9	100.4	10.2	100.5	100.7	9.7	100.7	100.9	10.5	108.6	109.2	10.7
E/O-16.4	82.2	83.3	11.6	83.4	83.7	11.1	83.5	84.0	12.7	91.1	93.1	11.7
E/O-21.3	70.2	72.4	13.8	71.3	71.5	12.1	69.9	72.5	14.6	78.5	80.7	12.7

Figure 5-2 shows that the HT-TGIC profiles measured in Column 1 (d_p = 5 μm), Column 2 (d_p = 3 μm), and Column 3 (d_p = 7 μm) are very similar. This observation is confirmed by the data in Table 5-2 showing that the values for T_P, T_μ and σ are essentially the same within experimental error. Albeit the values of σ for Column 3 are slightly higher than those for the other two columns. Those differences, however, do not seem to be statistically significant. Figure 5-3 indicates that the shapes of the HT-TGIC profiles of a blend of E/O-9.8 and E/O-16.4 (50/50 wt.%) are influenced only slightly by the average particle size of the Hypercarb column packing. Figure 5-4 shows similar results for a different blend (E/O-5.6 and E/O-16.4, 50/50 wt.%). In both figures, the peaks shift very slightly for the different columns, but no change in peak resolution results from using packing with average diameters of 3 μm, 5 μm or

7 μm. Consequently, HT-TGIC peak position and shape are not substantially affected by the average size of the PGC particles for individual samples and blends. Since the average particle size has a negligible effect on the HT-TGIC profiles, columns packed with larger particles are recommended to avoid possible plugging and to reduce the pressure during the analysis.

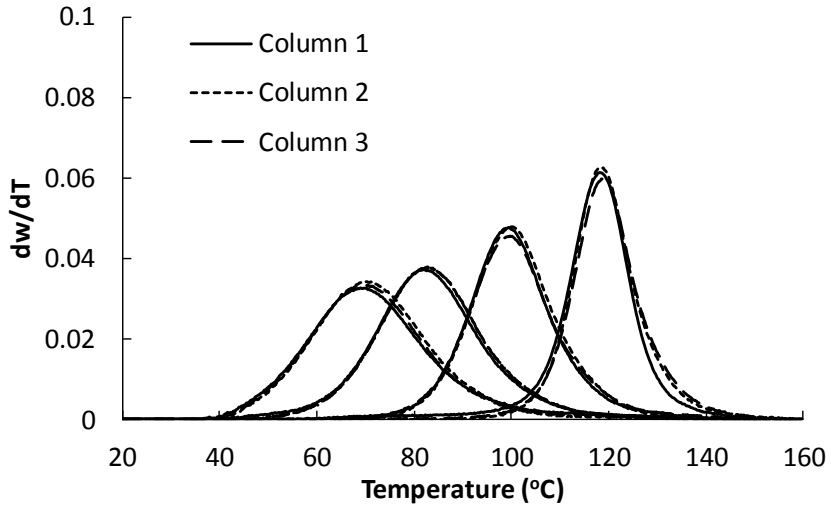

Figure 5-2. HT-TGIC profiles of four ethylene/1-octene copolymers (E/O-5.6, E/O-9.8, E/O-16.4, and E/O-21.3) measured in three Hypercarb columns having packing with distinct average particle sizes.

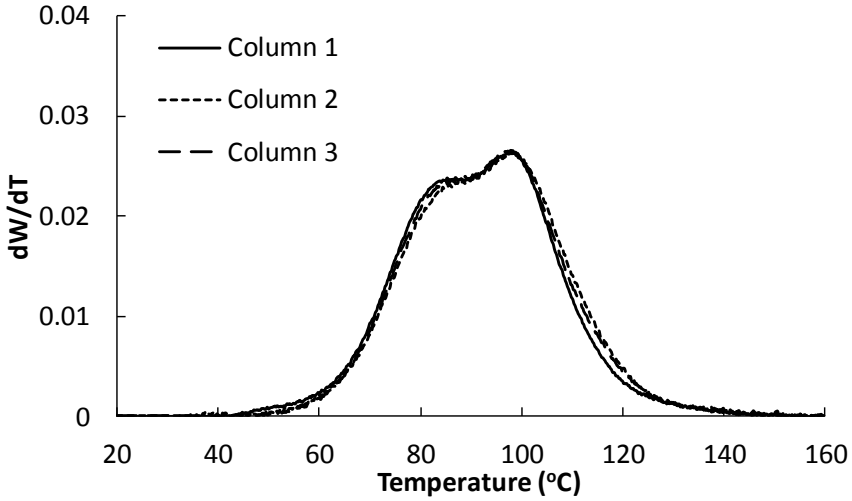

Figure 5-3. HT-TGIC profiles of the blend of E/O-9.8 and E/O-16.4 (50/50 wt.%), analyzed in three Hypercarb columns having packing with distinct average particle sizes.

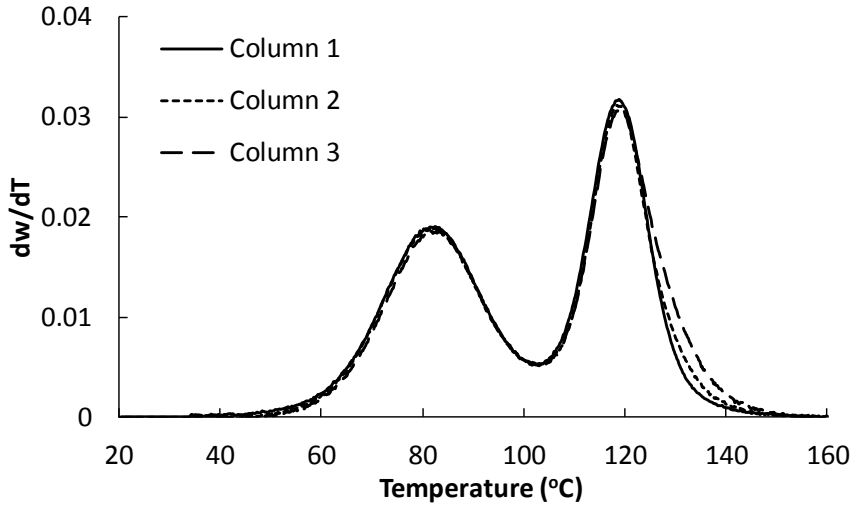

Figure 5-4. HT-TGIC profiles of the blend of E/O-5.6 and E/O-16.4 (50/50 wt.%), analyzed in three Hypercarb columns having packing with distinct average particle sizes.

5.2.3 Effect of Column Length on HT-TGIC Profiles

The same four samples were analyzed using two Hypercarb columns with different lengths: Column 1 (L = 100 mm) and Column 4 (L =250 mm). Column length influences peak temperatures of the individual samples as illustrated in Figure 5-5 and shown in Table 5-2. The chromatograms of copolymers analyzed in the longer column (Column 4) have higher peak temperatures than those measured in the shorter column (Column 1). This should not be misinterpreted as a change in polymer desorption temperature. The peaks shift to higher temperatures because, by the time the sample reaches the detector at the end of the column, the temperature will be higher when the longer column is used. When the HT-TGIC profiles measured in Column 4 are shifted by 9 to 11°C to make them superimpose those measured with Column 1, both sets of profiles looked very similar, as shown in Figure 5-6. The profiles measured in the 250 mm column look a little broader (also compare the σ values in Table 5-2), as expected from more pronounced axial diffusion effects in a longer column. Apart from this minor difference, column length does not seem to have much influence on HT-TGIC fractionation.

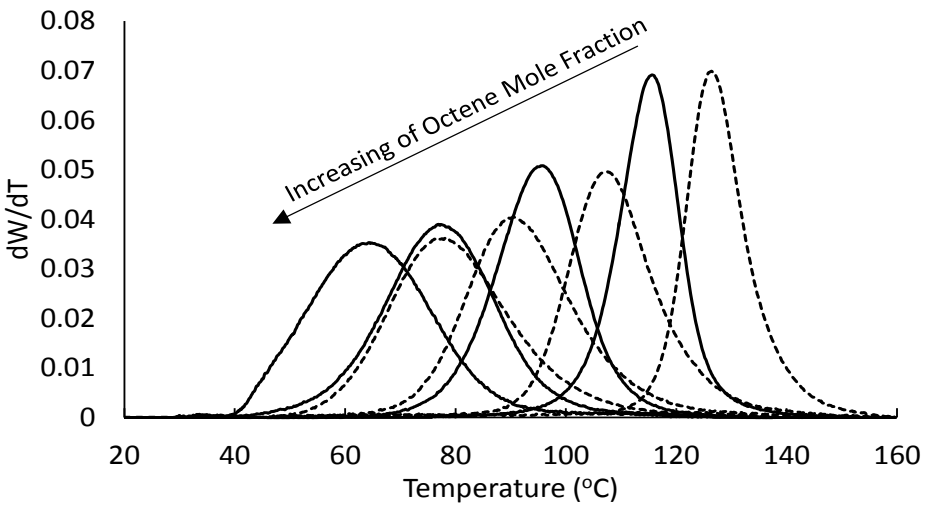

Figure 5-5. HT-TGIC profiles of four ethylene/1-octene copolymers (E/O-5.6, E/O-9.8, E/O-16.4, and E/O-21.3) analyzed in two Hypercarb columns having different lengths: *L* = 250 mm (dotted line) and *L* = 100 mm (continuous line).

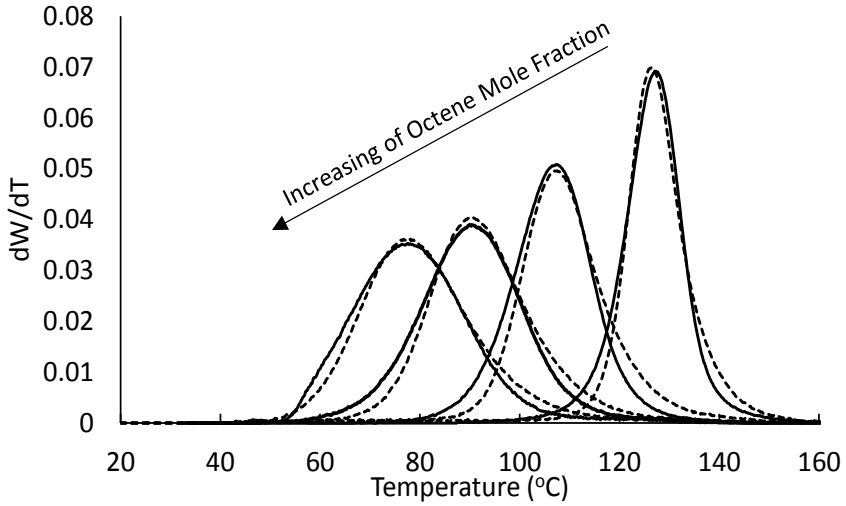

Figure 5-6. HT-TGIC profiles of four ethylene/1-octene copolymers (E/O-5.6, E/O-9.8, E/O-16.4, and E/O-21.3) analyzed in two Hypercarb columns having different lengths: *L* = 250 mm (dotted line) and *L* = 100 mm (continuous line). The profiles measured in the shorter column have been shifted to higher temperatures.

Figure 5-7 and Figure 5-8 tell a similar story about two binary blends of these copolymers. Column length has a negligible effect on the fractionation of these materials. Since shorter

columns are less expensive and have decreased axial dispersion, they should be preferred for routine polyolefin analysis by HT-TGIC.

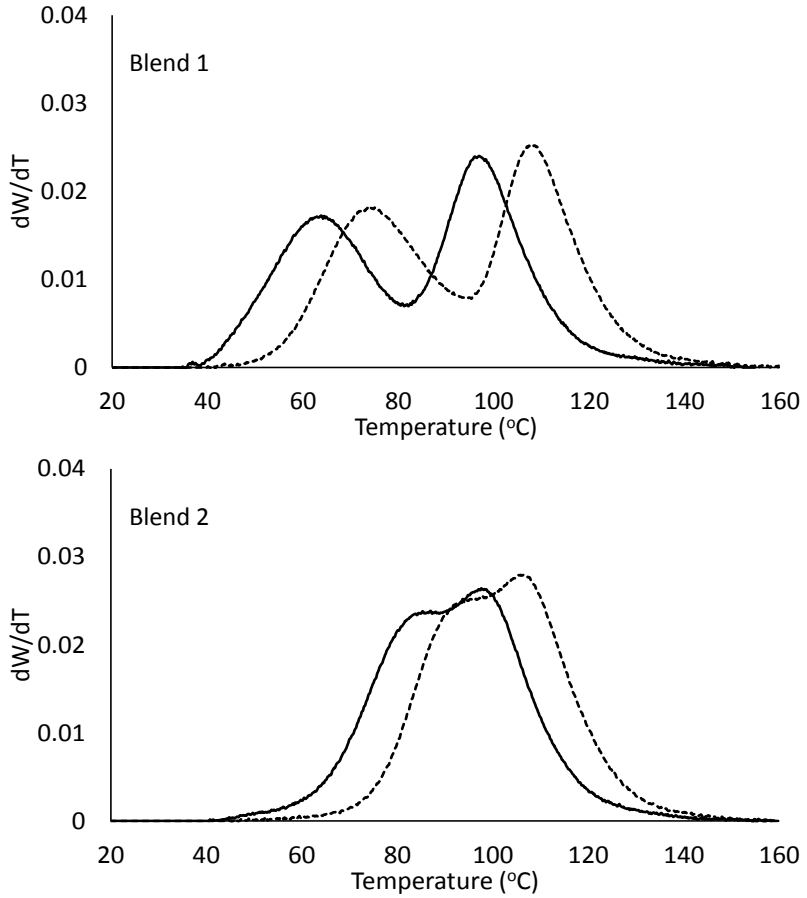

Figure 5-7. HT-TGIC profiles of Blend 1 (E/O-9.8 and E/O-23.2, 50/50 wt.%) and Blend 2 (E/O-9.8 and E/O-16.4, 50/50 wt.%) measured in two Hypercarb columns having different lengths: *L* = 250 mm (dotted line) and *L* = 100 mm (continuous line).

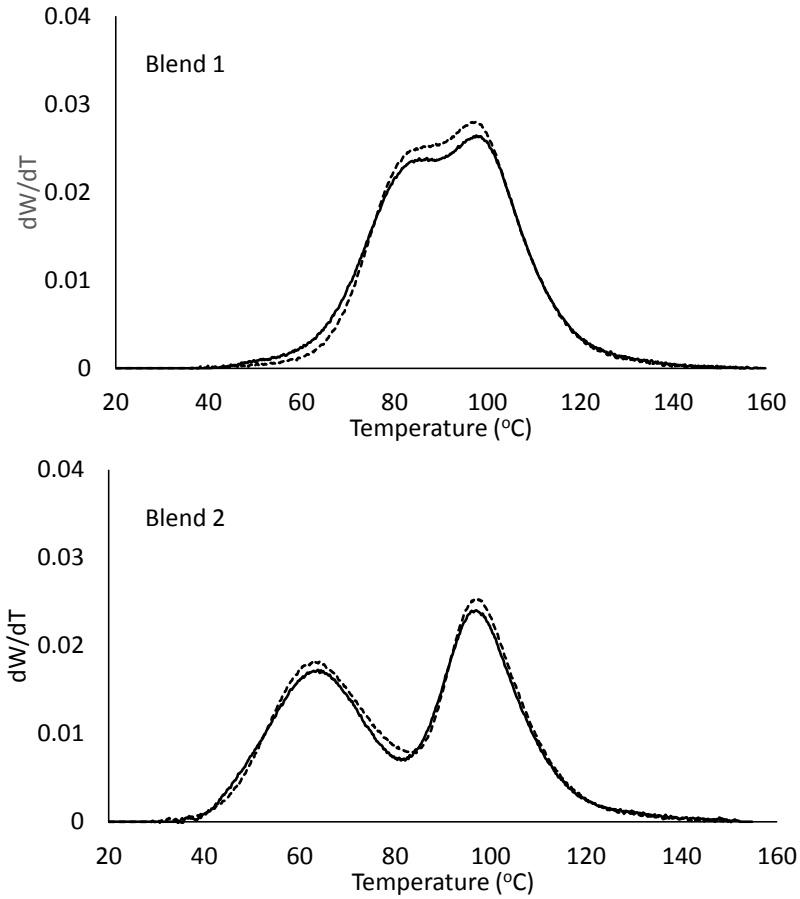

Figure 5-8. HT-TGIC profiles of Blend 1 (E/O-9.8 and E/O-23.2, 50/50 wt.%) and Blend 2 (E/O-9.8 and E/O-16.4, 50/50 wt.%) measured in two different Hypercarb columns having different lengths: *L* = 250 mm (dotted line) and *L* = 100 mm (continuous line). The profiles measured in the longer column have been shifted to lower temperatures.

5.3 Conclusions

High-temperature thermal gradient interaction chromatography is becoming an important technique to measure the CCD of polyolefins, on par with more traditional methods such as TREF, CRYSTAF and CEF. In this chapter, we extended the investigations on the factors that affect the fractionation of ethylene/α-olefin copolymers by HT-TGIC reported in Chapter 4, by considering the effects of column length and average particle size of the PGC packing.

We compared Hypercarb columns having two lengths (100 and 250 mm) and three average particle sizes (3, 5, and 7 μm). Neither column length nor particle size played an important role on the fractionation of polyolefins and their blends. It is preferable to use shorter columns with larger particles, since peak broadening due to axial dispersion is more severe in longer columns, and higher operation pressures and plugging during analysis are more likely to happen in columns packed with smaller particles.

For binary blends, we observed that the fraction of the component with high comonomer content could affect the peak position of the fraction with low comonomer content, perhaps because of co-desorption effects. The cause of this behavior is not clear at present, but it should be kept in mind when interpreting the results of blends analyzed by HT-TGIC.

Chapter 6. Joint Effect of Polyolefin Chain Length and Comonomer Fraction on HT-TGIC [3]

6.1 Introduction

Several factors influence the shape and position of HT-TGIC chromatograms, notably polymer microstructure, analytical conditions and, to a lesser extent, solvent type. This chapter investigates the joint influence of chain length and comonomer content of a series of polyethylene and ethylene/1-octene copolymers having similar 1-octene fractions (0 – 13 mol%) and a wide range of molecular weights on HT-TGIC fractionation (Category II). Stockmayer distribution and Monte Carlo model that was used to simulate the distributions for the longest (LESD) and overall ethylene sequence length (OESD) were established for these samples to explain the observed behavior of HT-TGIC profiles and to interpret the experimental results. Also, these samples were used to study the HT-TGIC of blends having different 1-octene contents and chain length.

6.2 Polyethylene Synthesis

Section 3.1 in Chapter 3 explained the copolymerization conditions, copolymerization procedure, materials and 300 autoclave reactor used to synthesize the copolymer samples of Category II. This category (used in this chapter) included one series of ethylene homopolymers with a distinct number average molecular weight (M_n) (Series H) and five series of ethylene/1-octene copolymers with similar 1-octene content per series, but different M_n. (Series C1, C2.6, C3.7, C7.8, and C13).

[3] The results discussed in this chapter have been published in (A. Z. Al-Khazaal, J. B. P. Soares, *Macromolecular Chemistry and Physics*, **2016**).[98]

6.3 polyethylene Analysis

The characterization techniques used to analyze ethylene/1-octene copolymer samples in Category II were explained in Section 3.2 in Chapter 3. GPC measured the MWDs of all samples. The FTIR calibration curve was established to estimate mole fraction of 1-octene in copolymer samples. HT-TGIC was used to determine the CCD and peak elution temperature.

6.4 Monte Carlo Simulation

Monte Carlo simulation is a powerful technique used to predict the CCD of copolymers and the distribution of stereoregularity in the case of polypropylene. In this chapter, Monte Carlo method were applied in MATLAB R2014 to estimate the microstructure of the ethylene/1-octene copolymer samples of Category II. Figure 6-1 shows the flow chart of the computer program used to run the model. In this approach, the Monte Carlo model depended on the propagation probability (*pp*) that the chain propagates by monomer with a probability of adding comonomer. The value of the 1-octene composition (F_O) was directly used as the probability of 1-octene propagation. The number average molecular weight (M_n) and the 1-octene mole fraction (F_O) were the only values used to determine the simulation parameters. The number average chain length (r_n) that is related to the propagation probability can be calculated for each sample from M_n and F_O with the following expression,

$$r_n = \frac{M_n}{(1 - F_O) \times MW_E + F_O \times MW_O} \tag{6.1}$$

where MW_E is the molar mass of ethylene, and MW_O is the molar mass of 1-octene.

Therefore, the propagation probability was determined with the following expression,

$$pp = \frac{r_n}{1 + r_n} \tag{6.2}$$

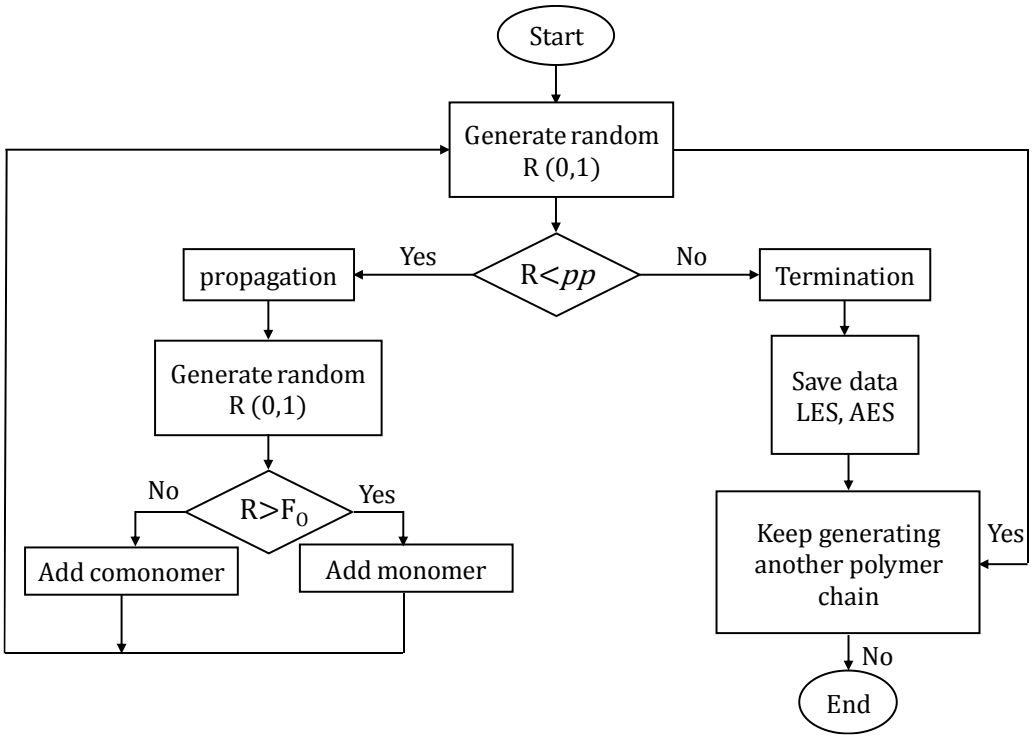

Figure 6-1. Algorithm of Monte Carlo simulation program

One hundred thousand chains were simulated for each sample. At the termination of each chain, the length of the ethylene sequence (ES) and the longest ethylene sequence were recorded, and then the average ethylene sequence length (AES) and the average longest ethylene sequence length (LES) were estimated for each sample. Equations (6.3) and (6.4) show how the Monte Carlo model calculates AES and LES for a population of *n* polymer chains containing a total number of ethylene segments *m*, and Figure 6-2 illustrates some of these sequences. At the end of the program, the procedure generated distributions of longest ethylene sequences (LESD) and overall ethylene sequence (OESD).

$$AES = \frac{\sum_i \sum_j ES_{i,j}}{m} \tag{6.3}$$

$$LES = \frac{\sum_i LES_i}{n} \tag{6.4}$$

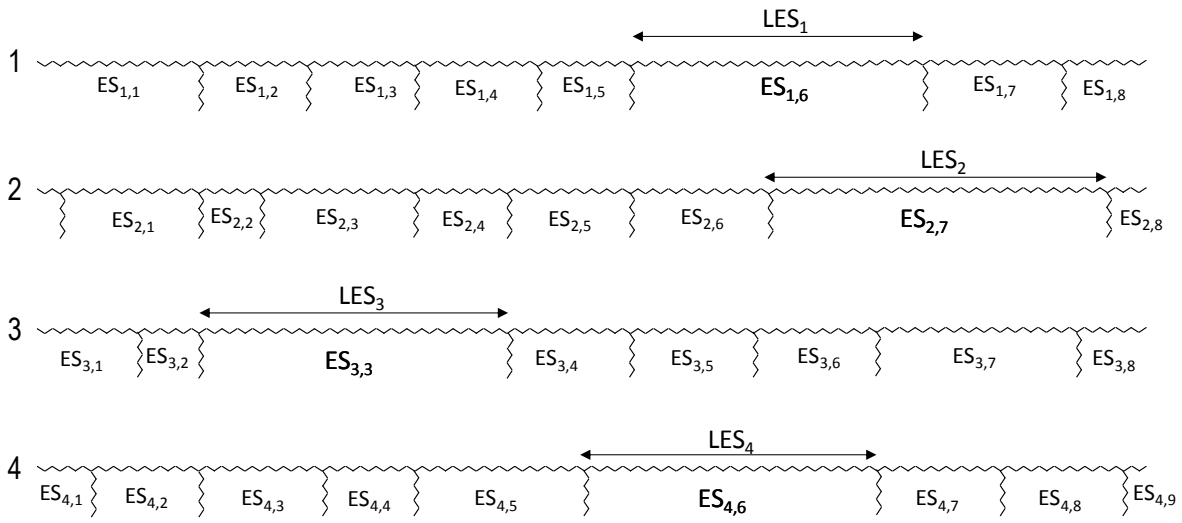

Figure 6-2. An Example of AES and LES calculation in Monte Carlo simulation

6.5 Results and Discussion

Monrabal *et al.*[87,88] suggested that the adsorption strength of ethylene/1-olefin copolymers on graphite was proportional to the available contact surface area of the polymer chain on the atomic level flat support surface. A sample with no or few short chain branches (SCBs) interacts strongly with the support because it has longer ethylene sequences and a larger contact surface area. Such a sample will adsorb on (or desorb from) the surface at higher temperatures than a sample having many SCBs and shorter ethylene sequences, as depicted in Figure 6-3. We will combine our experimental HT-TGIC measurements with Monte Carlo simulations of ethylene sequence length distributions of our copolymers to examine if this hypothesis can explain the joint effect of molecular weight and chemical composition on HT-TGIC fractionation.

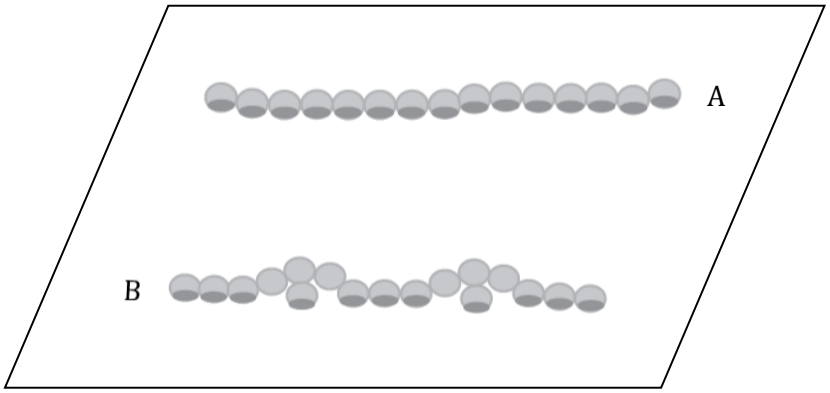

Figure 6-3. Adsorption of polyethylene on an atomic level flat surface: A) without SCB, longer ethylene sequences, stronger interaction, and B) with SCB, shorter ethylene sequences, weaker interactions.[87]

the mean elution temperature (T_μ), variance (σ^2), and standard deviation (σ) of HT-TGIC profiles were defined using Equation 4.1 to 4.3.

Peak temperatures (T_P), T_μ and σ for all samples are listed in Tables 6-1 to 6-6. These tables also listed the number average chain lengths (r_n) for each sample. Even though they are correlated, we will use r_n preferentially to M_n in our discussion, since the length of the chains, not their molecular weights, is supposed to be the main factor controlling interactions between polymer chain and the support in HT-TGIC columns.

The average ethylene sequence length (AES) and the average longest ethylene sequence length (LES) of each sample estimated by Monte Carlo simulation are also mentioned in Tables 6-1 to 6-6. Since ethylene homopolymers have no SCBs, AES and LES are both equal to r_n for these samples.

Table 6-1. HT-GPC and HT-TGIC data for ethylene homopolymers.

Sample ID	HT-GPC			HT-TGIC		
	M_n (g/mol)	PDI	r_n	T_P (°C)	σ	T_μ (°C)
H-1.0	970	1.8	35	122.3	21.4	96.5
H-1.2	1 200	1.8	44	126.5	20.8	104.5
H-1.7	1 700	2.3	62	129.9	19.6	113.7
H-2.7	2 700	2.1	97	132.4	12.9	123.5
H-3.6	3 600	2.2	131	134.0	10.4	126.4
H-9.2	9 200	2.1	329	135.9	8.4	130.8
H-12.2	12 200	2.0	436	136.2	5.6	134.4
H-21.0	21 000	2.1	748	136.7	4.9	135.9
H-25.3	25 300	2.1	904	136.8	3.8	136.4
H-56.6	56 600	2.1	2021	137.2	3.3	136.4
H-75.0	75 000	2.2	2680	137.2	2.9	137.3
H-97.0	97 000	2.1	3464	137.1	2.8	137.5

Table 6-2. HT-GPC and HT-TGIC data for ethylene/1-octene copolymers with 1.0 mol % of 1-octene.

Sample ID	HT-GPC					HT-TGIC		
	M_n (g/mol)	PDI	r_n	AES	LES	T_P (°C)	σ	T_μ (°C)
C1-1.4	1 400	1.8	50	33	35	114.8	19.3	100.0
C1-1.7	1 700	1.8	61	37	40	119.1	16.8	104.5
C1-2.4	2 400	2.3	84	45	52	125.5	14.6	112.8
C1-4.6	4 600	2.1	162	61	70	129.6	12.9	122.2
C1-8.2	8 200	2.2	286	74	100	131.6	9.6	127.5
C1-15.6	15 600	2.1	540	84	156	132.3	6.3	130.6
C1-19.5	19 500	2.0	678	87	178	132.5	5.7	131.2
C1-27.1	27 800	2.1	943	90	210	132.7	3.9	132.1
C1-36.3	36 300	2.1	1260	92	240	132.9	3.4	132.6
C1-68.1	68 100	2.2	2360	95	305	132.9	2.9	132.7
C1-129.4	129 400	2.1	4485	96	371	132.7	2.7	132.7

Table 6-3. HT-GPC and HT-TGIC data for ethylene/1-octene copolymers with 2.6 mol % of 1-octene.

Sample ID	HT-GPC					HT-TGIC		
	M_n (g/mol)	PDI	r_n	AES	LES	T_P (°C)	σ	T_μ (°C)
C2.6-1.5	1 500	1.7	51	21	22	93.1	19.5	84.7
C2.6-1.7	1 700	1.8	58	23	25	99.7	18.1	92.7
C2.6-2.0	2 000	1.8	69	24	31	104.4	17.5	96.1
C2.6-3.4	3 400	2.0	113	28	39	114.8	15.4	105.3
C2.6-4.8	4 800	2.0	159	30	50	119.5	13.3	111.9
C2.6-7.0	7 000	2.2	235	32	64	121.3	10.1	116.3
C2.6-14.1	14 100	2.1	469	34	90	123.1	7.1	120.4
C2.6-23.6	23 600	2.5	785	35	111	124.3	6.2	122.6
C2.6-36.0	36 000	2.2	1193	36	127	124.5	5.3	123.5
C2.6-61.1	61 100	2.2	2025	37	148	124.5	4.1	124.6
C2.6-115.7	115 700	2.2	3833	37	173	124.6	3.8	124.6

Table 6-4. HT-GPC and HT-TGIC data for ethylene/1-octene copolymers with 3.7 mol % of 1-octene.

Sample ID	HT-GPC					HT-TGIC		
	M_n (g/mol)	PDI	r_n	AES	LES	T_P (°C)	σ	T_μ (°C)
C3.7-2.3	2 300	1.9	73	19	28	96.8	16.1	88.4
C3.7-5.4	5 400	2.1	172	22	46	111.4	13.3	105.3
C3.7-7.2	7 200	2.0	233	23	53	113.3	11.1	108.5
C3.7-10.6	10 600	2.1	340	24	63	114.5	11.0	110.5
C3.7-16.8	16 800	2.0	539	24	76	115.8	8.4	113.6
C3.7-29.2	29 200	2.1	938	25	91	117.0	7.6	115.4
C3.7-34.8	34 800	2.2	1118	25	95	117.7	6.7	117.3
C3.7-52.2	52 200	2.1	1672	25	106	117.8	5.6	117.4
C3.7-85.2	85 200	2.1	2736	25	120	117.8	4.7	117.5

Table 6-5. HT-GPC and HT-TGIC data for ethylene/1-octene copolymers with 7.8 mol % of 1-octene.

Sample ID	HT-GPC					HT-TGIC		
	M_n (g/mol)	PDI	r_n	AES	LES	T_P (°C)	σ	T_μ (°C)
C7.8-1.9	1 900	1.6	56	10	16	55.3	12.2	50.0
C7.8-2.9	2 900	1.8	83	10	23	76.1	16.0	73.2
C7.8-4.6	4 600	2.0	132	11	27	82.6	14.0	79.4
C7.8-9.7	9 700	2.1	279	11	37	90.6	13.4	84.8
C7.8-18.5	18 500	2.1	534	11	45	96.0	10.3	93.1
C7.8-40.1	40 100	2.1	1160	12	55	98.2	9.4	98.8
C7.8-55.7	55 700	2.1	1611	12	59	98.2	7.9	98.0
C7.8-117.0	117 000	2.1	3384	12	68	98.3	7.0	98.2

Table 6-6. HT-GPC and HT-TGIC data for ethylene/1-octene copolymers with 12.9 mol % of 1-octene.

Sample ID	HT-GPC					HT-TGIC		
	M_n (g/mol)	PDI	r_n	AES	LES	T_P (°C)	σ	T_μ (°C)
C13-2.5	2 500	1.5	64	6	14	23.5	2.3	25.8
C13-4.5	4 500	2.0	116	6	18	53.9	10.6	59.5
C13-9.4	9 400	2.0	242	6	24	63.5	10.2	62.9
C13-15.4	15 400	1.9	397	7	28	68.9	10.9	67.7
C13-28.0	28 000	2.1	729	7	32	71.5	11.7	69.6
C13-48.8	48 800	2.1	1256	7	36	73.5	11.4	72.0
C13-57.3	57 300	2.2	1476	7	38	73.7	10.5	73.2
C13-127.0	127 000	2.1	3266	7	43	73.7	9.0	73.5

6.5.1 Chain Length and 1-Octene Mole Fraction Effect on HT-TGIC of Individual Polymer Samples

Figure 6-4 compares HT-TGIC profiles of all polyethylenes and ethylene/1-octene copolymers. For a given comonomer fraction, the HT-TGIC profiles broaden and shift towards lower temperatures when r_n decreases. More noticeably, when the 1-octene content increases, the HT-TGIC chromatograms shift to lower temperatures and become broader. This behavior is related to the shortening of the length of the ethylene sequences between short chain branching points,[87,88] which depends on SCB frequency but also on the r_n of the polymer sample. Therefore, samples with longer average ethylene sequences (lower SCB and higher r_n) will adsorb at higher temperatures onto the porous graphitic support than samples with shorter AES (higher SCB and lower r_n).

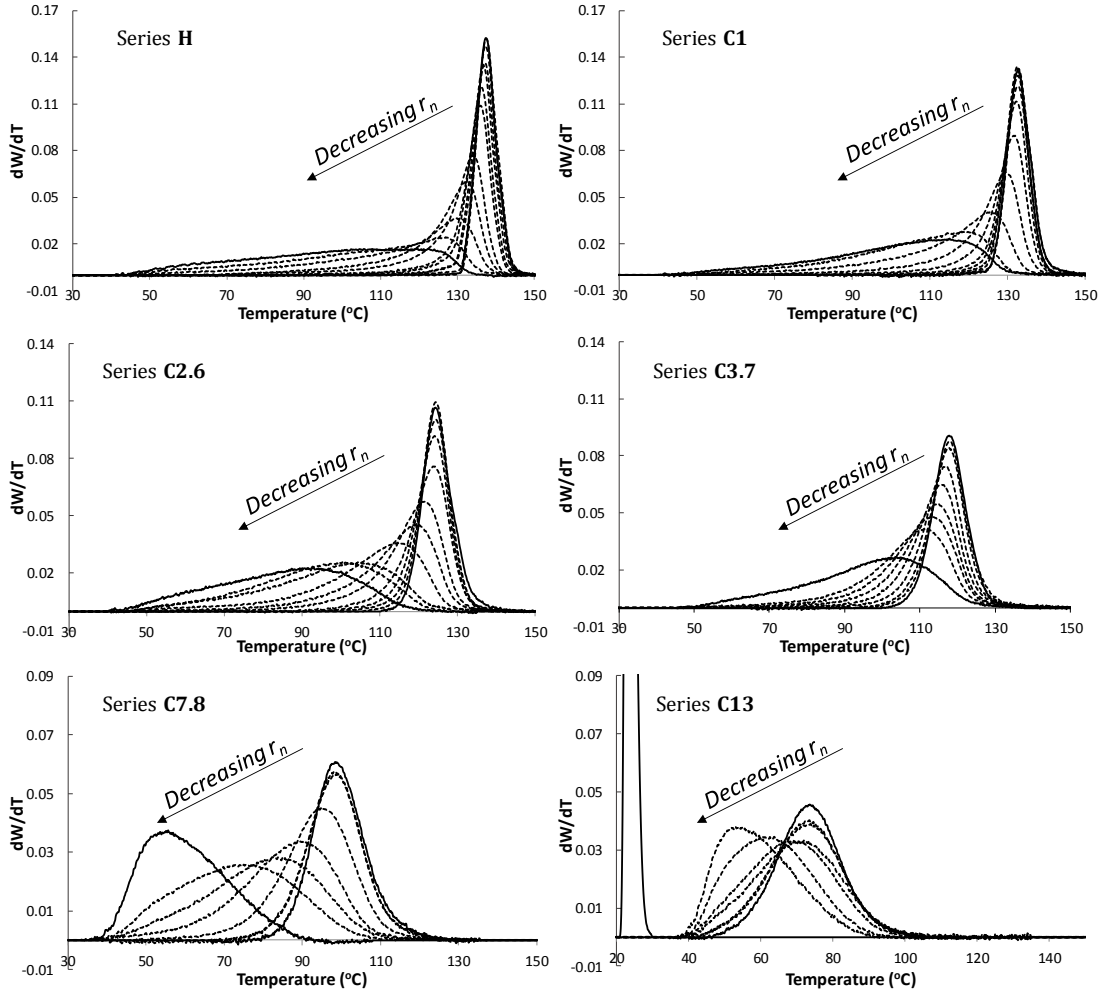

Figure 6-4. HT-TGIC profiles of polyethylenes and ethylene/1-octene copolymers with different r_n.

Figure 6-5, however, shows that the AES estimated with Monte Carlo simulation for these samples does not depend strongly on r_n, especially for samples with higher 1-octene contents, which is not surprising since 1-octene incorporation is the dominant factor controlling AES in these copolymers. Considering that the shapes and peak positions of the HT-TGIC profiles of samples with high comonomer content (such as C7.8 and C13) depend on r_n, AES cannot be used to explain r_n (or M_n) effects on HT-TGIC profiles.

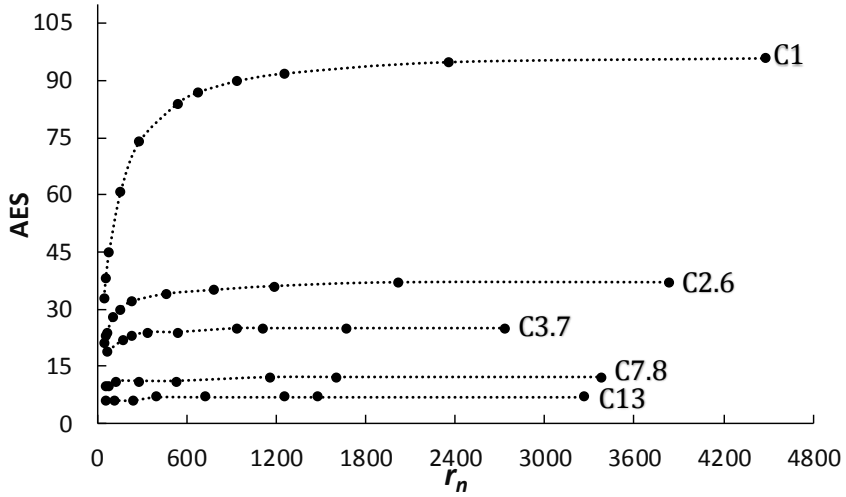

Figure 6-5. Average ethylene sequences (AES) depend weakly on r_n for ethylene/1-octene copolymers with a high 1-octene fraction.

Figure 6-6 shows that the average longest ethylene sequence length (LES) depends on r_n even for samples with higher 1-octene content, even though this dependency is more pronounced for samples with lower 1-octene fractions. Therefore, it seems that LES may explain r_n effects on HT-TGIC profiles more adequately than AES. Assuming that the length of the ethylene segments is responsible for the interaction between the support and the polymer chains, the longest ethylene sequences in the polymer should control, or at least substantially influence, the retention of the polymer in the HT-TGIC columns. For a given copolymer series this interaction weakens as LES decreases due to a reduction in r_n, and the peaks shift to lower temperatures.

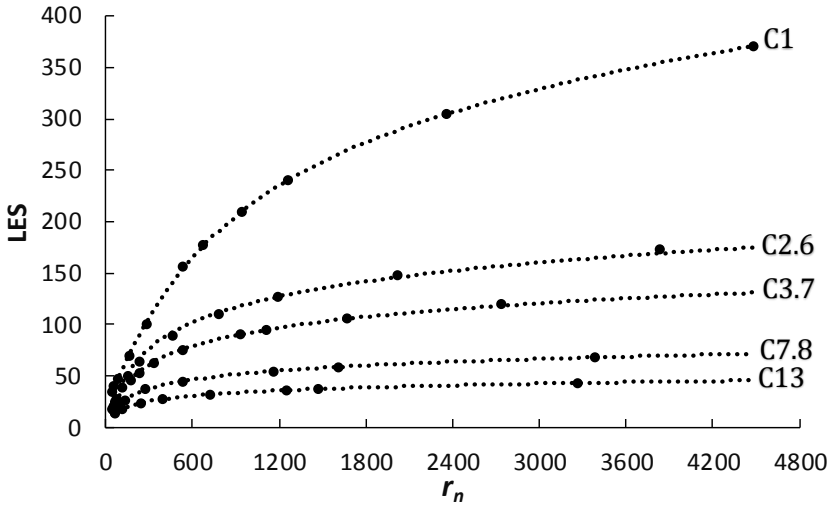

Figure 6-6. Average longest ethylene sequences (LES) depend more strongly on r_n for ethylene/1-octene copolymers.

It is illustrative to compare the overall ethylene sequence distribution (OESD) and the longest ethylene sequence distribution (LESD) estimated by Monte Carlo simulation for the five sets of ethylene/1-octene copolymers (Figure 6-7). The OESD does not depend substantially on copolymer molecular weight, particularly for samples with higher 1-octene content, but the LESD shifts to lower averages and becomes narrower when r_n decreases. The shift to lower LES correlates to the shift to lower temperatures of the experimental HT-TGIC profiles, *but contrarily to the experimental observations*, the LESD becomes narrower, not broader, as r_n decreases. This indicates that although we may loosely associate the change in HT-TGIC peak position to decreasing LES, the shape of the LES distribution cannot explain, and in fact contradicts, the broadening we observe in the HT-TGIC profiles as r_n decreases.

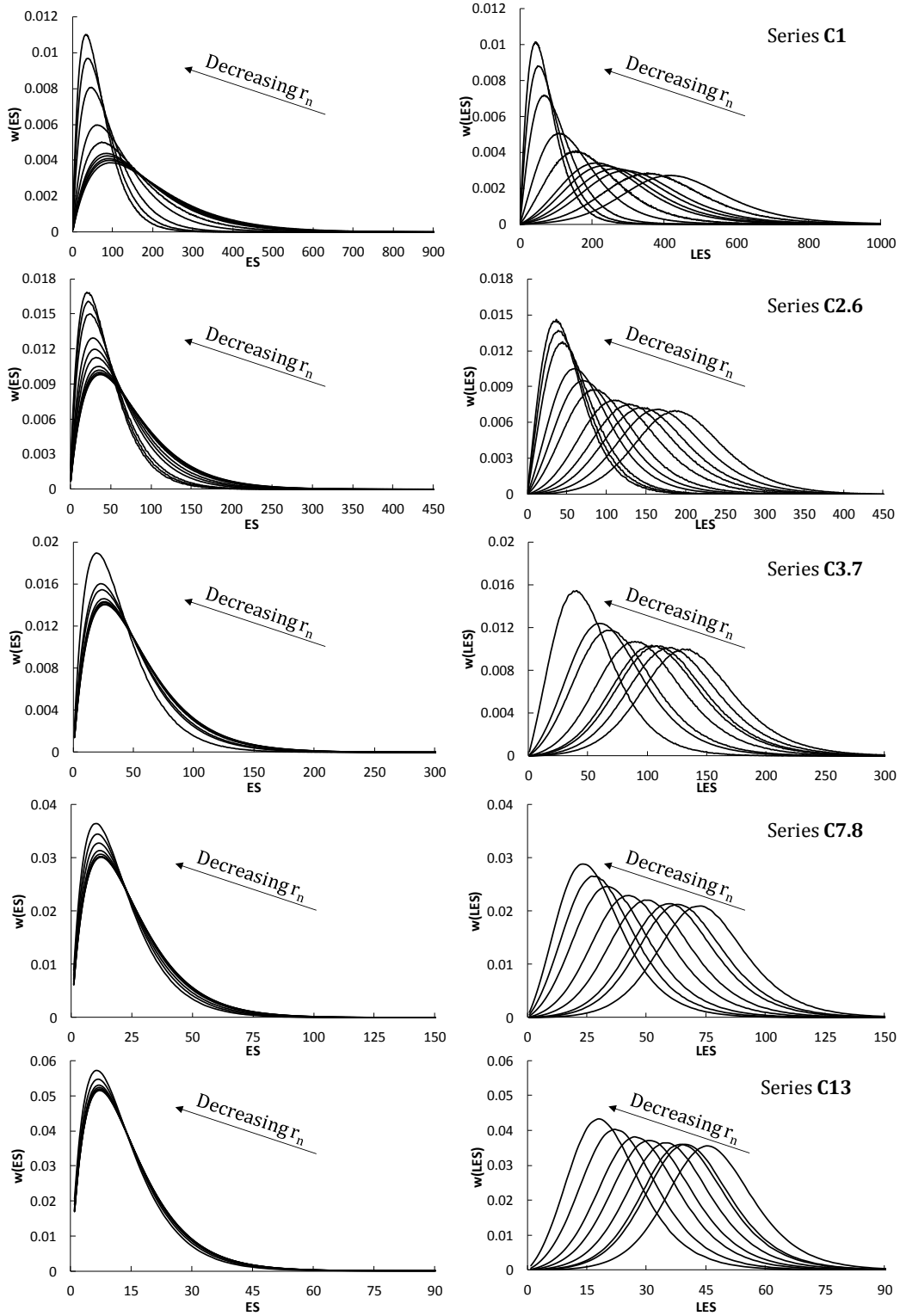

Figure 6-7. Overall ethylene sequence distributions (left), and longest ethylene sequence distributions (right) of ethylene/1-octene copolymers become narrow, and shift towards lower averages as r_n decreases.

Figure 6-8 shows that the peak elution temperature decreases exponentially below a critical r_n value ($\hat{r}_n$) for homopolymers and all five copolymer series. The value of T_P does not depend significantly on chain size for M_n > 24 000 g/mol or r_n > 850 for the homopolymer group, but $\hat{r}_n$ increases almost linearly with increasing mole fraction of 1-octene for the copolymer series, as illustrated in Figure 6-9. Therefore, the effect of r_n on HT-TGIC profiles is more pronounced for copolymers with increasing 1-octene contents. It seems that the porous graphite support in HT-TGIC columns has a moderate size exclusion effect, at least for chains with lower r_n. The fact that copolymers with higher comonomer content have higher critical r_n support this observation, since their hydrodynamic volumes would be lower. Interestingly, Sun *et al.*[93] reported a linear relation between the radius of gyration ratio and the fraction of 1-olefin for several ethylene/1-olefin copolymers, which agrees with our observations in Figure 6-9. In fact, porous graphic surface supports have been claimed for size exclusion chromatography separations in a recent patent by Dow Global Technologies.[94]

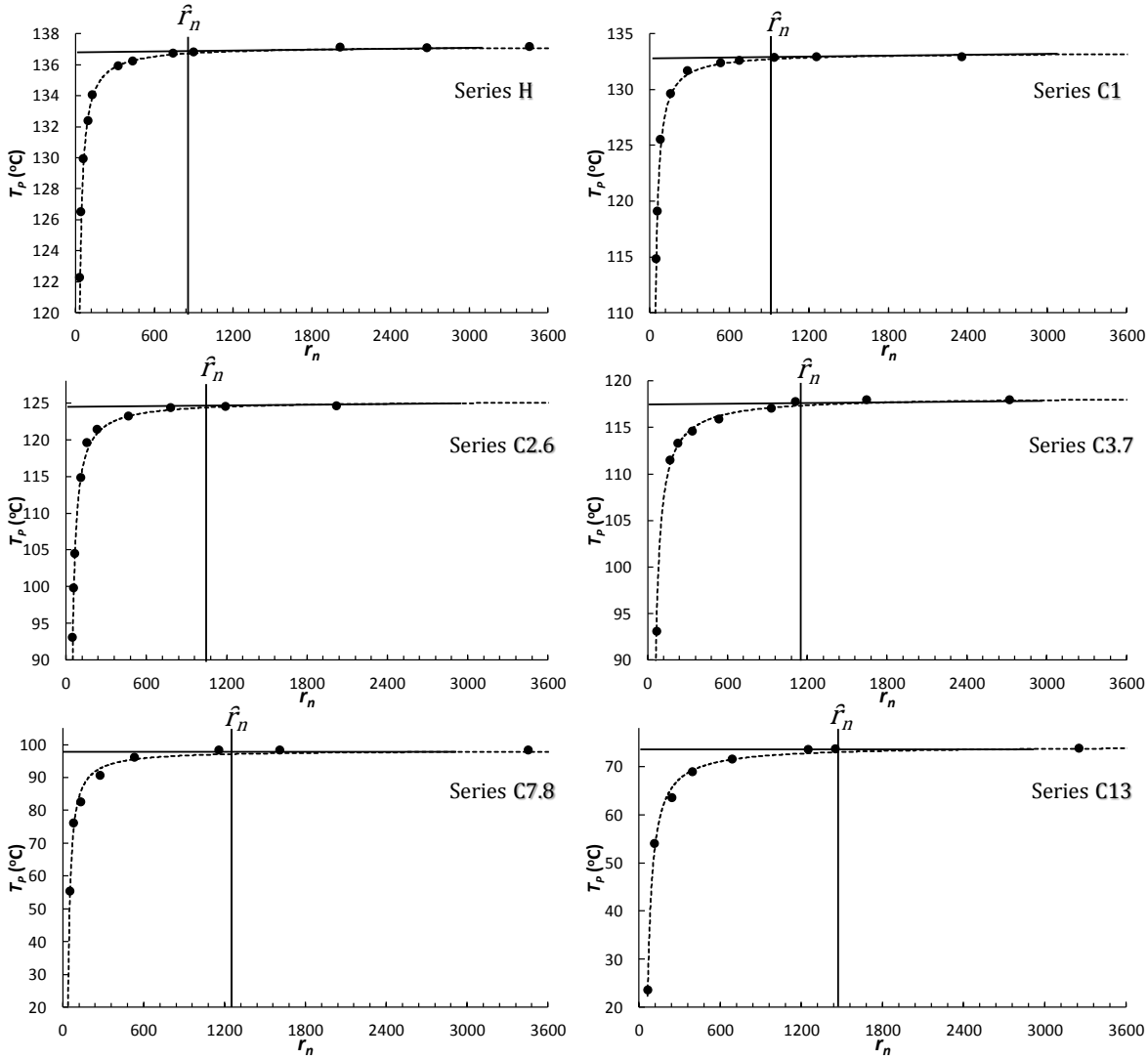

Figure 6-8. Elution peak temperature versus r_n for polyethylene and ethylene/1-octene copolymers, showing how the critical r_n ($\hat{r}_n$) gets higher when the fraction of 1-octene in the copolymer increases.

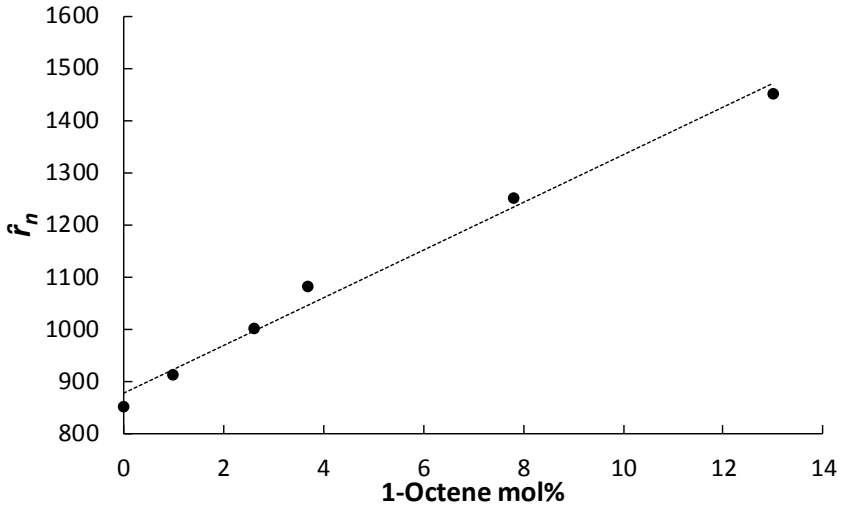

Figure 6-9. Relationship between the critical r_n ($\hat{r}_n$) and mole fraction of 1-octene in the copolymer.

Figure 6-10 shows that T_P does not depend on AES for copolymers with higher 1-octene samples, since copolymers with similar AES may have very different T_P values, as clearly illustrated within the shadowed area in Figure 6-10, but also apparent in other parts of the plot. A similar plot for LES (Figure 6-11) leads to a similar, and even more definite conclusion: Copolymers with similar LES have different T_P values if they have different 1-octene fractions. These plots prove that neither AES nor LES explain the shift in HT-TGIC peak temperature below $\hat{r}_n$.

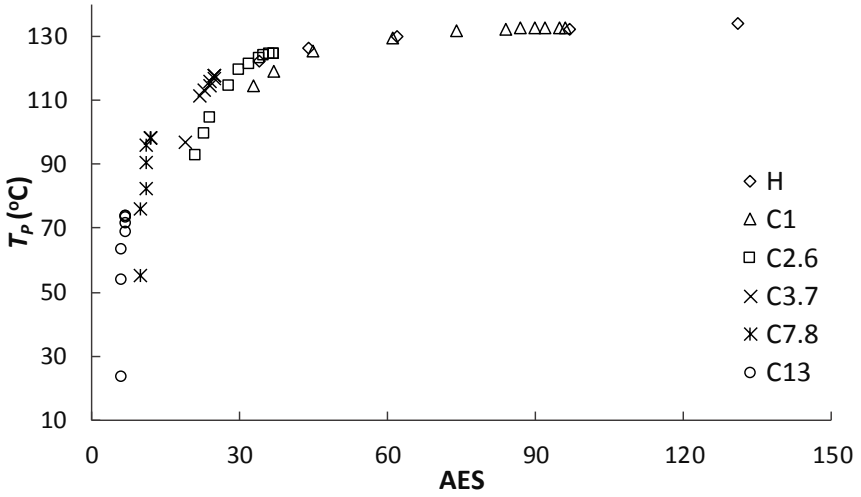

Figure 6-10. Peak temperatures do not depend on AES for samples with higher 1-octene fractions (C7.8 and C13).

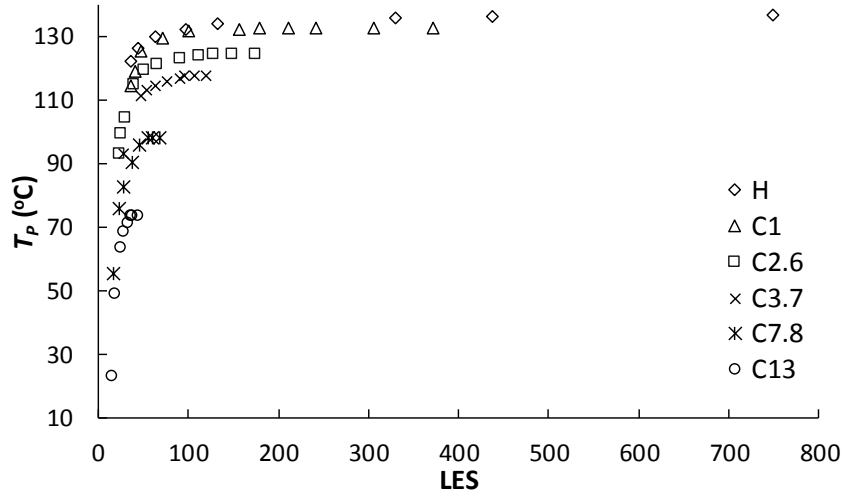

Figure 6-11. Peak temperatures do not depend on LES for all sets of ethylene/1-octene copolymers.

Interestingly, the plot of T_P x $1/r_n$ is approximately linear (Figure 6-12) for samples below $\hat{r}_n$. Since r_n and LES are related, the plot for T_P x 1/LES is also nearly linear (Figure 6-13). The slopes of these curves become steeper with increasing 1-octene fraction, showing that the HT-TGIC profiles of copolymer samples with higher comonomer contents are more sensitive to chain length effects (Figure 6-14).

This last finding indicates that LES is not a suitable variable to explain changes in HT-TGIC profiles due to changes in polymer chain length. We had already demonstrated in Figure 6-7 that lowering the copolymer average chain length caused the LES distribution to narrow, while the actual HT-TGIC profiles became broader (Figure 6-4). Now we showed that the T_P of copolymers with higher 1-octene fractions depend more strongly on r_n, but Figure 6-6 shows that LES for these samples depends only weakly on r_n. Therefore, neither LES or AES can describe adequately the fractionation mechanism of HT-TGIC. A more complex model, likely involving Van der Waals interactions between the support surface and polymer chains, polymer radius of gyration, and branching frequency and length is likely needed to explain the fundamental mechanism of HT-TGIC fractionation.

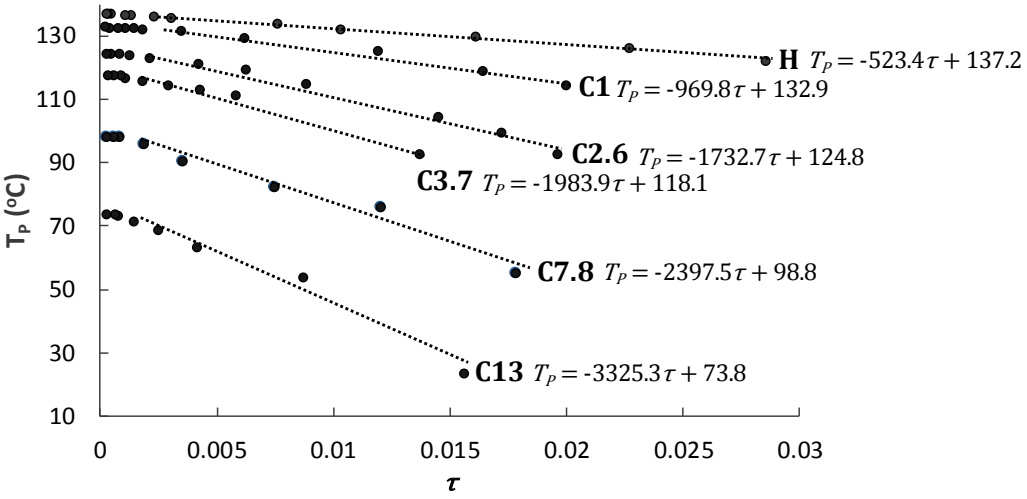

Figure 6-12. Elution peak temperatures versus $1/r_n$.

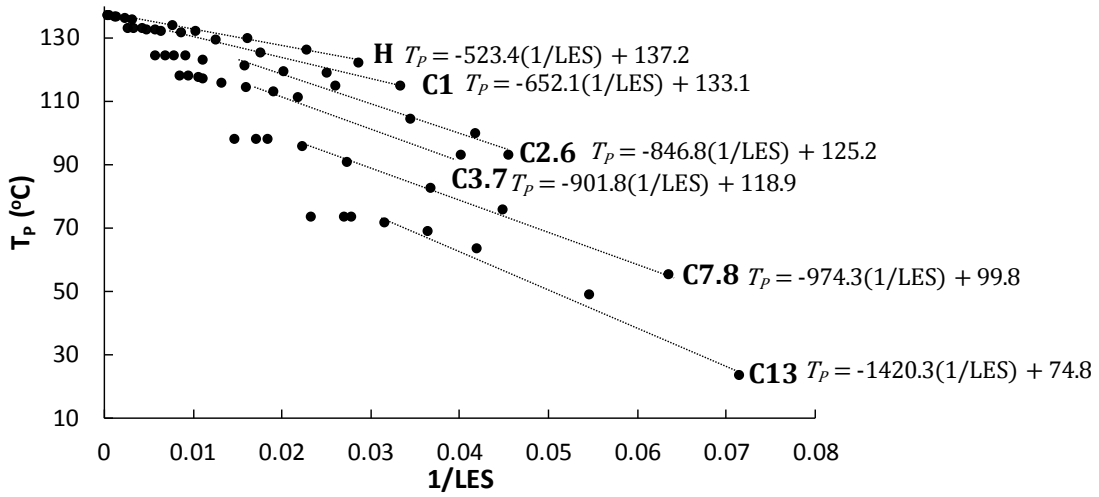

Figure 6-13. Elution peak temperatures versus 1/LES.

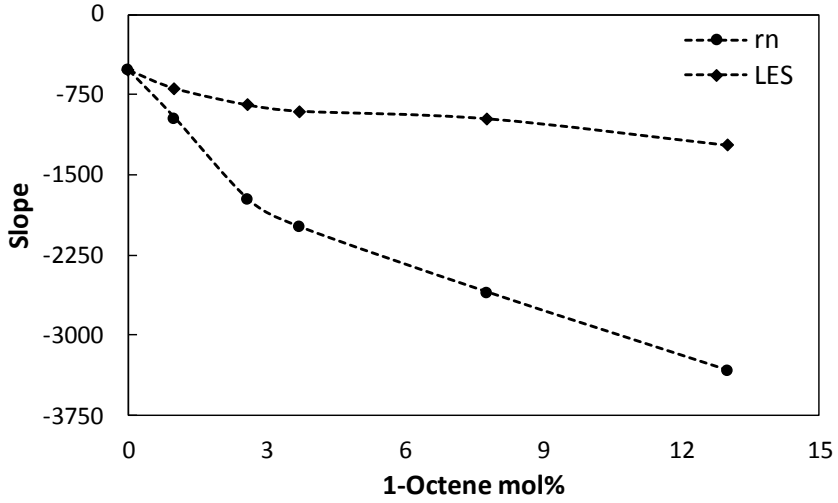

Figure 6-14. Slope of the curves shown in Figure 6-12 and Figure 6-13 versus 1-octene content in the copolymer.

Figure 6-15 summarizes the joint effect of chain length and 1-octene fraction on HT-TGIC peak temperature. Because of the nearly linear relationship, we choose to express this dependency as a function of $1/r_n$. A similar plot can be created using 1/LES, but it does not bring any new light to this problem, as LES clearly fails to describe the effect of chain length on HT-TGIC fractionation. We could have also substituted the 1-octene mol% axis in Figure 6-15 by CH_3/1000 C atoms to include the effect of chain ends on T_p, but this change would be minor for low r_n values, and negligible for polymers with higher r_n.

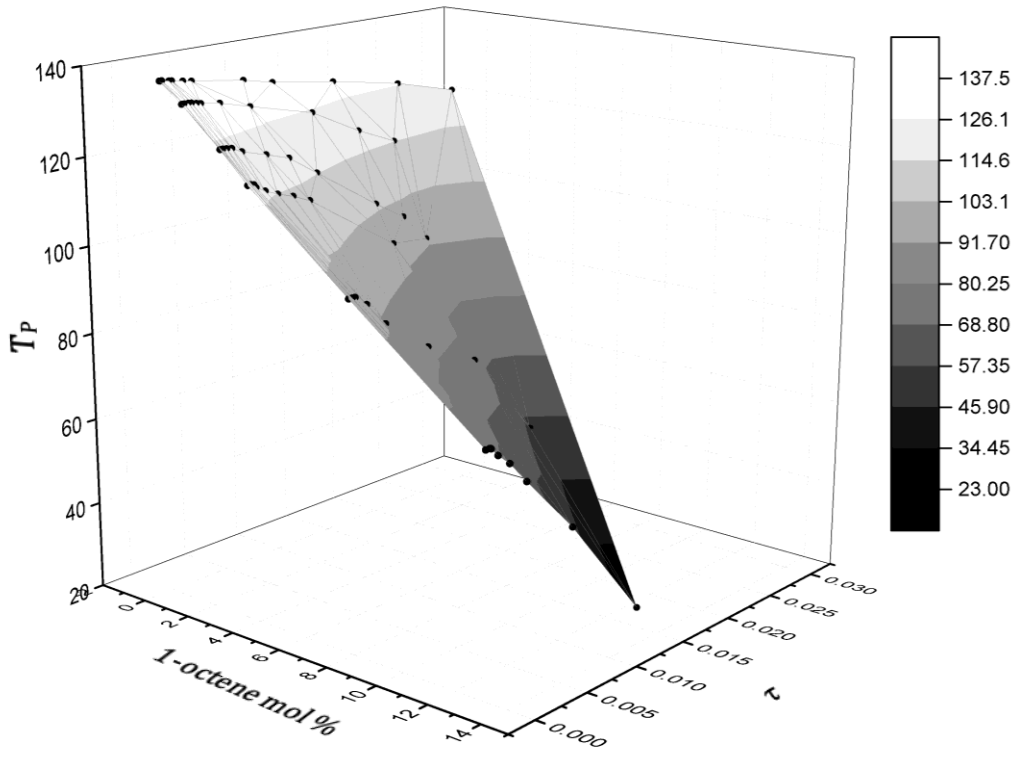

Figure 6-15. Joint effect of 1-octene mol% and r_n on HT-TGIC peak temperature.

6.5.2 Using Stockmayer Bivariate Distribution to Interpret HT-TGIC Profiles

The CCD of ethylene/1-olefin copolymers made with a single-site catalyst follows the chemical composition component of Stockmayer bivariate distribution,

$$w(y) = \int_0^\infty w(r, y).dr = \frac{3}{4 \times \sqrt{2\beta\tau}\left(1 + \frac{y^2}{2\beta\tau}\right)^{5/2}} \tag{6.5}$$

where $y = F_E - \bar{F}_E$, F_E is the molar fraction of ethylene in a copolymer chain, $\bar{F}_E$ is the average molar fraction of ethylene in the whole copolymer sample, τ is the reciprocal of r_n,

$$\tau = \frac{1}{r_n} \tag{6.6}$$

and β is a function of $\bar{F}_E$ and the product of the catalyst reactivity ratios ($r_1 r_2$),

$$\beta = \bar{F}_E(1 - \bar{F}_E) \cdot \sqrt{1 - 4\bar{F}_E(1 - \bar{F}_E) \cdot [1 - r_1 r_2]} \tag{6.7}$$

The lumped parameter $\beta\tau$ is equal to the variance (σ_s^2) of the Stockmayer distribution,

$$\sigma_s^2 = \beta\tau = \int (y - \hat{y})^2 \cdot w(y) \cdot dy \tag{6.8}$$

$$\sigma_s = \sqrt{\beta\tau} \tag{6.9}$$

We can use Equation (6.5) to evaluate whether HT-TGIC profiles are direct measurements of the CCD, or if peak broadening by axial dispersion or other effects influences the analysis.

We selected two samples with high r_n from each copolymer series investigated in this chapter (Table 6-7) to compare them with the Stockmayer distribution. These samples were selected because we wanted to avoid peak shift and broadening effects on the HT-TGIC due to the chain length.

Figure 6-16 shows the linear calibration curve for our HT-TGIC instrument, relating elution temperature (T_e) and the comonomer molar fraction (F_O),

$$F_E = 1 - F_O = 1 - (-0.002 \times T_e + 0.2749) \tag{6.10}$$

Since $y = F_E - \bar{F}_E$, then,

$$y = [1 - (-0.002 \times T_e + 0.2749)] - \bar{F}_E \tag{6.11}$$

Table 6-7. Stockmayer parameters and HT-TGIC-measured CCDs.

Sample ID	HT-TGIC			Stockmayer Parameters			σ_T/σ_S
	T_P (oC)	Avg. F_E	$\sigma_T \times 10^2$	$\tau \times 10^4$	$\beta \times 10^2$	$\sigma_S \times 10^2$	
C1-36.3	132.8	0.990	0.69	7.93	1.08	0.29	**2.4**
C1-68.1	132.9	0.990	0.51	4.23	1.08	0.21	**2.3**
C2.6-36.0	124.5	0.974	1.08	8.38	3.11	0.51	**2.1**
C2.6-61.1	124.5	0.974	0.85	4.93	3.11	0.39	**2.2**
C3.7-34.8	117.7	0.962	1.33	8.94	4.75	0.65	**2.0**
C3.7-52.1	117.8	0.962	1.08	5.58	4.75	0.51	**2.1**
C7.8-40.1	98.2	0.921	1.88	8.72	11.28	0.99	**1.9**
C7.8-55.7	98.2	0.921	1.67	6.21	11.28	0.83	**2.0**
C13-48.8	73.5	0.871	2.31	7.96	20.28	1.27	**1.8**
C13-57.3	73.6	0.871	2.11	6.47	20.28	1.14	**1.8**

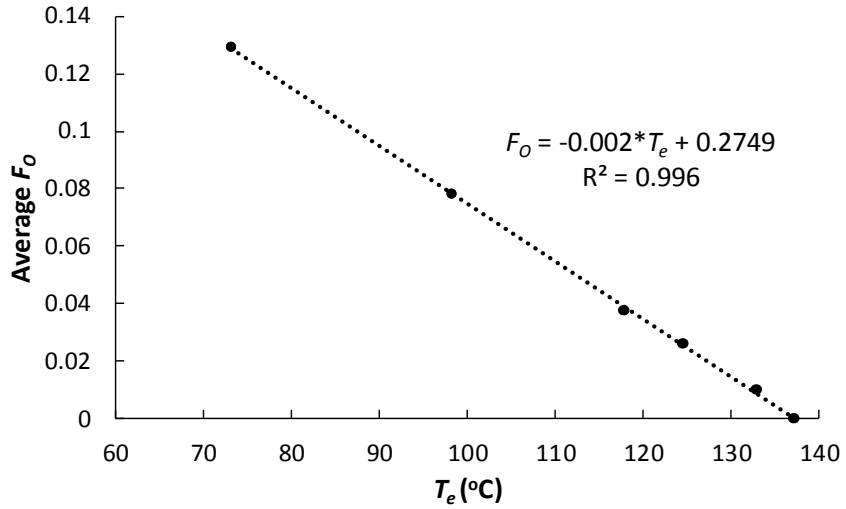

Figure 6-16. HT-TGIC calibration curve.

Figure 6-17 compares HT-TGIC chromatograms and Stockmayer CCDs based on the elution temperature for these samples. According to a previous estimate from the group,[95] we used r_1 r_2 = 6.07 to calculate the parameter β. The calibration curve presented in Figure 6-16 was used to obtain the HT-TGIC-measured CCDs.

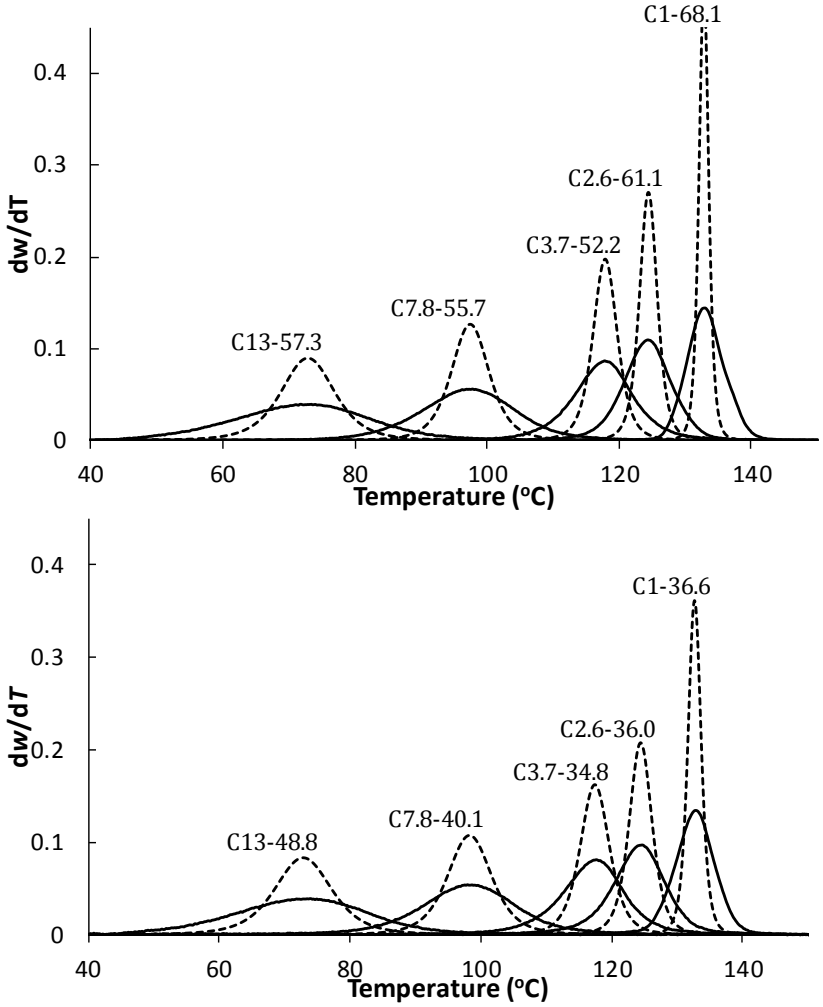

Figure 6-17. Comparison experimental (continuous line) and predicted (dotted line) HT-TGIC profiles.

The experimental HT-TGIC chromatograms are broader than the ones predicted by the Stockmayer distribution, perhaps because axial dispersion - a common phenomenon in most chromatography measurements - affects these profiles. We examined this possibility by plotting the ratio of the standard deviations of HT-TGIC profiles and Stockmayer distribution (σ_T / σ_s) in Figure 6-18. Interestingly, this ratio is nearly constant, increasing only slightly for samples with higher ethylene fraction. This suggests that axial dispersion in HT-TGIC is relatively independent of the 1-octene fraction for these samples.

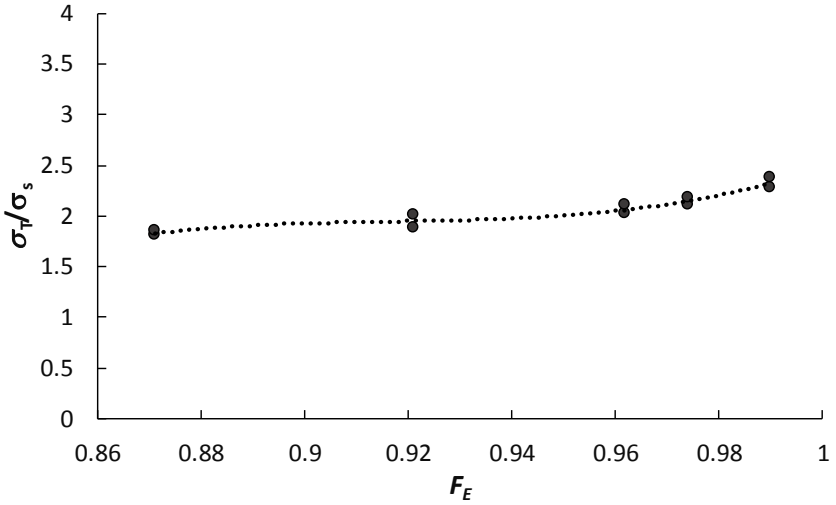

Figure 6-18. Relation between (σ_T/σ_S) and F_E for the samples in Figure 17.

We adjusted the Stockmayer distributions to fit the experimental HT-TGIC profiles by substituting the value of the product $\beta\tau(\sigma_s^2)$ with σ_T^2 determined for the equivalent HT-TGIC profile (Equation 6.5), as shown in Figure 6-19. These results show that the "broadened" Stockmayer distribution fits the HT-TGIC profiles surprisingly well, suggesting that symmetrical axial dispersion may be indeed responsible for the observed broader HT-TGIC profiles. In principle, correcting for axial dispersion should permit us to estimate the actual CCDs of polyolefins analyzed by HT-TGIC. This is an important finding, since it shows that for chain lengths above the critical r_n, HT-TGIC profiles reflect the actual distribution of 1-olefin in the copolymer. Furthermore, it may be possible to develop a fundamental model for axial dispersion in the HT-TGIC columns that takes into account flow rates and polymer molecular diffusivity during the fractionation.

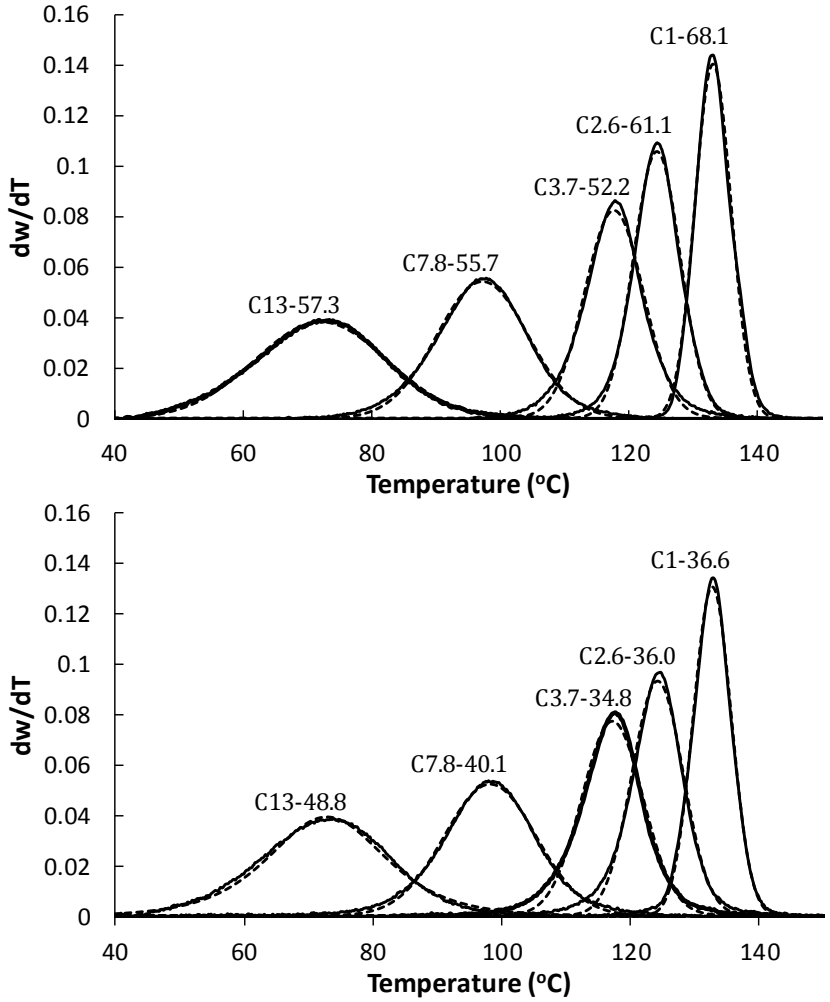

Figure 6-19. Comparison of HT-TGIC profiles and broadened Stockmayer distributions.

6.5.3 Chain Length and 1-Octene Mole Fraction Effect on the HT-TGIC Analysis of Blends

When HT-TGIC analyzes binary blends of ethylene/1-olefin copolymers, sometimes copolymers of different compositions affect each other's HT-TGIC profiles, a phenomenon that has been attributed to co-adsorption and/or co-desorption of these species. The copolymer microstructure and analytical conditions influence this phenomenon. The co-desorption index (CDI) was defined to quantify these effects using Equation 4.4.

We selected two blend groups, Group A (comprising samples from series C1 and C3.7) and Group B (comprising samples from series C3.7 and C13), to study the effect of r_n and 1-octene fraction on HT-TGIC fractionation. Each blend was labeled as shown in Figure 6-20, where the components of the blends are separated by a comma, with the first letter indicating the 1-octene level (L = low, H = high), and the second letter representing the M_n level. The co-desorption index of each blend is presented in Table 6-8.

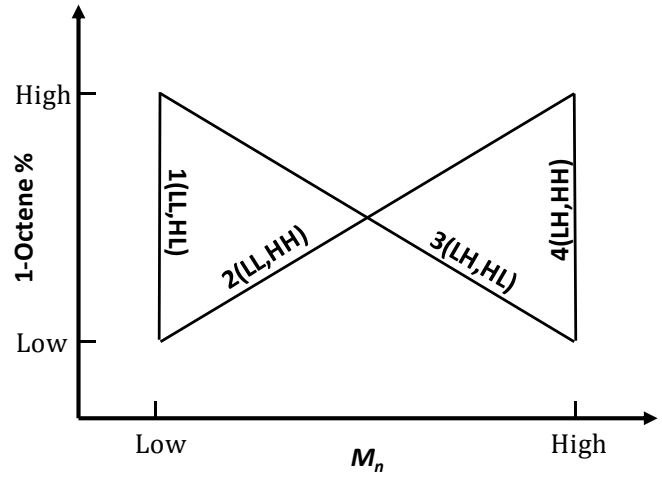

Figure 6-20. Nomenclature for the dual-resin blends.

Table 6-8. Co-desorption index of the two major group blends.

Blend ID	Sample ID	LES	AES	Sample ID	LES	AES	AES Ratio	LES Ratio	CC Ratio	CDI
A1(LL,HL)	C1-4.6	70	61	C3.7-5.4	46	22	2.8	1.5	3.7	0.112
A2(LL,HH)	C1-4.6	70	61	C3.7-52.2	106	25	2.5	1.5	3.7	**0.330**
A3(LH,HL)	C1-68.1	305	95	C3.7-5.4	46	22	4.3	6.6	3.7	0.122
A4(LH,HH)	C1-68.1	305	95	C3.7-52.2	106	25	3.8	2.9	3.7	0.113
B1(LL,HL)	C3.7-5.4	46	22	C13-4.5	18	6	3.6	2.5	3.5	0.134
B2(LL,HH)	C3.7-5.4	46	22	C13-57.3	38	7	3.1	1.2	3.5	**0.338**
B3(LH,HL)	C3.7-52.2	106	25	C13-4.5	18	6	4.1	5.9	3.5	0.165
B4(LH,HH)	C3.7-52.2	106	25	C13-57.3	38	7	3.6	2.8	3.5	0.136

Figure 6-21 and Figure 6-22 compared the experimental and predicted HT-TGIC profiles of Group-A and Group-B blends, respectively. In both groups, r_n had no significant impact on the HT-TGIC profile when one of the blend components had low 1-octene mole fraction and high r_n (blends A3, A4, B3, and B4). Furthermore, when both components of the blend (A1 and B1) had low r_n, the value of the co-desorption index was small. On the other hand, the experimental and predicted HT-TGIC profiles did not match when one of the blend components had low 1-octene mole fraction and low r_n (A2 and B2). The component with low 1-octene fraction and low r_n in the blend seemed to increase the co-desorption index.

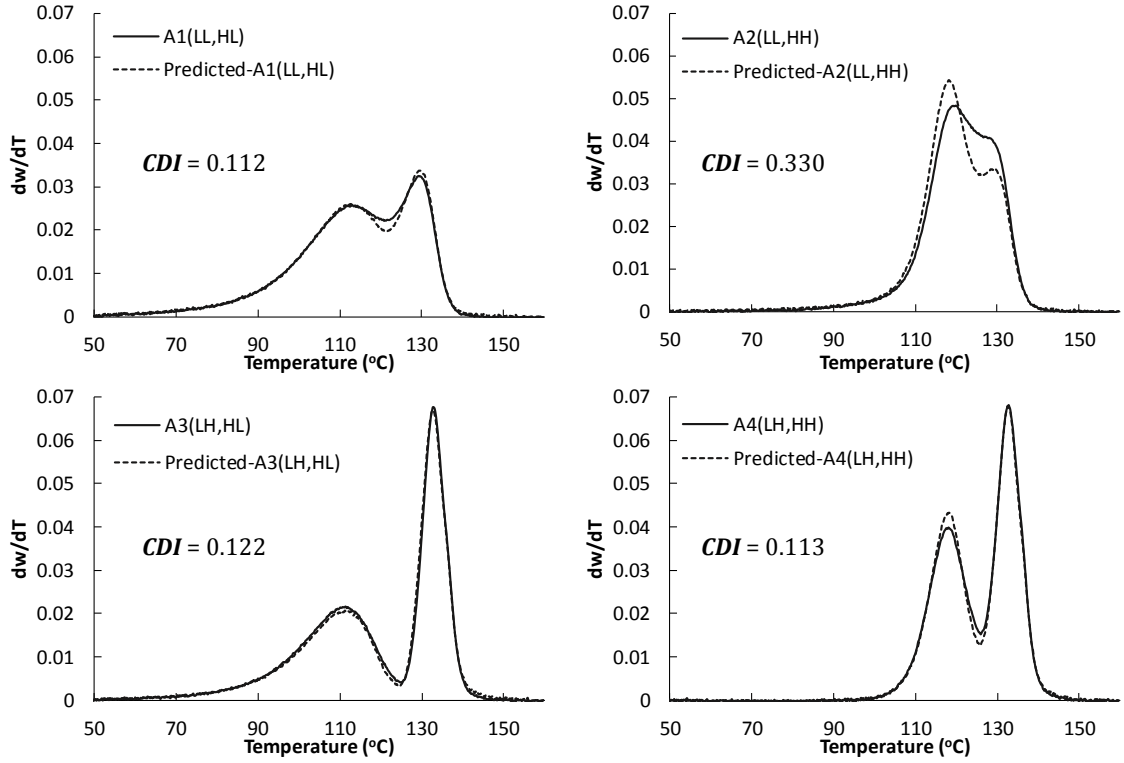

Figure 6-21. Experimental and predicted HT-TGIC profiles of Group-A blends.

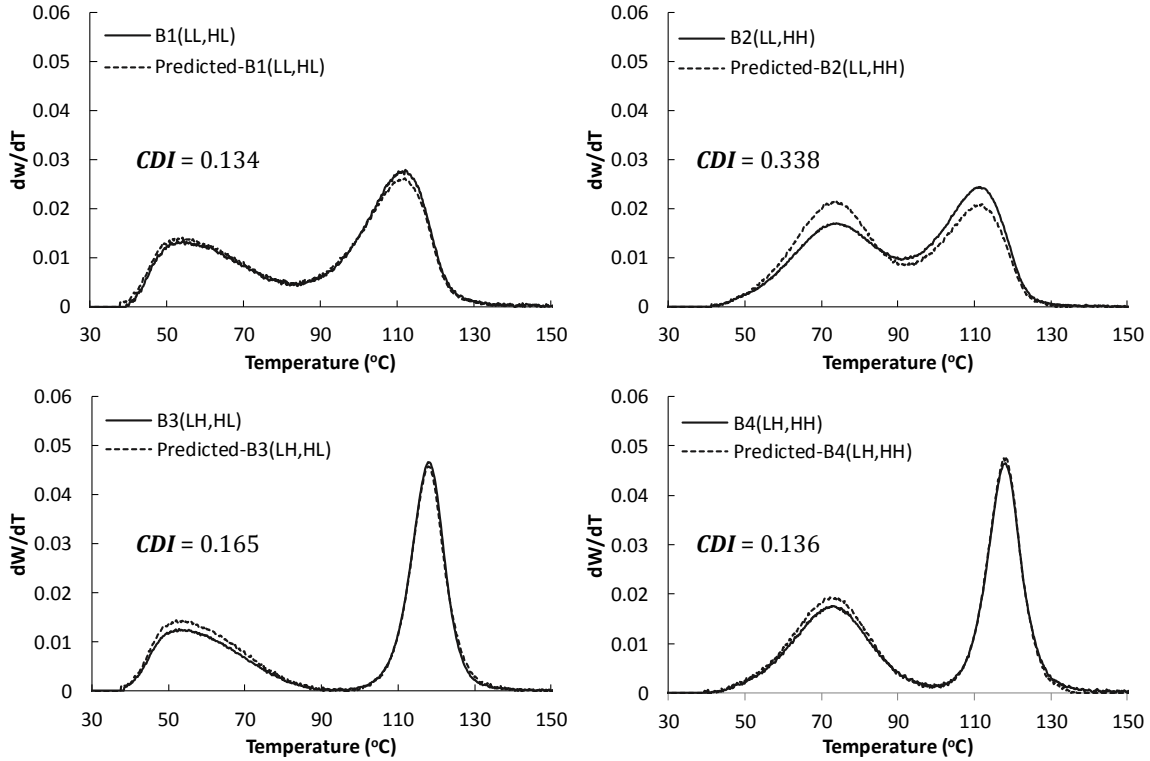

Figure 6-22. Experimental and predicted HT-TGIC profiles of Group-B blends.

We extended the study of Blend-A2 and Blend-B2 by choosing four other different blends (Table 6-9), all having one component with low r_n, to test whether our observations with Blends A and B extended to other cases. Figure 6-23 shows that their predicted profiles did not agree well with their experimental profiles, and that they had a high value of co-desorption index.

Table 6-9. Additional blends used to study the effect of M_n on the co-desorption index.

Blend ID	Sample ID	LES	AES	Sample ID	LES	AES	AES Ratio	LES Ratio	CC Ratio	CDI
C2(LL,HH)	H-2.7	97	97	C3.7-52.2	106	25	3.9	1.1	-	**0.331**
D2(LL,HH)	C1-4.6	70	61	C7.8-55.7	59	12	5.1	1.2	7.8	**0.271**
E2(LL,HH)	C2.6-4.8	50	30	C9.8-67.1*	54	9	3.3	1.1	3.7	**0.316**
F2(LL,HH)	C7.8-4.6	27	11	C16.4-61.3*	30	5	2.2	1.1	2.1	**0.244**

* These samples are from Category I

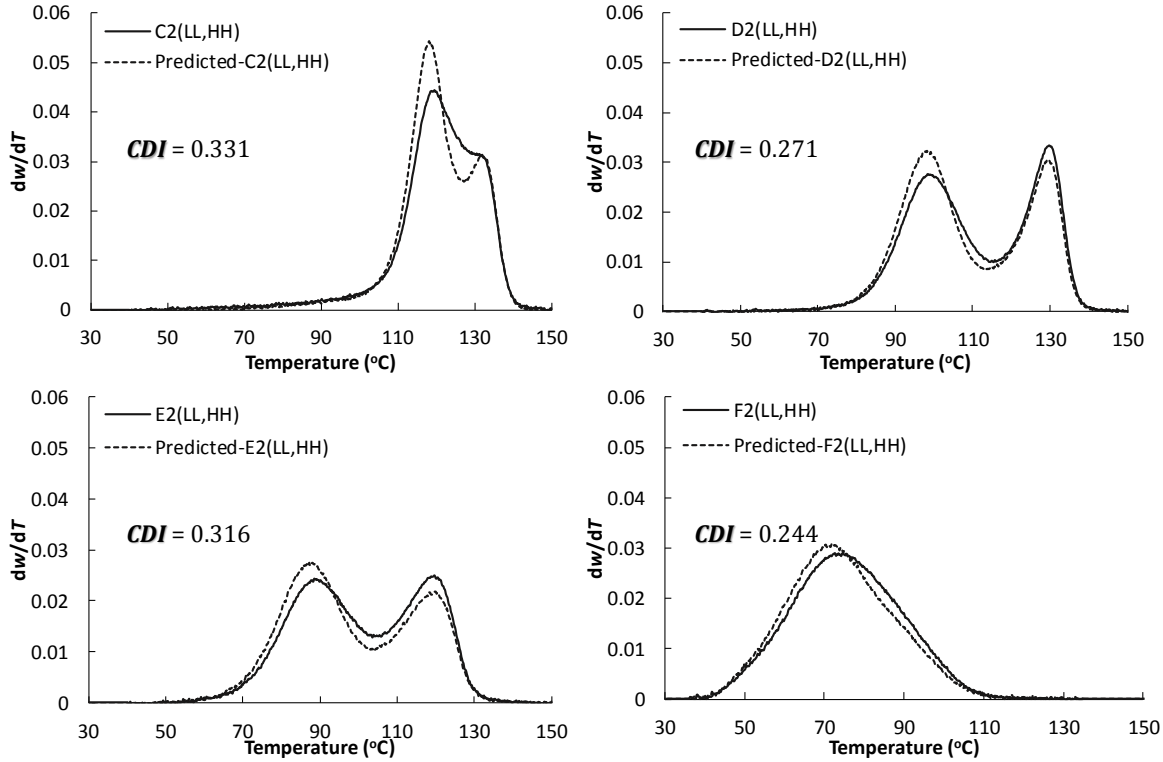

Figure 6-23. Experimental and predicted HT-TGIC profiles of Blend-C2, Blend-D2, Blend-E2, and Blend-F2.

We calculated the ratio of AESs for both components in each blend to figure out whether similar AES among the blend components favored co-adsorption/co-desorption. Figure 6-24 shows that CDI does not correlate with the AES ratio of the blend components.

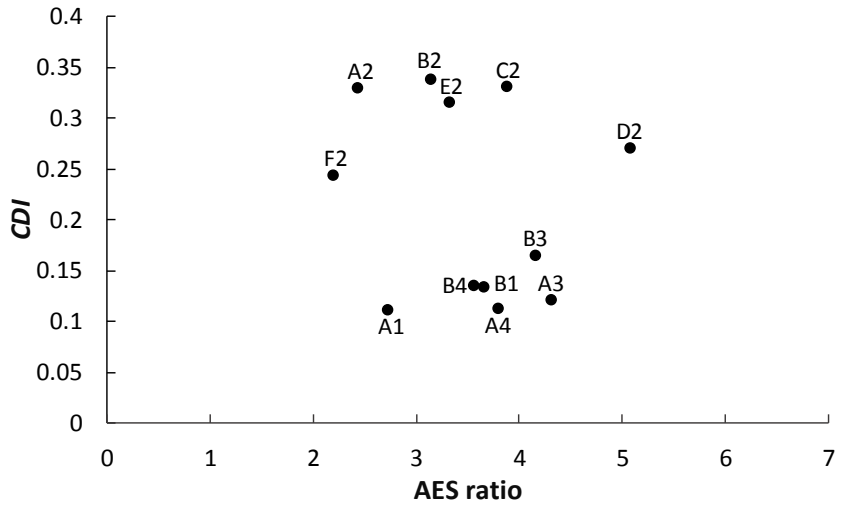

Figure 6-24. Relation between co-adsorption index and AES ratio of all blends.

The plot of the LES ratio versus CDI apparently divides these blends into two main regions: a high CDI range (CDI > 0.2, see shaded area in Figure 6-25) where co-adsorption is more prevalent, and a low CDI range (CDI < 0.2). Most samples having LES ratios close to 1 have a relative high CDI, except for Blend-A1. This seems to suggest, equivocally as we will explain below, that samples with similar LES are more likely to co-adsorb onto the support surface.

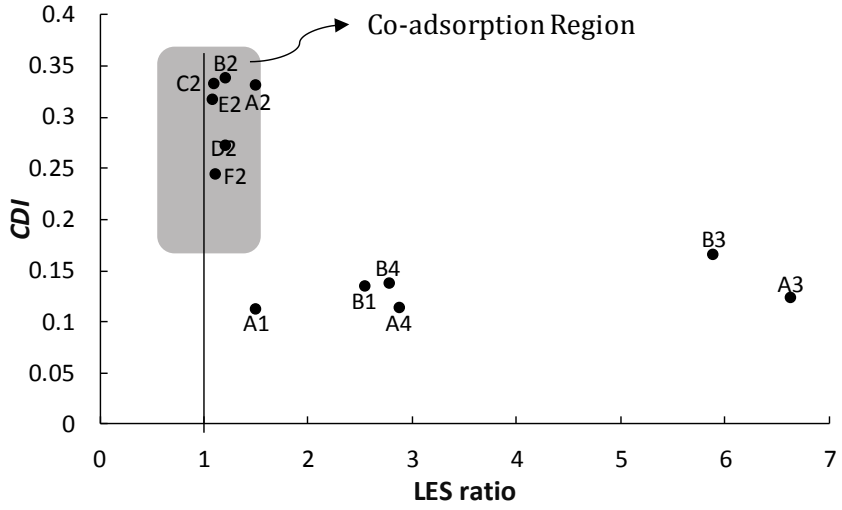

Figure 6-25. Relation between the co-adsorption index and LES ratio of all blends.

However, we cannot understand these results properly if we ignore the effect of the 1-octene content ratio on CDI. Figure 6-26 shows the combined effect of the LES ratio and the chemical

composition (CC) ratio on CDI. The 3D plot shows that for a given CC ratio, CDI will increase with increasing LES ratio, that is, as the chain lengths become more dissimilar in length; it also shows that for the same LES ratio, CDI will increase when the chains have more similar comonomer molar fractions (smaller CC ratios). Therefore, similar comonomer contents, not similar LES, favor co-desorption on the HT-TGIC support.

We arrive at a similar conclusion by plotting CDI versus CC ratio and r_n ratio, as shown in Figure 6-27. For a given CC ratio, chains with more dissimilar r_n will have a higher CDI. This is the opposite of what would be expected if the fractionation mechanism in HT-TGIC was governed mainly by the adsorption of ethylene sequences on the support surface since, in this case, one would expect samples with similar LES to co-elute from the column. Rather, it seems that copolymers with low r_n and low 1-octene fraction somehow affect the adsorption behavior of the other component, causing them to elute from the column at higher temperatures, as shown in Figures 23 to 25.

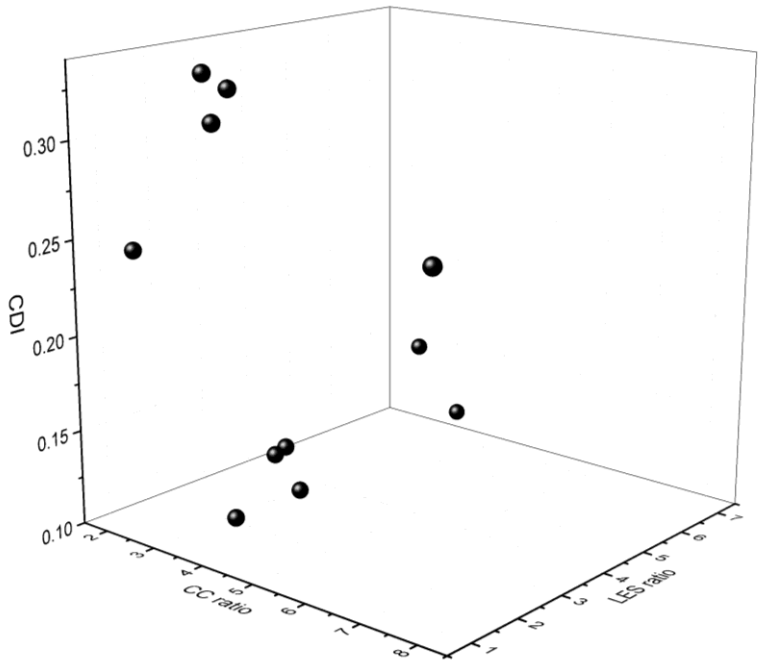

Figure 6-26. 3D plot showing how the co-desorption index (CDI) varies with CC ratio and LES ratio.

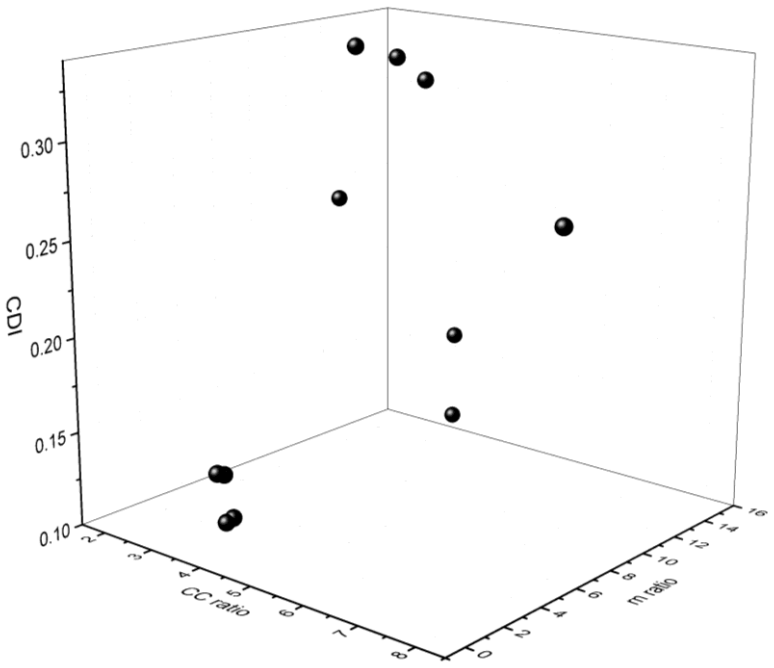

Figure 6-27. 3D plot showing how the co-desorption index (CDI) varies with CC ratio and r_n ratio.

6.6 Conclusions

We investigated the joint influence of 1-octene fraction and number average chain length (r_n) on HT-TGIC profiles using one series of polyethylenes and five series of ethylene/1-octene copolymers having different average chain lengths but similar 1-octene fractions. The peak elution temperature (T_P) decreases exponentially below a critical r_n value that depends linearly on the fraction of 1-octene in the copolymer, and copolymers with more 1-octene have a higher critical r_n. Interestingly, the value of T_P decreased approximately linearly with $1/r_n$ below the value of critical r_n.

We investigated the hypothesis that longer ethylene sequences in the polymer made the chains adsorb more strongly onto the support using distributions for the overall ethylene sequence (OESD) and average longest ethylene sequences (LESD) generated by Monte Carlo simulation, but neither distribution provided an adequate correlation between T_P and ethylene

sequences. The mechanism of fractionation in HT-TGIC is more complex than these simple models can predict.

Stockmayer distribution, on the other hand, describes the shapes of the HT-TGIC profiles of copolymers above the critical r_n correctly, but systematically predicts narrower distributions than the experimental ones. Interestingly, it is easy to correct these distributions by applying a symmetrical broadening factor that depends only slightly on 1-octene fraction, suggesting that axial dispersion may be responsible by this broadening. This finding indicates that we could apply an axial dispersion correction factor to transform HT-TGIC profiles into the actual chemical composition distributions of these copolymers, provided that the samples are above the critical r_n.

We combined some of the copolymer samples to study the effect of co-adsorption/co-desorption on the HT-TGIC of binary blends. Interestingly, when the blend components had very different average longest ethylene sequence lengths but similar average comonomer fractions, they affected each other's profiles more significantly. This effect was particularly noticeable when one of the blend components had low r_n and low 1-octene fraction. Even though the reason for this effect is not clear, we could not relate it to similarities between the average longest ethylene sequences (LES) of the two blend components, which discards the hypothesis that LES is a factor controlling the co-adsorption of these copolymers.[4]

[4] Appendix D shows the results of using the *weight* average ethylene sequence length (W_AES) and *weight* average longest ethylene sequence length (W_LES) instead of AES and LES. This alternative way of calculating these sequences did not affect the conclusions of this chapter.

Chapter 7. Conclusions and Recommendations

7.1 Conclusions

High-temperature thermal gradient interaction chromatography has become an important technique to measure the CCD of polyolefins, on par with more traditional methods such as TREF, CRYSTAF and CEF. HT-TGIC has better advantages over these techniques; 1) it can analyze ethylene/1-olefin copolymers over a wider compositional range, since the fractionation mechanism is not based on polymer crystallization; 2) it requires shorter analysis times because adsorption/desorption processes are faster than polymer crystallization; and 3) it is free of co-crystallization effects that plague TREF, CRYSTAF and CEF.

The main objective of this research was to study HT-TGIC fractionation systematically to better understand its mechanism and to propose operation conditions to maximize peak resolution and minimize analysis times. To achieve these objectives, we used several sets of ethylene/1-octene copolymers made with a single site catalyst under controlled conditions.

We used a 2^3 experimental factorial design to study the influence of analytical operation conditions on the shape and position of the HT-TGIC chromatograms of individual ethylene/1-octene copolymer samples and binary blends. During the adsorption cycle, the cooling rate had no significant effect on the desorption temperature or broadness of the HT-TGIC chromatograms of both individual samples and blends. This indicates that interactions between the polyethylene chains and the graphite surface are not strongly affected by how fast the column is cooled. Therefore, it is recommended that the fastest cooling rate is used to reduce analysis time.

Operating parameters for the desorption cycle – heating rate and elution flow rate, as well as their interactions – influenced peak temperature values, breadth of HT-TGIC profiles, and co-desorption. Increasing the heating rate shifts HT-TGIC peaks to higher temperatures since the desorption temperature detected by the time that the solvent has reached the detector at the end

of the column is higher. Furthermore, slow elution flow rates broaden the HT-TGIC profile and shift its peak temperature to a higher value due to an increase in residence time of the polymer solution in the column. The preferred analytical conditions are a cooling rate of 5 ºC/min, a heating rate of 3 °C/min, and an elution flow rate of 0.5 mL/min. These conditions reduce the co-desorption index (better resolution) and minimize the analysis time for the range of samples covered in this research.

We also considered the effects of column length and particle size averages of the porous graphite carbon packing on the fractionation of ethylene/1-octene copolymers by HT-TGIC. Two lengths (100 and 250 mm) and three average particle sizes (3, 5, and 7 μm) of Hypercarb columns were compared. Neither average particle size nor column length played an important role to enhance the resolution of HT-TGIC profile of polyolefins and their blends. Therefore, it is preferable to use shorter columns with larger particles, since peak broadening due to axial dispersion is more severe in longer columns, and higher operation pressures and plugging during analysis are more likely to happen in columns packed with smaller particles.

We also investigated the joint influence of 1-octene fraction and number average chain length (r_n) on HT-TGIC profiles. Below a critical r_n value, the peak elution temperature of each polymer series decreased exponentially, and the profile broadened. Interestingly, the critical r_n value increases linearly with increasing the fraction of 1-octene in the copolymer and the value of the peak elution temperature decreased approximately linearly with $1/r_n$ below the critical r_n value.

We used Monte Carlo simulation to generate the distributions of overall ethylene sequence (OESD) and longest ethylene sequence (LESD) to test the hypothesis that longer ethylene sequences in the polymer made the chains adsorb more strongly onto the support. We found out that the fractionation mechanism in HT-TGIC is more complex than these simple models describe because both distributions did not provide an adequate correlation between the shape and position peak of HT-TGIC profiles and ethylene sequences. On the other hand, for samples with chain length averages above the critical r_n, Stockmayer distribution describes the shapes

of the HT-TGIC chromatogram correctly, but systematically predicts narrower distributions than the experimental ones. Interestingly, these distributions can be made to match by applying a symmetrical broadening factor, suggesting that axial dispersion causes the observed peak broadening. This finding indicates that we could apply an axial dispersion correction factor to transform HT-TGIC profiles into the actual chemical composition distributions of these copolymers, provided that the samples are above the critical r_n.

Finally, we studied the effect of co-adsorption/co-desorption on the HT-TGIC of binary blends having components that varied in r_n and 1-octene fraction. For a given 1-octene fraction, the blend components affected each other's profiles more significantly when they had very different average longest ethylene sequence (LESs). This effect was particularly noticeable when one of the blend components had low r_n and low 1-octene fraction. Therefore, similar average longest ethylene sequences of the two blend components cannot be the cause of the co-adsorption/co-desorption phenomenon, which invalidates the hypothesis that LES is a factor controlling this phenomenon.

The main contributions of this thesis are summarized below.

1. Influence of analytical operation conditions.

    1.1. The cooling rate had no significant influence on the value of peak elution temperature and on the shape of the HT-TGIC profiles of individual samples and their blends.

    1.2. Desorption parameters (heating rate and elution flow rate) and their interactions affected the peak elution temperature and the broadness of HT-TGIC profile of individual samples and their blends.

    1.3. The preferred analytical conditions (CR= 5 °C/min, HR= 3 °C/min, F_E=0.5 mL/min) reduce the co-desorption index (better resolution) and minimize the analysis time for at least the range of samples covered in this thesis.

2. Effect of Hypercarb column type.

    2.1. Neither average particle size nor column length enhanced the resolution of HT-TGIC profile of polyolefins and their blends.

    2.2. It is preferable to use shorter columns with larger particles.

3. Joint effect of chain length and comonomer mole fraction.

    3.1. For a given comonomer content, the HT-TGIC chromatogram broadens and shifts towards lower temperatures, which is more pronounced for higher 1-octene mole fraction.

    3.2. In each series, the peak elution temperature decreased exponentially below a critical value for the chain length.

    3.3. LESD and OESD did not provide an adequate correlation between the shape and peak position of HT-TGIC profiles and ethylene sequences.

    3.4. For the samples having chain length average above the critical value, Stockmayer distribution describes the shapes of HT-TGIC profiles correctly, but systematically predicts narrower distributions than the experimental ones.

    3.5. Axial dispersion may broaden HT-TGIC profiles.

    3.6. Similar average longest ethylene sequences lengths of blend components is not the cause of the co-desorption phenomenon.

7.2 Recommendations and Future Work

HT-TGIC is the next major step in a long sequence of polyolefin CCD-characterization techniques that started in the eighties with TREF. Understanding the fractionation mechanism of HT-TGIC was the main target in this research. To extend the scope of this work, the following investigations are suggested:

1. Repeating this study to ethylene/1-olefin copolymers with comonomers other than 1-octene will permit understanding the effect of olefin type on HT-TGIC profiles. Ethylene/1-olefin copolymers samples having similar chain lengths and comonomer contents will help investigate the effect of SCB length on HT-TGIC fractionation. Of particular importance would be very long SCB, perhaps reaching up to long chain branch (LCB) values to check whether HT-TGIC could be used to measure small amounts to LCB in the polymer.
2. Ethylene polymerization with non-linear comonomer (branched or aromatic) should be considered to investigate the effect of SCB topology on HT-TGIC profiles.
3. A series of polypropylenes with different tacticities should be synthesized to investigate how HT-TGIC fractionates polypropylene according to stereo- and regio-defects.
4. It would be interesting to develop a fundamental model for axial dispersion in the HT-TGIC columns that takes into account flow rates and polymer molecular diffusivity during the fractionation.
5. All this information combined may eventually lead to the development of a universal calibration curve for HT-TGIC, similarly to the universal calibration curve for gel permeation chromatography. If achievable, this would make HT-TGIC one of the most useful techniques to characterize olefin copolymers.

Bibliography

1. Soares J, Mckenna T. *Introduction to Polyolefins*. In: *Polyolefin Reaction Engineering*. Vol Verlag Gmb. First Ed. Weinheim, Germany: Wiley-VCH; **2012**:1-13.

2. Soares J, Mckenna T, et al. *Coordination Polymerization*. In: *Polymer Reaction Engineering*. Vol Verlag Gmb. First Ed. Blackwell Publishing; **2008**:365-430.

3. Parvez MA, Rahaman M, et al. *Effect of long chain branching on the properties of polyethylene synthesized via metallocene catalysis*. Polymer Science Series B. **2014**;56(6):707-720.

4. Soares J. *Polyolefins with Long Chain Branches Made with Single-Site Coordination Catalysts: A Review of Mathematical Modeling Techniques for Polymer Microstructure*. Macromolecular Materials and Engineering. **2004**;289(1):70-87.

5. Yan D, Wang WJ, et al. *Effect of long chain branching on rheological properties of metallocene polyethylene*. Polymer. **1999**;40(7):1737-1744.

6. Kaminsky W, Laban A. *Metallocene catalysis*. Applied Catalysis A: General. **2001**;222(1):47-61.

7. Natta G. *Kinetic studies of α-olefin polymerization*. Journal of Polymer Science. **1959**;34(127):21-48.

8. Natta G, Pino P, et al. *Crystalline High Polymers of A-Olefins*. Journal of the American Chemical Society. **1955**;77(6):1708-1710.

9. Mortazavi M, Arabi H, et al. *Copolymerization of ethylene/a-olefins using bis(2-phenylindenyl)zirconium dichloride metallocene catalyst: Structural study of comonomer distribution*. Polymer International. **2010**;59(1):1258-1265.

10. Soares J, Simon L. *Coordination Polymerization*. In: *Handbook of Polymer Reaction*

Engineering. Vol Willey-VCH. First Ed. Weinheim, Germany; **2008**:365-430.

11. Yoon J, Lee D, et al. *Thermal and mechanical properties of ethylene / a-olefin copolymers produced over (2-MeInd) 2 ZrCl 2 / MAO system*. Polymer. **2000**;41(12):4523-4530.

12. Gupta P, Wilkes GL, et al. *Does the length of the short chain branch affect the mechanical properties of linear low density polyethylenes? An investigation based on films of copolymers of ethylene/1-butene, ethylene/1-hexene and ethylene/1-octene synthesized by a single site metall*. Polymer. **2005**;46(20):8819-8837.

13. Kaminsky W, Arndt M. *Metallocenes for Polymer Catalysis*. In: *Polymer Synthesis/Polymer Catalysis*. Vol 127. Springer-Verlag Berlin Heidelberg; **1997**:143-187.

14. Kaminsky W, Piel C, et al. *Polymerization of ethene and longer chained olefins by metallocene catalysis*. Macromolecular Symposia. **2005**;226(1):25-34.

15. Kissin Y. *Multicenter nature of titanium-based Ziegler-Natta catalysts: Comparison of ethylene and propylene polymerization reactions*. Journal of Polymer Science, Part A: Polymer Chemistry. **2003**;41(12):1745-1758.

16. Kissin Y. *General Description of Transdition Metal Catalysts and Catalytic Polymerization Reactions*. In: *Alkene Polymerization Reactions with Transition Metal Catalysts*. Vol 173. First Ed. Amsterdam, Netherlands: Elsevier; **2008**:1-34.

17. Breslow DS, Newburg NR. *Bis-(Cyclopentadienyl)-Titanium Dichloride — Alkylaluminum Complexls As Catalysts for the Polymerization of Ethylene*. Journal of the American Chemical Society. **1957**;79(18):5072-5073.

18. Kaminsky W, Steiger R. *Polymerization of olefins with homogeneous zirconocene/alumoxane catalysts*. Polyhedron. **1988**;7(22-23):2375-2381.

19. Kaminsky W. *Highly active metallocene catalysts for olefin polymerization*. J Am Chem Soc, Dalton Trans. **1998**;9:1413-1418.

20. Kaminsky W, Miri M, et al. *Bis(cyclopentadienyl)zirkon-verbindungen und aluminoxan als Ziegler-Katalysatoren für die polymerisation und copolymerisation von olefinen*. Die Makromolekulare Chemie, Rapid Communications. **1983**;4(6):417-421.

21. Kaminsky W. *Discovery of Methylaluminoxane as Cocatalyst for Olefin Polymerization*. Macromolecules. **2012**;45(1):3289-3297.

22. Kaminsky W. *The discovery of metallocene catalysts and their present state of the art*. Journal of Polymer Science, Part A: Polymer Chemistry. **2004**;42(16):3911-3921.

23. Kaminsky W, Külper K, et al. *Olefinpolymerization with highly active soluble zirconium compounds using aluminoxane as co-catalyst*. Makromolekulare Chemie, Macromolecular Symposia. **1986**;3(1):377-387.

24. Mehdiabadi S, Soares JBP. *Ethylene homopolymerization kinetics with a constrained geometry catalyst in a solution reactor*. Macromolecules. **2012**;45(4):1777-1791.

25. Piel T, Saarinen T, et al. *Effect of Metallocene Structures on their Performance in Ethene Polymerisation*. Macromolecular Chemistry and Physics. **2007**;208(8):851-861.

26. Soares J, Mckenna T. *Polyolefin Microstructural Characterization*. In: *Polyolefin Reaction Engineering*. Vol Verlag Gmb. First Ed. Weinheim, Germany: Wiley-VCH; **2012**:15-52.

27. Soares JBP, Mckenna T. *Polymerization Catalysis and Mechanism*. In: *Polyoelfin Reaction Engineering*. First Ed. Weinheim, Germany: Wiley-VCH; **2012**:53-86.

28. Soares J, Perez O. *Coordination polymerization*. In: *Handbook of Polymer Synthesis, Chracterization, and Processing*. Vol Willey-VCH. First. ; **2013**:85-104.

29. Böhm LL. *The Ethylene Polymerization with Ziegler Catalysts: Fifty Years after the Discovery*. Angewandte Chemie - International Edition. **2003**;42(41):5010-5030.

30. Anantawaraskul S, Soares J, et al. *Fractionation of semicrystalline polymers by crystallization analysis fractionation and temperature rising elution fractionation*. In:

Polymer Analysis Polymer Theory. Vol 182. Springer Berlin Heidelberg; **2005**:1-54.

31. Soares J, Hamielec A. *Temperature rising elution fractionation of linear polyolefins*. Polymer. **1995**;36(8):1639-1654.

32. Wild L, Ryle TR, et al. *Determination of Branching Distributions in Polyethylene and Ethylene Copolymers*. Journal of Polymer Science, Polymer Physics Edition. **1982**;20:441-455.

33. Monrabal B. *CRYSTAF: Crystallization Analysis Fractionation. a new approach to the compostion analysis of semicrystalline polymer*. Macromolecular Symposia. **1996**;110(1):81-86.

34. Monrabal B. *Crystallization analysis fractionation: A new technique for the analysis of branching distribution in polyolefins*. Journal of Applied Polymer Science. **1994**;52(4):491-499.

35. Nieto J, Oswald T, et al. *Crystallizability of ethylene homopolymers by crystallization analysis fractionation*. Journal of Polymer Science, Part B: Polymer Physics. **2001**;39(14):1616-1628.

36. Soares J, Anantawaraskul S. *Crystallization analysis fractionation*. Journal of Polymer Science, Part B: Polymer Physics. **2005**;43(13):1557-1570.

37. Stadler F, Takahashi T, et al. *Crystal structure of ethene-/α-olefin copolymers with various long comonomers (C8–C26)*. European Polymer Journal. **2011**;47(5):1048-1053.

38. Monrabal B, Sancho-Tello J, et al. *Crystallization elution fractionation. A new separation process for polyolefin resins*. Macromolecular Symposia. **2007**;257(1):71-79.

39. Alghyamah A. *Comparison Between CEF and HT-TGIC of Polyolefins Made by Ziegler-Natta and Metallocene Catalysts*. In: *Chemical Engineering, University of Waterloo*. waterloo, Ontario, Canada; **2012**:150-210.

40. Monrabal B, Romero L, et al. *Advances in Crystallization Elution Fractionation*. Macromolecular Symposia. **2009**;282(1):14-24.

41. Anantawaraskul S, Soares JBP, et al. *Effect of molecular weight and average comonomer content on the crystallization analysis fractionation (Crystaf) of ethylene α-olefin copolymers*. Polymer. **2003**;44(8):2393-2401.

42. Alghyamah A, Soares J. *Crystallization Elution Fractionation of LLDPEs Made with Metallocene Catalysts*. Macromolecular Symposia. **2012**;312(1):43-50.

43. Anantawaraskul S, Soares J, et al. *Effect of Operation Parameters on Temperature Rising Elution Fractionation and Crystallization Analysis*. Journal of Polymer Science, Part B: Polymer Physics. **2003**;41(14):1762-1778.

44. Aust N, Gahleitner M, et al. *Optimization of run parameters of temperature-rising elution fractionation with the aid of a factorial design experiment*. Polymer Testing. **2006**;25(7):896-903.

45. Chokputtanawuttilerd N, Anantawaraskul S, et al. *Effect of operating conditions on dynamic crystallization of ethylene/1-octene copolymers*. Macromolecular Chemistry and Physics. **2013**;214(22):2591-2601.

46. Somnukguande P, Anantawaraskul S, et al. *Effect of Chain Microstructure and Cooling Rate on Crystaf Calibration Curves: An Experimental Study*. Macromolecular Symposia. **2012**;312(1):191-196.

47. Anantawaraskul S, Soares J, et al. *Cocrystallization of blends of ethylene/1-olefin copolymers: An investigation with crystallization analysis fractionation (Crystaf)*. Macromolecular Chemistry and Physics. **2004**;205(6):771-777.

48. Anantawaraskul S, Somnukguande P, et al. *Application of a Crystallization Kinetics Model to Simulatethe Effect of Operation Conditions on Crystaf Profiles andCalibration Curves*. Journal of Polymer Science Part B: Polymer physics. **2009**;47(9):866-876.

49. Monrabal B, Javier B, et al. *Characterization of homogeneous ethylene/1-octene*

copolymers made with a single-site catalyst. CRYSTAF analysis and calibration. Journal of Polymer Science Part A: Polymer Chemistry. **1999**;37(1):89-93.

50. Sarzotti D, Soares J, et al. *Ethylene/1-hexene copolymers synthesized with a single-site catalyst: Crystallization analysis fractionation, modeling, and reactivity ratio estimation*. Journal of Polymer Science Part B: Polymer Physics. **2002**;40(23):2595-2611.

51. Al-Khazaal A. *Characterization of Ethylene/a-Olefin Copolymer Made with a Single-Site Catalyst Using Crystallization Elution Fractionation*. In: *Chemical Engineering, University of Waterloo*. waterloo, Ontario, Canada; **2011**:80-95.

52. Beigzadeh D, Soares JBP, et al. *Modeling of Fractionation in CRYSTAF Using Monte Carlo Simulation of Crystallizable Sequence Lengths : Ethylene / 1- octene Copolymers Synthesized with Single-Site – Type Catalysts*. Journal of Applied Polymer Science. **2001**;80:2200-2206.

53. Costeux S, Anantawaraskul S, et al. *Distribution of the longest ethylene sequence in ethylene/α-olefin copolymers synthesized with single-site-type catalysts*. Macromolecular Theory and Simulations. **2002**;11(3):326-341.

54. Soares JBP, Beigzadeh D, et al. *Mathematical modelling and control of chemical composition distribution of ethylene/α-olefin copolymers made with single and combined metallocene catalysts*. Polymer Reaction Engineering. **2000**;8(3):241-270.

55. Soares J. *Mathematical modelling of the microstructure of polyolefins made by coordination polymerization: A review*. Chemical Engineering Science. **2001**;56:4131-4153.

56. Berek D. *Coupled liquid chromatographic techniques for the separation of complex polymers*. Progress in Polymer Science (Oxford). **2000**;25(7):873-908.

57. Chang T. *Recent advances in liquid chromatography analysis of synthetic polymers*. Advances in Polymer Science. **2003**;163(1):1-60.

58. Kazakevich Y, Fadeev A. *Adsorption characterization of oligo(dimethylsiloxane)-modified silicas: An example of highly hydrophobic surfaces with non-aliphatic architecture*. Langmuir. **2002**;18(8):3117-3122.

59. Macko T, Pasch H, et al. *Adsorption of polyethylene standards from decalin on liquid chromatography column packings*. Journal of Chromatography A. **2003**;1002(1-2):55-62.

60. Macko T, Pasch H, et al. *Elution behavior of polyethylene in polar mobile phases on a non-polar sorbent.* Journal of chromatography A. **2003**;988(1):69-76.

61. Heinz L, Pasch H. *High-temperature gradient HPLC for the separation of polyethylene-polypropylene blends*. Polymer. **2005**;46(26):12040-12045.

62. Lehtinen A, Paukkeri R. *Fractionation of polypropylene according to molecular weight and tacticity*. Macromolecular Chemistry and Physics. **1994**;195(5):1539-1556.

63. Albrecht A, Heinz L, et al. *Separation and characterization of ethylene-propylene copolymers by high-temperature gradient HPLC coupled to FTIR spectroscopy*. Macromolecular Symposia. **2007**;257(1):46-55.

64. Macko T, Pasch H, et al. *Adsorption of polypropylene from dilute solutions on a zeolite column packing.* Journal of separation science. **2005**;28(1):59-64.

65. Chitta R, Macko T, et al. *Elution behavior of polyethylene and polypropylene standards on carbon sorbents*. Journal of Chromatography A. **2010**;1217(49):7717-7722.

66. Macko T, Brüll R, et al. *Separation of propene/1-alkene and ethylene/1-alkene copolymers by high-temperature adsorption liquid chromatography*. Polymer. **2009**;50(23):5443-5448.

67. Macko T, Brüll R, et al. *Separation of short-chain branched polyolefins by high-temperature gradient adsorption liquid chromatography.* Analytical and bioanalytical chemistry. **2011**;399(4):1547-1556.

68. Macko T, Brüll R, et al. *Characterization of Ethylene-Propylene Copolymers with High-Temperature Gradient Adsorption Liquid Chromatography and CRYSTAF*. Journal of Applied Polymer Science. **2011**;122(5):3211-3217.

69. Macko T, Brüll R, et al. *A review on the development of liquid chromatography systems for polyolefins.* Journal of Separation Science. **2010**;33(22):3446-3454.

70. Macko T, Pasch H. *Separation of Linear Polyethylene from Isotactic, Atactic, and Syndiotactic Polypropylene by High-Temperature Adsorption Liquid Chromatography*. Macromolecules. **2009**;42(16):6063-6067.

71. Chitta R, MacKo T, et al. *Separation of ethylene-propylene copolymers and ethylene-propylene-diene terpolymers using high-temperature interactive liquid chromatography*. Journal of Polymer Science, Part A: Polymer Chemistry. **2011**;49(8):1840-1846.

72. Ginzburg A, MacKo T, et al. *Characterization of polyolefins by comprehensive high-temperature two-dimensional liquid chromatography (HT 2D-LC)*. European Polymer Journal. **2011**;47(3):319-329.

73. Ginzburg A, Macko T, et al. *Characterization of functionalized polyolefins by high-temperature two-dimensional liquid chromatography*. Journal of Chromatography A. **2013**;1285:40-47.

74. Ginzburg A, Macko T, et al. *High-temperature two-dimensional liquid chromatography of ethylene-vinylacetate copolymers*. Journal of Chromatography A. **2010**;1217(44):6867-6874.

75. Roy A, Miller M, et al. *Development of Comprehensive Two-Dimensional High Temperature Liquid Chromatography Â Gel Permeation Chromatography for Characterization of Polyolefins* . Macromolecules. **2010**;43(8):3710-3720.

76. Mekap D, Macko T, et al. *Multiple-Injection Method in High- Temperature Two-Dimensional Liquid*. Macromolecular Chemistry and Physics. **2014**;215(1):314-319.

77. Cong R, Degroot AW, et al. *A new technique for characterizing comonomer distribution in polyolefins: High-temperature thermal gradient interaction chromatography (HT-TGIC)*. Macromolecules. **2011**;44(8):3062-3072.

78. Cong R, Degroot AW, et al. *High temperature thermal gradient interaction chromatography (HT-TGIC) for microstructure analysis of polyolefins*. Macromolecular Symposia. **2012**;312(1):108-114.

79. Pasch H, Malik M, et al. *Recent advances in high-temperature fractionation of polyolefins*. Advances in Polymer Science. **2013**;251(1):77-140.

80. Monrabal B, Mayo N, et al. *Crystallization elution fractionation and thermal gradient interaction chromatography. Techniques comparison*. Macromolecular Symposia. **2012**;312(1):115-129.

81. Alghyamah A, Soares J. *Effect of Solvent Type on High-Temperature Thermal Gradient Interaction Chromatography of Polyethylene and Ethylene – 1-Octene Copolymers*. Macromolecular Chemistry and Physics. **2015**;216(1):38-48.

82. Alghyamah A, Soares J. *Fractionation of Ethylene/1-Octene Copolymers by High-Temperature Thermal Gradient Interaction Chromatography*. Industrial & Engineering Chemistry Research. **2014**;53(22):9228-9235.

83. Mekap D, Malz F, et al. *Studying the Interactions of Polyethylene with Graphite in the Presence of Solvent by High Temperature Thermal Gradient Interactive Chromatography, Thermal Gradient Nuclear Magnetic Resonance Spectroscopy, and Solution Differential Scanning Calorimetry*. Macromolecules. **2014**;47:7939-7946.

84. Mekap D, Macko T, et al. *Studying Binary Solvent Mixtures as Mobile Phase for Thermal Gradient Interactive Chromatography (TGIC) of Poly(ethylene- stat -1-octene)*. Industrial & Engineering Chemistry Research. **2014**;53(39):15183-15191.

85. Inwong N, Anantawaraskul S, et al. *High Temperature Thermal Gradient Interaction Chromatography (HT-TGIC) for Blends of Ethylene/1-Octene Copolymers: A*

Mathematical Model. Macromolecular Symposia. **2015**;354(1):361-366.

86. Inwong N, Anantawaraskul S, et al. *High Temperature Thermal Gradient Interaction Chromatography (HT-TGIC) of Ethylene / 1-Octene Copolymers : Model Development and Validation*. Macromolecular Symposia. **2015**;356(1):54-60.

87. Monrabal B, Lõpez E, et al. *Advances in thermal gradient interaction chromatography and crystallization techniques for composition analysis in polyolefins*. Macromolecular Symposia. **2013**;330:9-21.

88. Monrabal B. *Separation of Ethylene-Propylene Copolymers by Crystallization and Adsorption Mechanisms. A Journey Inside the Analytical Techniques*. Macromolecular Symposia. **2015**;356(1):147-166.

89. DePooter M, Smith P. *Determination of the composition of common linear low density polyethylene copolymers by 13C-NMR spectroscopy*. Journal of Applied Polymer Science. **1991**;42(2):399-408.

90. ASTM-D5017-96. *Standard Test Method for Determination of Linear Low Dinsity Polyethylene (LLDPE) Compsition by Carbon-13 Nuclear Magnetic Resonance*. American Society for Testing and Materials. **2009**;1(1):1-7.

91. ASTM-D6645-01. *Standard Test Method for Methyl (Comonomer) Content in Polyethylene by Infrared*. American Society for Testing and Materials. **2010**;1(1):1-4.

92. Montgomery D. *The 2k Factorial Design*. In: *Design and Analysis of Experiments*. 8th ed. WILEY; **2012**:233-292.

93. Sun T, Brant P, et al. *Effect of Short Chain Branching on the Coil Dimensions of Polyolefins in Dilute Solution*. Macromolecules. **2001**;39(19):6812-6820.

94. Cong R, Parrott AR, et al. *Size Exclusion Chromatography of Polymers*. WO 2012166861 A1. **2012**.

95. Mehdiabadi S. *Synthesis, Characterization and Polymerization Kinetic Study of Long*

Chain Branched Polyolefins Made with Two Single-Site Catalysts. In: *Chemical Engineering, University of Waterloo*. waterloo, Ontario, Canada; **2011**:202-208.

96. Al-Khazaal AZ, Soares JBP. *Characterization of Ethylene/α-Olefin Copolymers Using High-Temperature Thermal Gradient Interaction Chromatography*. Macromolecular Chemistry and Physics. **2014**;215(5):465-475.

97. Al-Khazaal AZ, Soares JBP. *Effect of Column Type on Polyolefin Fractionation by High-Temperature Thermal Gradient Interaction Chromatography*. Macromolecular Symposia. **2015**;356(1):10-18.

98. Al-Khazaal AZ, Soares JBP. *Joint Effect of Poly(ethylene-co-1-octene) Chain Length and 1-Octene Fraction on High-Temperature Thermal Gradient Interaction Chromatography*. Macromolecular Chemistry and Physics. **2016**;1(1):1-20

Appendices

Appendix A-Mathematical Model for Average Chain Length Control

The number average chain length of polyolefins (r_n) is given by,

$$r_n = \frac{R_P}{R_t} \tag{A.1}$$

where R_p and R_t are the propagation rate and the chain transfer rate, respectively. The propagation rate can be approximated by the expression,

$$R_p = k_p[E][C^*] \tag{A.2}$$

where k_p is the apparent propagation rate constant, $[E]$ is the ethylene concentration, and $[C^*]$ is the catalyst concentration. For simplicity, the concentration of octene was not considered implicitly in Equation (A.2), but it lumped with the apparent propagation rate constant k_p.

The chain transfer rate was also modeled with a simple equation,

$$R_t = k_{t_1}[O] + k_{t_2} + k_{t_3}[E] \tag{A.3}$$

where $[O]$ is the concentration of octene in the reactor, k_{t1} is the transfer to octene rate constant, k_{t2} is the β-hydride elimination rate constant, and k_{t3} is the transfer to ethylene rate constant.

Substituting Equation (A.2) and (A.3) into Equation (A.1), one gets,

$$r_n = \frac{k_p[E]}{k_{t_1}[O] + k_{t_2} + k_{t_3}[E]} \tag{A.4}$$

Therefore,

$$\frac{1}{r_n} = \frac{k_{t_1}}{k_p}\frac{[O]}{[E]} + \frac{k_{t_2}}{k_p}\frac{1}{[E]} + \frac{k_{t_3}}{k_p} \tag{A.5}$$

Assuming that Arrhenius law applies to all rate constants in Equation (A.5),

$$\frac{1}{r_n} = \frac{A_{t_1}}{A_p}\frac{[O]}{[E]}\exp\left(\frac{-\left(E_{t1} - E_p\right)}{RT}\right) + \frac{A_{t_1}}{A_p}\frac{1}{[E]}\exp\left(\frac{-\left(E_{t2} - E_p\right)}{RT}\right) + \frac{A_{t_1}}{A_p}\exp\left(\frac{-\left(E_{t3} - E_p\right)}{RT}\right) \tag{A.6}$$

which can be rearranged to the more compact form,

$$\frac{1}{r_n} = \varphi_1\frac{[O]}{[E]}\exp\left(\frac{-\Delta E_1}{RT}\right) + \varphi_2\frac{1}{[E]}\exp\left(\frac{-\Delta E_2}{RT}\right) + \varphi_3\exp\left(\frac{-\Delta E_3}{RT}\right) \tag{A.7}$$

where ΔE_i and φ_i are adjustable parameters.

A set of polymerization experiments (Table A.1) was designed to estimate the parameters ΔE_i and φ_i in Equation A.7 as shown in Table A.2. Figure A.1 shows the experimental and predicted M_n for the many samples used.

Table B.1. Polymerization conditions for a set of ethylene/1-octene copolymer samples.

No.	Ethylene (psig)	Temperature (°C)	1-Octene (mol/mL)
1	160	111	0.551
2	120	147.5	0.041
3	100	121	0.391
4	120	137	0.071
5	120	131	0.095
6	130	130	0.257
7	120	122	0.153
8	160	140	0.385
9	120	111	0.217
10	120	105	0.282
11	100	120	0.168
12	120	102.8	0.363
13	120	142	0.055
14	100	120	0.021
15	158	121	0.128
16	100	120	0.427
17	120	124	0.125
18	120	119	0.178
19	120	106.1	0.317
20	158	141	0.131

Table B.2. Estimation of ΔE_i and φ_i parameters in Equation A.7

ΔE_1	φ_1	ΔE_2	φ_2	ΔE_3	φ_3
45100.5	89.1	40109.2	101.2	8.64E-7	0.0

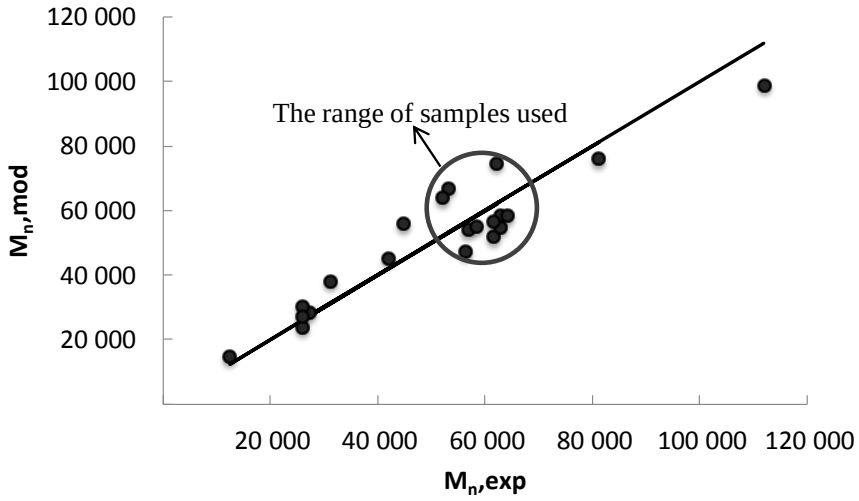

Figure B.1. Experimental and predicted M_n for all the samples.

Appendix B- ^{13}C NMR Analysis

^{13}C NMR spectra of ethylene/1-octene copolymer samples in Category I, containing different comonomer fractions.

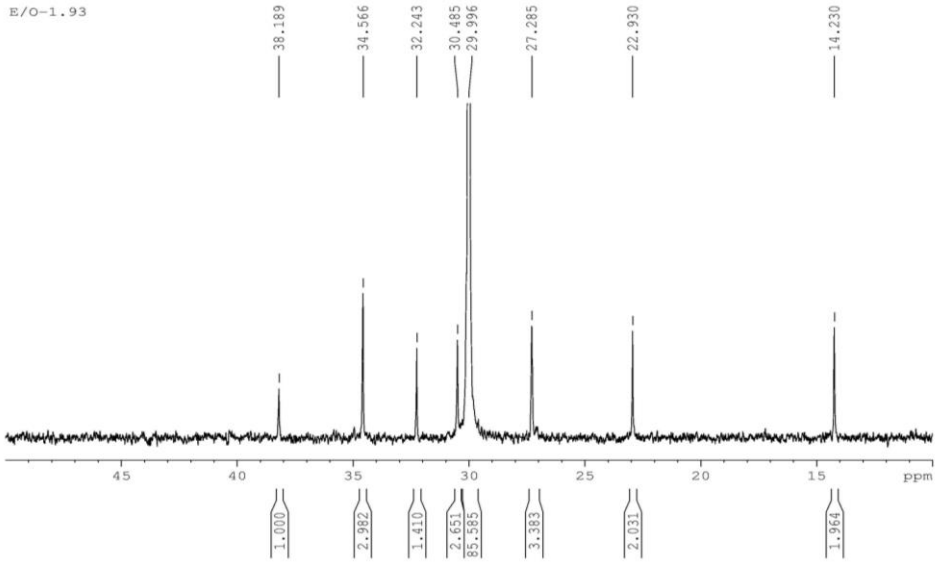

Figure B-1. ^{13}C NMR spectra of ethylene/1-octene copolymer (E/O-1.9), containing 1.9 % 1-octene.

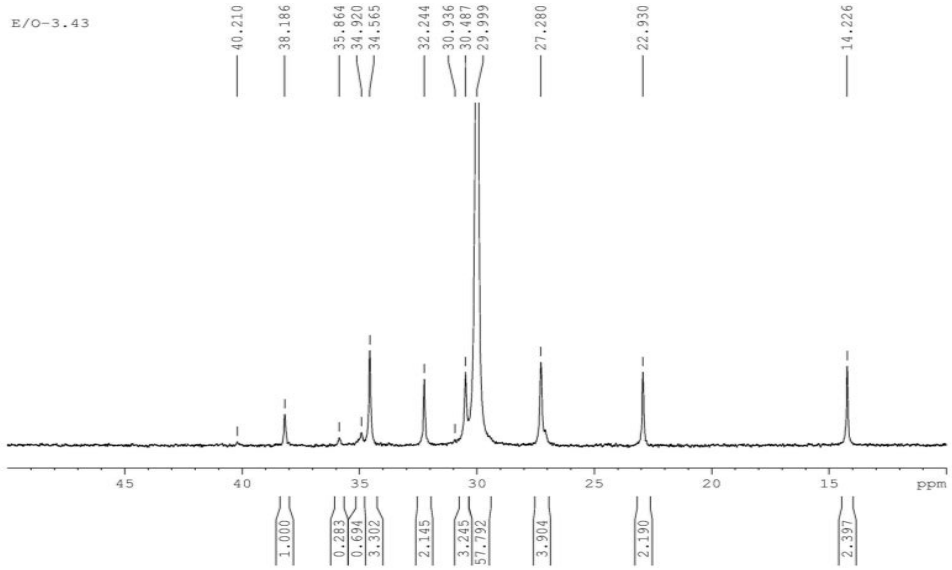

Figure B-2. ^{13}C NMR spectra of ethylene/1-octene copolymer (E/O-3.4), containing 3.4 % 1-octene.

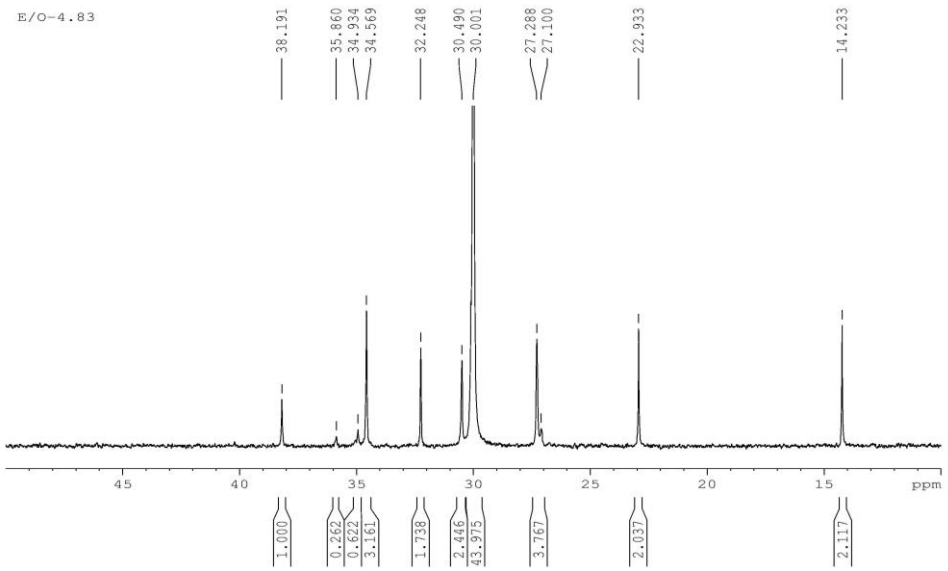

Figure B-3. ^{13}C NMR spectra of ethylene/1-octene copolymer (E/O-4.8), containing 4.8 % 1-octene.

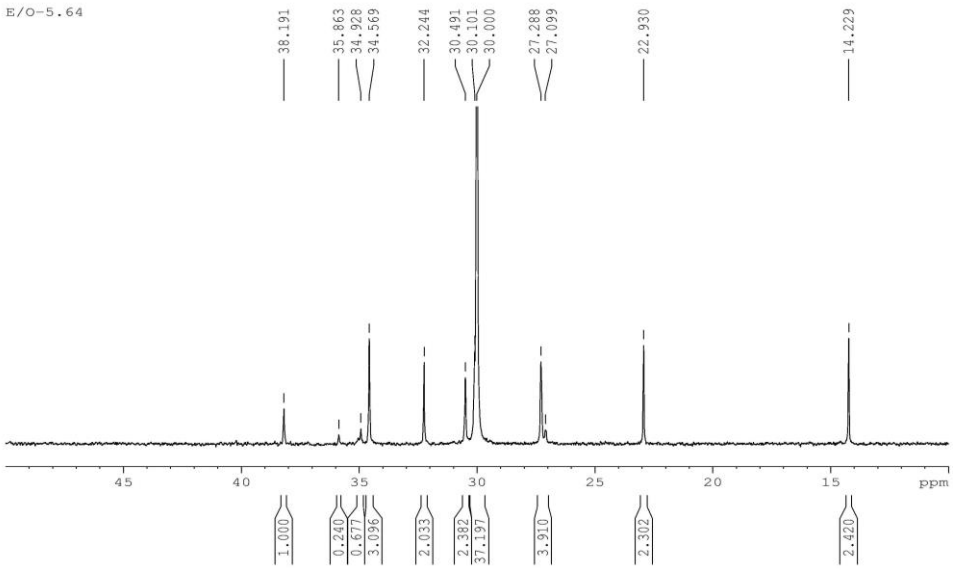

Figure B-4. ^{13}C NMR spectra of ethylene/1-octene copolymer (E/O-5.6), containing 5.6 % 1-octene.

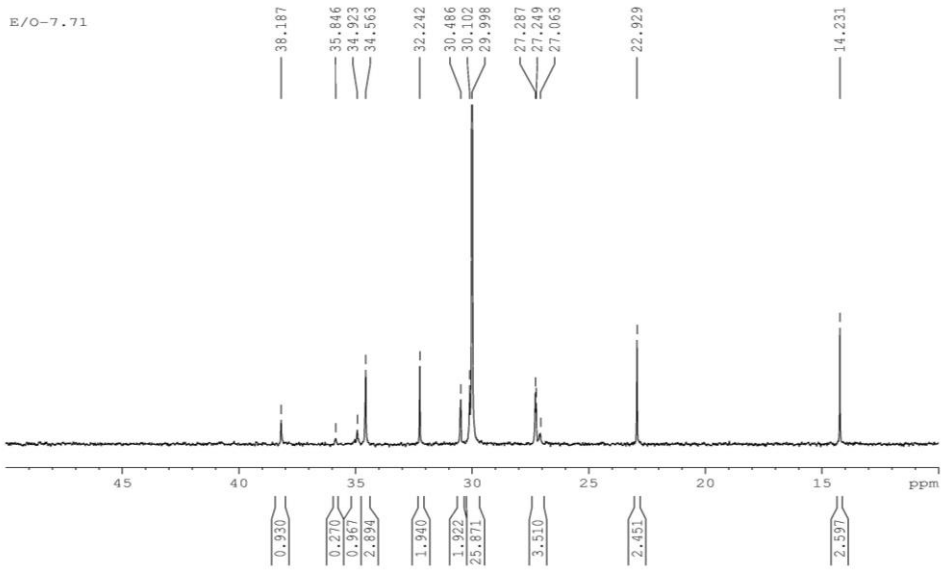

Figure B-5. ^{13}C NMR spectra of ethylene/1-octene copolymer (E/O-7.7), containing 7.7 % 1-octene.

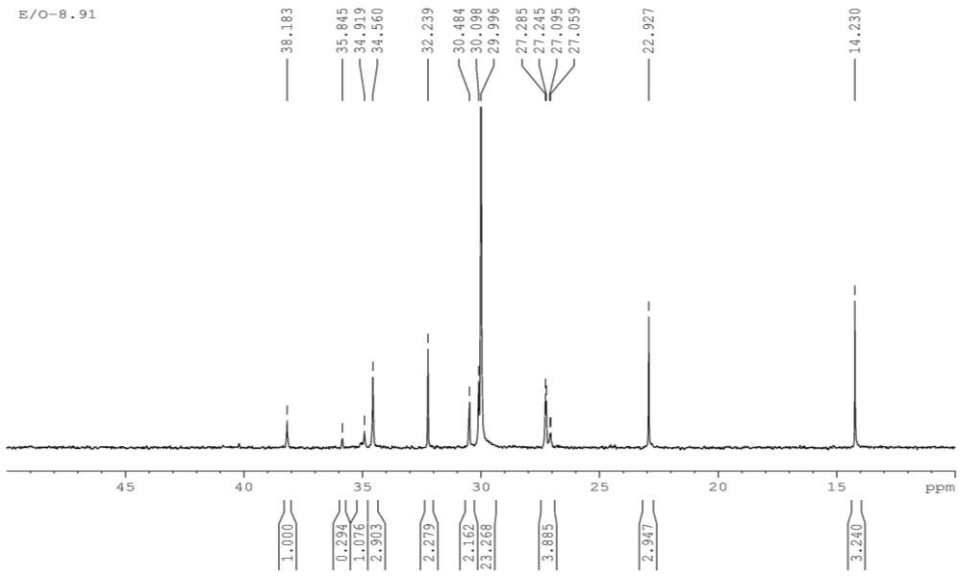

Figure B-6. ^{13}C NMR spectra of ethylene/1-octene copolymer (E/O-8.9), containing 8.9 % 1-octene.

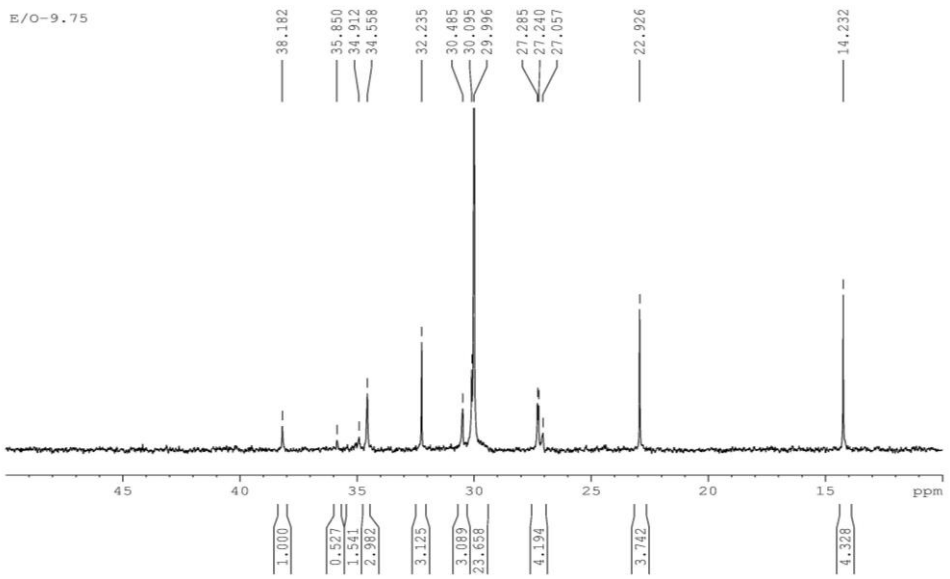

Figure B-7. ^{13}C NMR spectra of ethylene/1-octene copolymer (E/O-9.8), containing 9.8 % 1-octene.

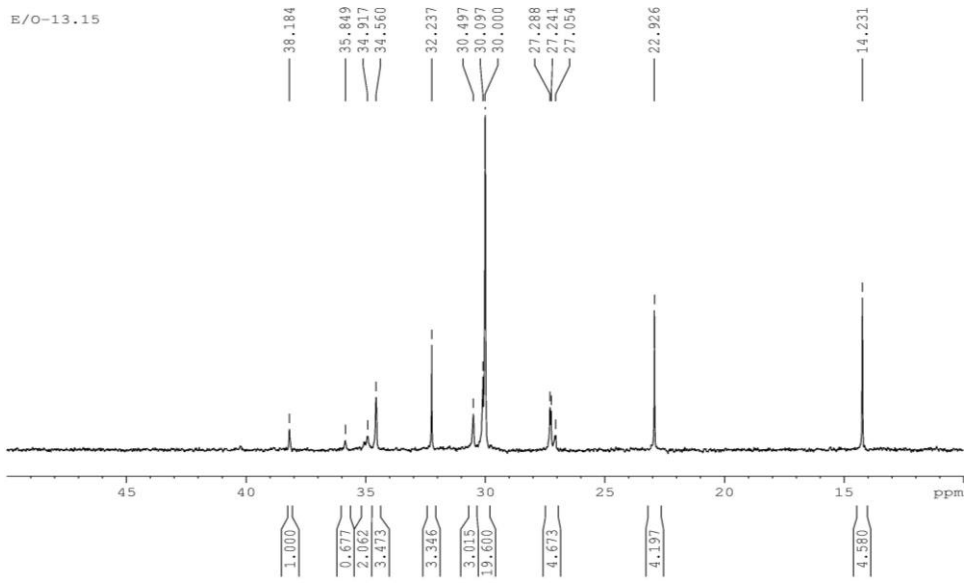

Figure B-8. ^{13}C NMR spectra of ethylene/1-octene copolymer (E/O-13.2), containing 13.2 % 1-octene.

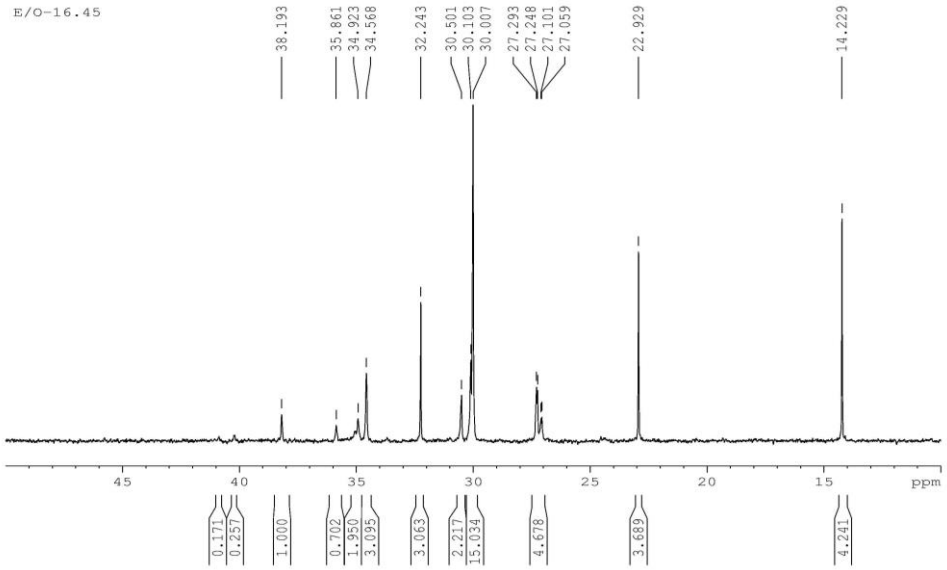

Figure B-9. ^{13}C NMR spectra of ethylene/1-octene copolymer (E/O-16.4), containing 16.4 % 1-octene.

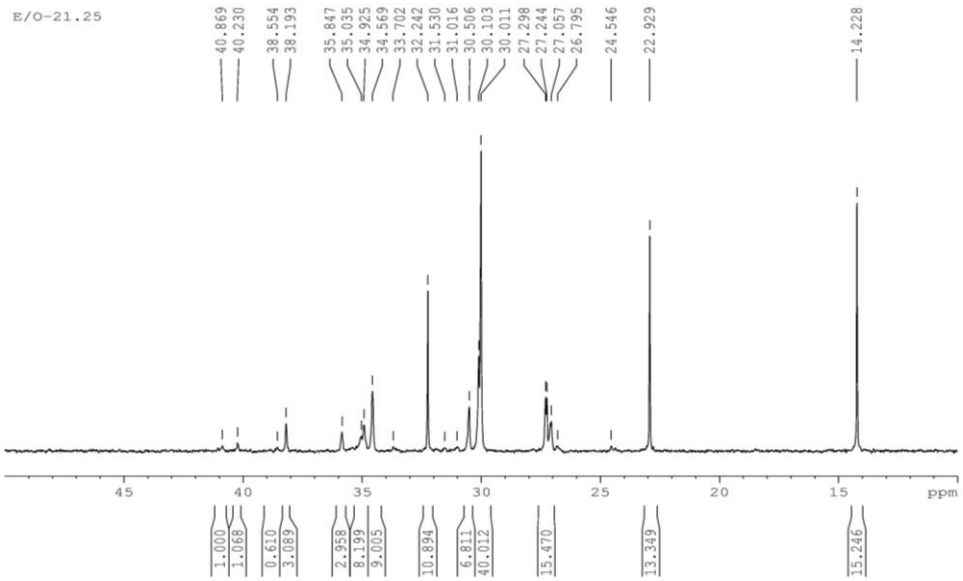

Figure B-10. ^{13}C NMR spectra of ethylene/1-octene copolymer (E/O-21.3), containing 21.3 % 1-octene.

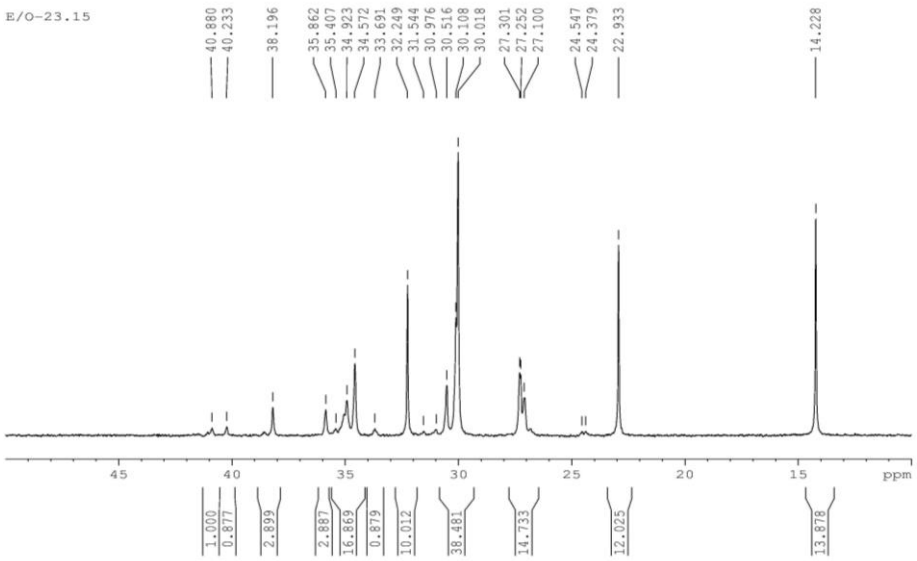

Figure B-11. ^{13}C NMR spectra of ethylene/1-octene copolymer (E/O-23.2), containing 23.2 % 1-octene.

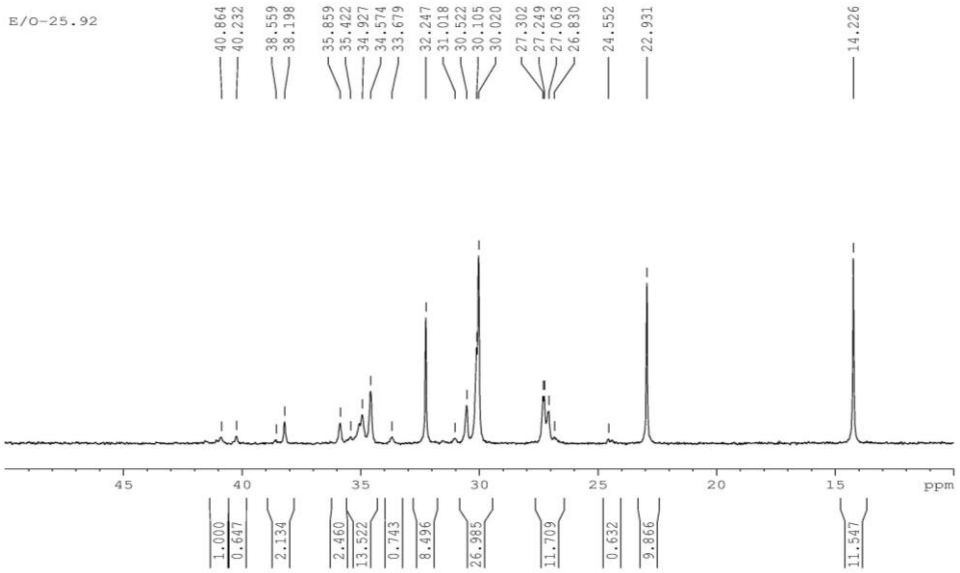

Figure B-12. ^{13}C NMR spectra of ethylene/1-octene copolymer (E/O-25.9), containing 25.9 % 1-octene.

Appendix C- Effects of CR, HR and F_E on HT-TGIC Profiles of E/O-9.8 and E/O-23.2 Samples

E/O-9.8 Sample

Table C-1. ANOVA TABLE for the temperature peak positions of E/O-9.8

Source of variance	Effect	Sum of Squares	Degree of freedom	Mean Squares	$F_{observed}$	$F_{critical}$ F(1,2,0.05)
Main Factor						
A	0.62	0.76	1	0.76	3.2	18.5
B	6.98	97.51	1	97.51	413.4*	
C	-6.68	89.18	1	89.18	378.0*	
Interaction						
AB	0.63	0.80	1	0.80	3.4	
AC	-0.91	1.65	1	1.65	7.0	
BC	-2.69	14.50	1	14.50	61.5*	
ABC	-1.01	2.05	1	2.05	8.7	
ERROR		0.47	2	0.24		

Table C-2. ANOVA TABLE for the standard variation values of E/O-9.8.

Source of variance	Effect	Sum of Squares	Degree of freedom	Mean Squares	$F_{observed}$	$F_{critical}$ F(1,2,0.05)
Main Factor						
A	-0.83	1.37	1	1.37	16.1	18.5
B	1.27	3.24	1	3.24	38.1*	
C	-1.32	3.50	1	3.50	41.2*	
Interaction						
AB	0.87	1.52	1	1.52	17.9	
AC	-0.28	0.16	1	0.16	1.9	
BC	-1.62	5.27	1	5.27	62.0*	
ABC	0.36	0.26	1	0.26	3.0	
ERROR		0.17	2	0.08		

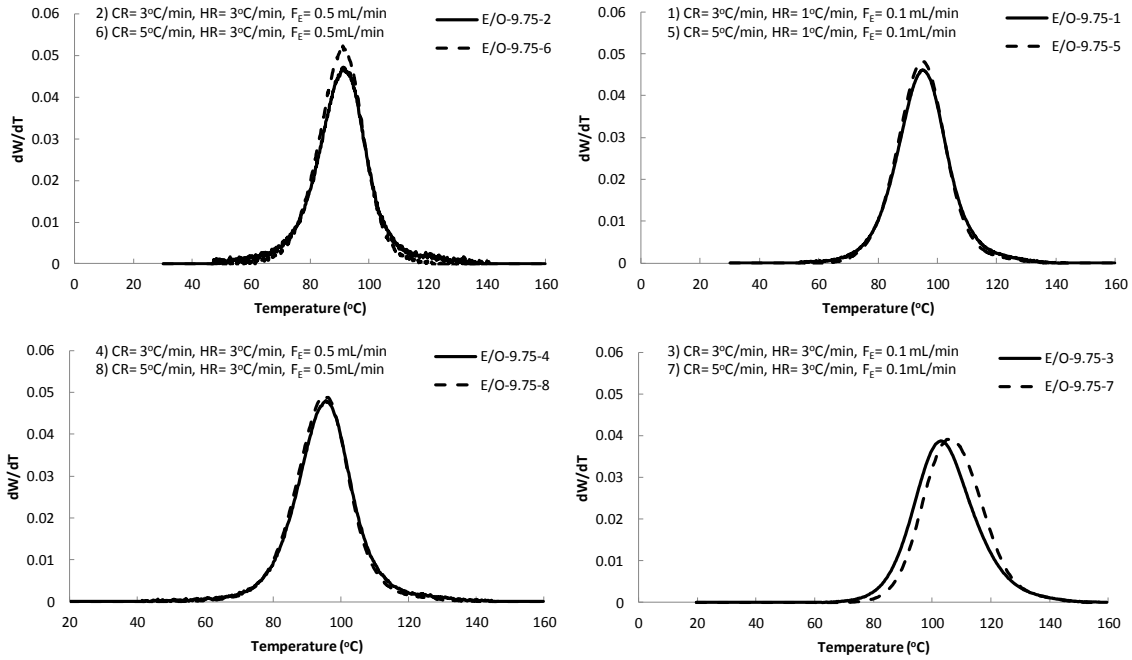

Figure C-1. Cooling rate effect on HT-TGIC profiles of sample E/O-9.8.

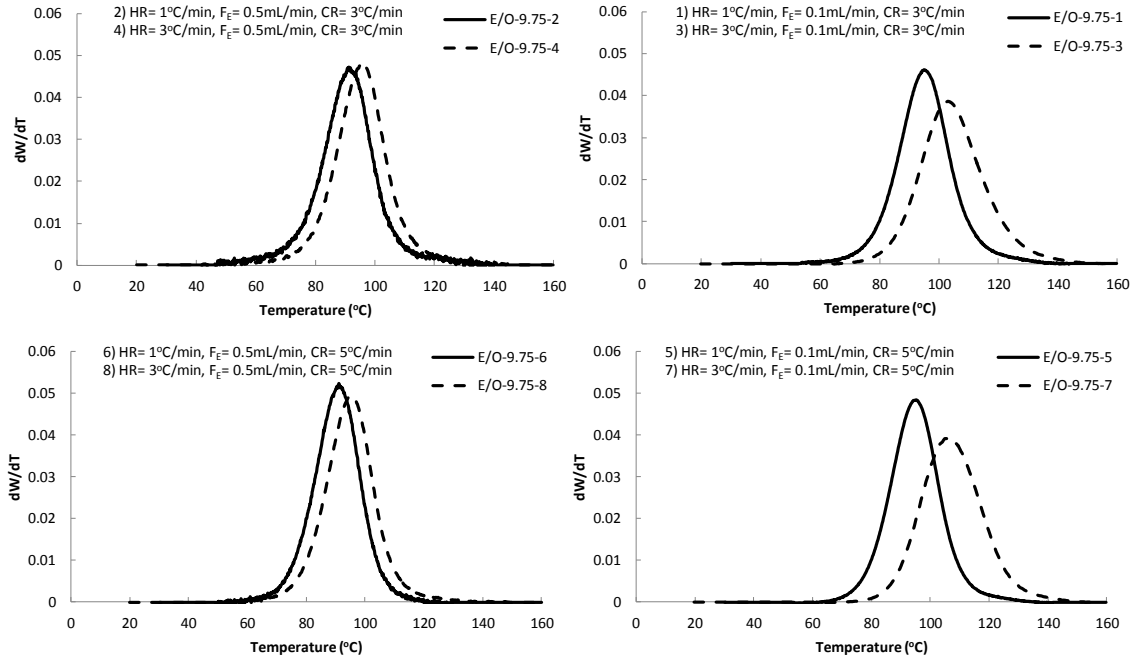

Figure C-2. Heating rate effect on HT-TGIC profile of sample E/O-9.8.

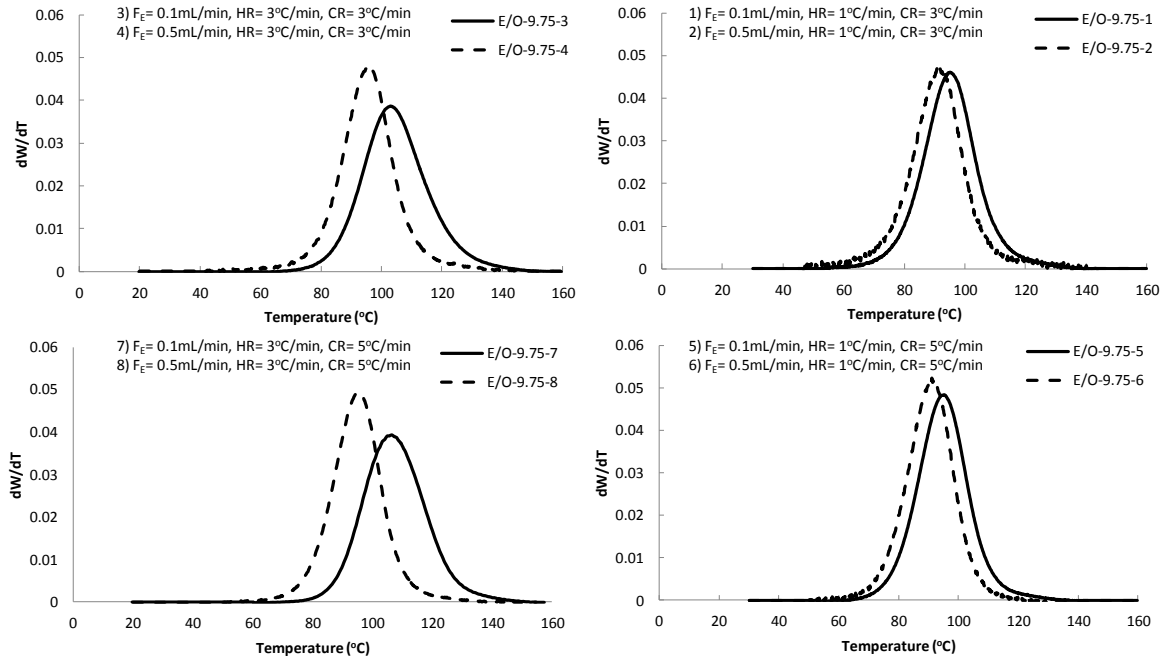

Figure C-3. Effect of elution flow rate on HT-TGIC profile of sample E/O-9.8.

E/O-23.2 Sample

Table C-3. ANOVA TABLE for the temperature peak positions of E/O-23.2.

Source of variance	Effect	Sum of Squares	Degree of freedom	Mean Squares	$F_{observed}$	$F_{critical}$ F(1,2,0.05)
Main Factor						
A	-1.62	5.23	1	5.23	14.4	18.5
B	5.84	68.15	1	68.15	187.6*	
C	-6.19	76.69	1	76.69	211.1*	
Interaction						
AB	0.64	0.83	1	0.83	2.3	
AC	-0.56	0.62	1	0.62	1.7	
BC	-3.44	23.70	1	23.70	65.2*	
ABC	-0.45	0.40	1	0.40	1.1	
ERROR		0.73	2	0.36		

Table C-4. ANOVA TABLE for the standard variation values of E/O-23.2.

Source of variance	Effect	Sum of Squares	Degree of freedom	Mean Squares	$F_{observed}$	$F_{critical}$ F(1,2,0.05)
Main Factor						
A	-0.18	0.06	1	0.06	1.9	18.5
B	1.11	2.44	1	2.44	33.6*	
C	0.98	1.90	1	1.90	26.2*	
Interaction						
AB	0.58	0.67	1	0.67	9.3	
AC	-0.08	0.01	1	0.01	0.2	
BC	-2.17	9.37	1	9.37	128.9*	
ABC	0.70	0.98	1	0.98	13.5	
ERROR		0.15	2	0.07		

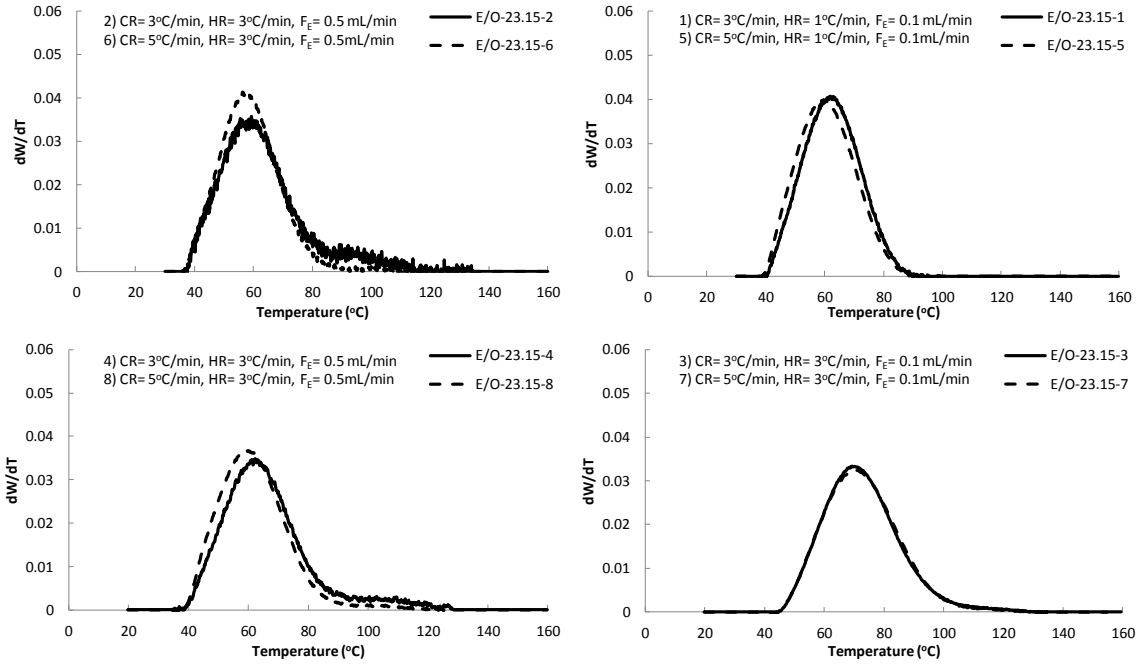

Figure C-4. Cooling rate effect on HT-TGIC profiles of sample E/O-23.2.

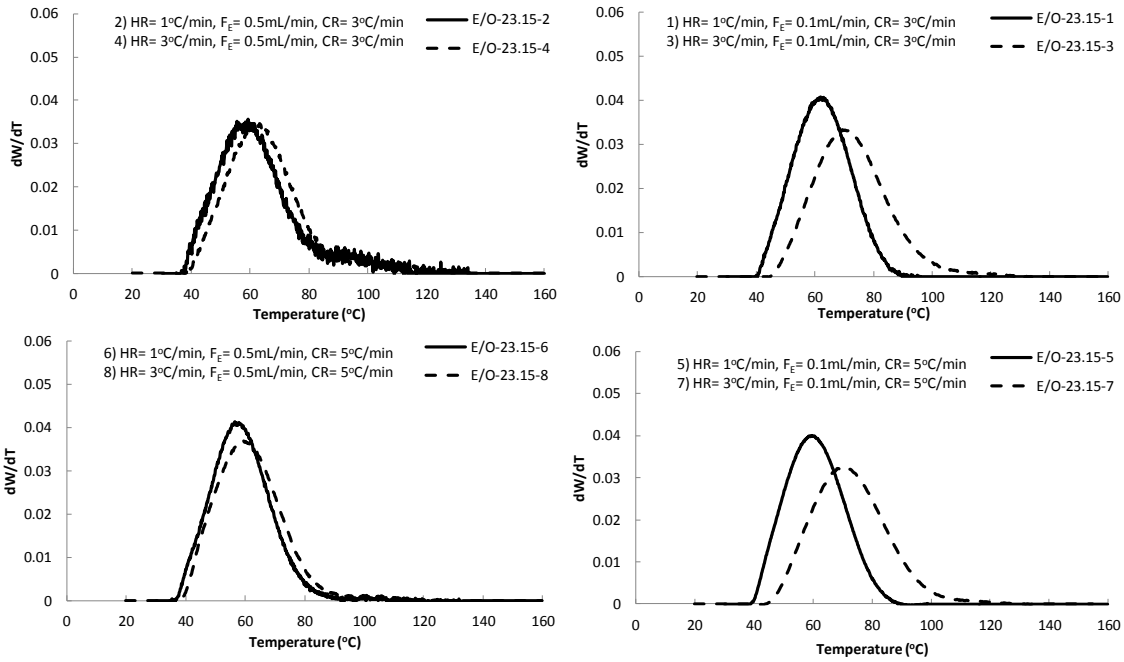

Figure C-5. Heating rate effect on HT-TGIC profile of sample E/O-23.2.

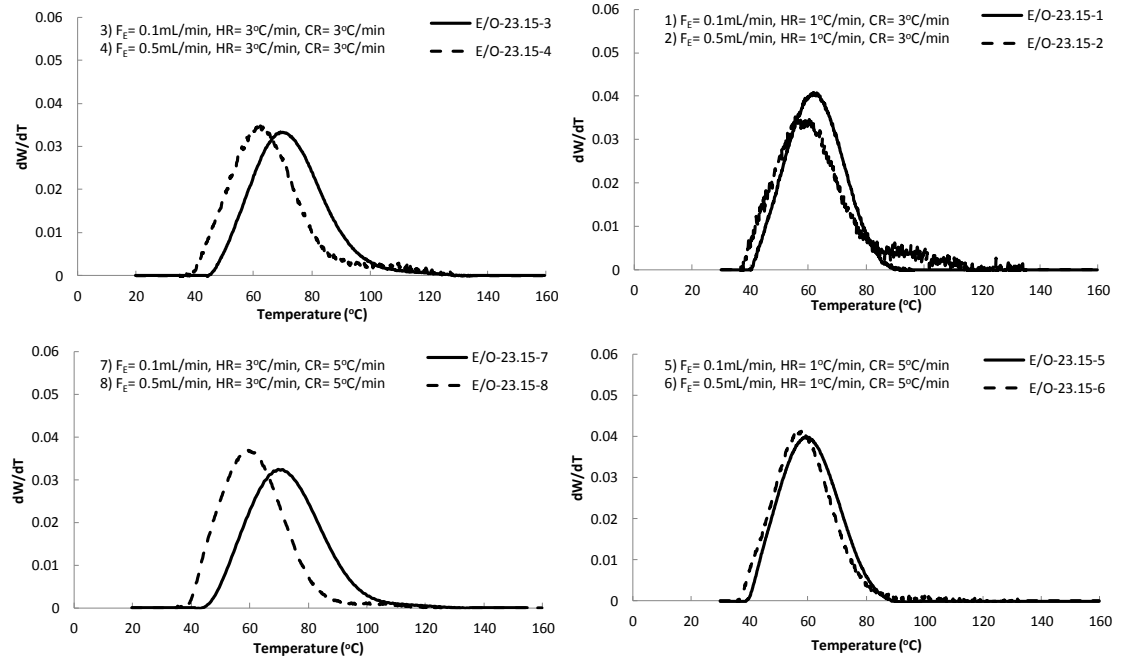

Figure C-6. Effect of elution flow rate on HT-TGIC profile of sample E/O-23.2.

Appendix D- W_AES and W_LES Results

In Chapter 6, we found that there is no simple correlation between the average ethylene sequence (AES) or average longest ethylene sequence (LES) and the HT-TGIC peak positions. To extend the investigations, we used our Monte Carlo model to calculate the *weight* average ethylene sequence (W_AES) and the *weight* average longest ethylene sequence (W_LES) of each ethylene/1-octene copolymer sample in Category II to find out whether these weight averages could be used to explain the joint effect of chain length and 1-octene mole fraction on the HT-TGIC fractionation for individual samples and their binary blends.

Tables D-1 to D-5 show the value of the W_AESs and the W_LESs of all ethylene/1-octene copolymer samples in Category II.

Table D-1. W_AES and W_LES values for ethylene/1-octene copolymers with 1.0 mol % of 1-octene.

Sample ID	r_n	W_AES	W_LES	T_P (°C)
C1-1.4	50	34	55	114.8
C1-1.7	61	43	61	119.1
C1-2.4	84	64	71	125.5
C1-4.6	162	84	120	129.6
C1-8.2	286	92	180	131.6
C1-15.6	540	97	250	132.3
C1-19.5	678	97	276	132.5
C1-27.1	943	98	312	132.7
C1-36.3	1260	99	343	132.9
C1-68.1	2360	99	409	132.9
C1-129.4	4485	99	475	132.7

Table D-2. W_AES and W_LES values for ethylene/1-octene copolymers with 2.6 mol % of 1-octene.

Sample ID	r_n	W_AES	W_LES	T_P (°C)
C2.6-1.5	51	30	38	93.1
C2.6-1.7	58	31	43	99.7
C2.6-2.0	69	32	50	104.4
C2.6-3.4	113	35	70	114.8
C2.6-4.8	159	36	84	119.5
C2.6-7.0	235	37	101	121.3
C2.6-14.1	469	37	129	123.1
C2.6-23.6	785	37	150	124.3
C2.6-36.0	1193	37	167	124.5
C2.6-61.1	2025	38	187	124.5
C2.6-115.7	3833	38	212	124.6

Table D-3. W_AES and W_LES values for ethylene/1-octene copolymers with 3.7 mol % of 1-octene.

Sample ID	r_n	W_AES	W_LES	T_P (°C)
C3.7-2.3	73	24	46	96.8
C3.7-5.4	172	25	72	111.4
C3.7-7.2	233	26	80	113.3
C3.7-10.6	340	26	91	114.5
C3.7-16.8	539	26	104	115.8
C3.7-29.2	938	26	119	117.0
C3.7-34.8	1118	26	124	117.7
C3.7-52.2	1672	26	135	117.8
C3.7-85.2	2736	26	148	117.8

Table D-4. W_AES and W_LES values for ethylene/1-octene copolymers with 7.8 mol % of 1-octene.

Sample ID	r_n	W_AES	W_LES	T_P (°C)
C7.8-1.9	56	12	28	55.3
C7.8-2.9	83	12	33	76.1
C7.8-4.6	132	12	40	82.6
C7.8-9.7	279	12	50	90.6
C7.8-18.5	534	12	57	96.0
C7.8-40.1	1160	12	67	98.2
C7.8-55.7	1611	12	71	98.2
C7.8-117.0	3384	12	80	98.3

Table D-4. W_AES and W_LES values for ethylene/1-octene copolymers with 12.9 mol % of 1-octene.

Sample ID	r_n	W_AES	W_LES	T_P (°C)
C13-2.5	64	7	21	23.5
C13-4.5	116	7	26	53.9
C13-9.4	242	7	31	63.5
C13-15.4	397	7	35	68.9
C13-28.0	729	7	39	71.5
C13-48.8	1256	7	43	73.5
C13-57.3	1476	7	45	73.7
C13-127.0	3266	7	50	73.7

Individual Sample Analysis

Figure D-1 illustrates that the W_AES value does not depend on chain length, especially at higher 1-octene mole fractions (similarly to Figure 6-5). This demonstrates that, like AES, W_AES cannot explain the effect of chain length on the HT-TGIC profile.

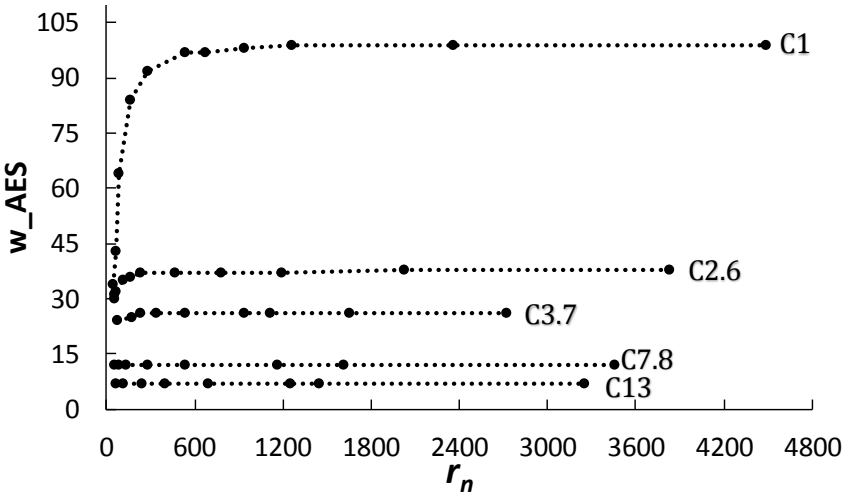

Figure D-1. Weight average ethylene sequence length (W_AES) depend weakly on r_n for ethylene/1-octene copolymers with a high 1-octene fraction.

Figure D-2 leads to the same conclusion (when compared to Figure 6-6) that the weight average longest ethylene sequence depends on the r_n for samples with higher 1-octene content; however, this dependency is more pronounced with lower 1-octene mole fraction.

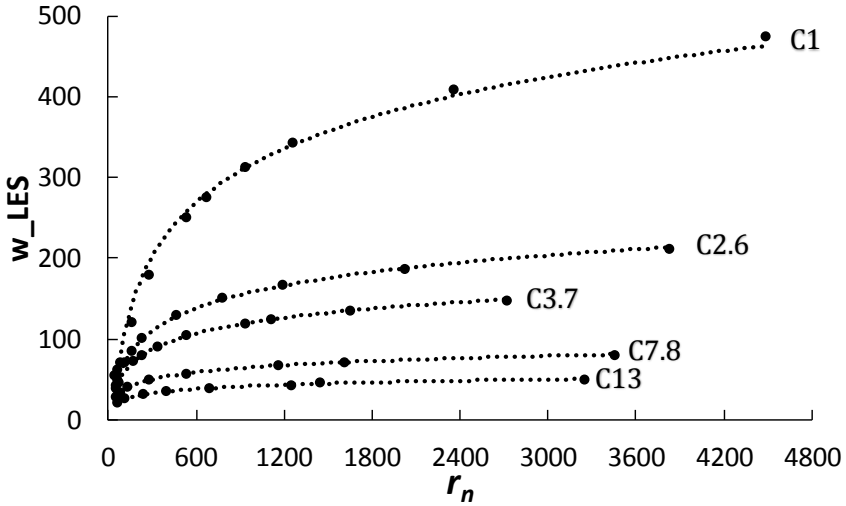

Figure D-2. Weight average longest ethylene sequence length (W_LES) depend on r_n for ethylene/1-octene copolymers with a high 1-octene fraction.

Figure D-3 shows that T_P does not depend on W_AES for copolymers with higher 1-octene samples, since copolymers with similar W_AES may have very different T_P values (similarly what was shown in Figure 6-10). Figure D-4 leads to same conclusion discussed in Figure 6-11, that samples with similar W_LES have very different peak temperatures if they have different 1-octene content. As a result, these plots prove that neither number or weight average ethylene sequences are the main factor controlling the fractionation mechanism of HT-TGIC.

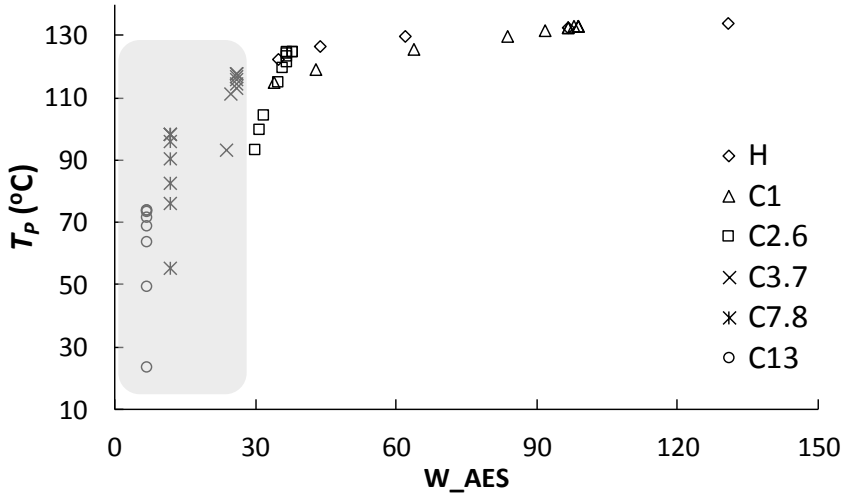

Figure D-3. Peak temperatures do not depend on W_AES for samples with higher 1-octene fractions.

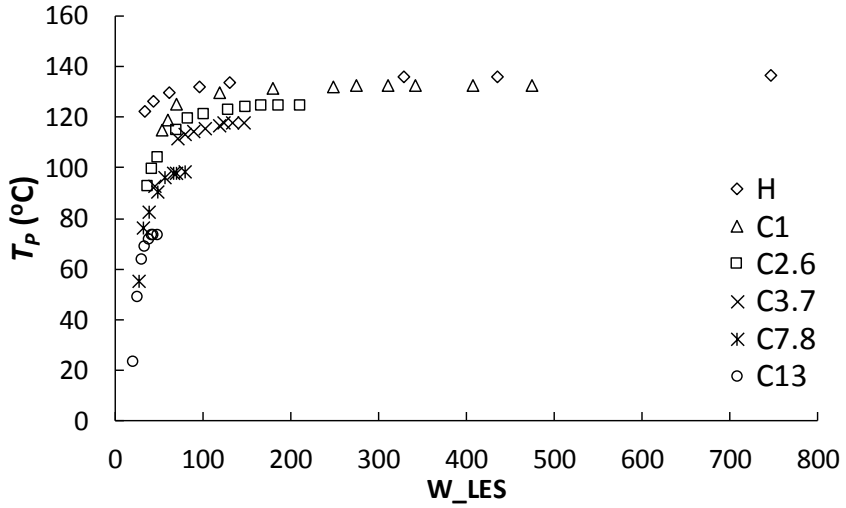

Figure D-4. Peak temperatures do not depend on W_LES for all sets of ethylene/1-octene copolymers.

Blend Analysis

We found that for a given comonomer content, the component blend affected each other HT-TGIC profile more significantly when they had similar average longest ethylene sequences. In this part, we consider the *weight* averages ratio to find out whether the final conclusions are different from what we observed in Chapter 6 using number, instead of weight, averages. Table D-6 shows the value of the W_AES ratio and the W_LES ratio of all blends investigated in Chapter 6.

Table D-6. W_AES ratio and W_LES ratio values and co-desorption index of all blends investigated.

Blend ID	W_AES Ratio	W_LES Ratio	CC Ratio	CDI
A1(LL,HL)	3.4	1.7	3.7	0.112
A2(LL,HH)	3.2	1.1	3.7	**0.330**
A3(LH,HL)	4.0	5.7	3.7	0.122
A4(LH,HH)	3.8	3.0	3.7	0.113
B1(LL,HL)	3.6	2.8	3.5	0.134
B2(LL,HH)	3.6	1.6	3.5	**0.338**
B3(LH,HL)	3.7	5.2	3.5	0.165
B4(LH,HH)	3.7	3.0	3.5	0.136
C2(LL,HH)	3.7	1.4	-	**0.331**
D2(LL,HH)	7.0	1.7	7.8	**0.271**
E2(LL,HH)	4.0	1.4	3.7	**0.316**
F2(LL,HH)	2.4	1.1	2.1	**0.244**

Figure D-5 illustrates that the co-desorption index does not correlate with W_AES ratio (similarly to was observed in Figure 6-24 for the AES ratio). Figure D-6 shows that only two blends (A2 and F2) having similar W_LES have a high relative CDI; however, co-desorption took place in different blends when the blend components had dissimilar W_LES, as clearly

shown in Table D-6. This indicate that the similarity of W_LES between the blend components is not the factor controlling the co-desorption phenomena.

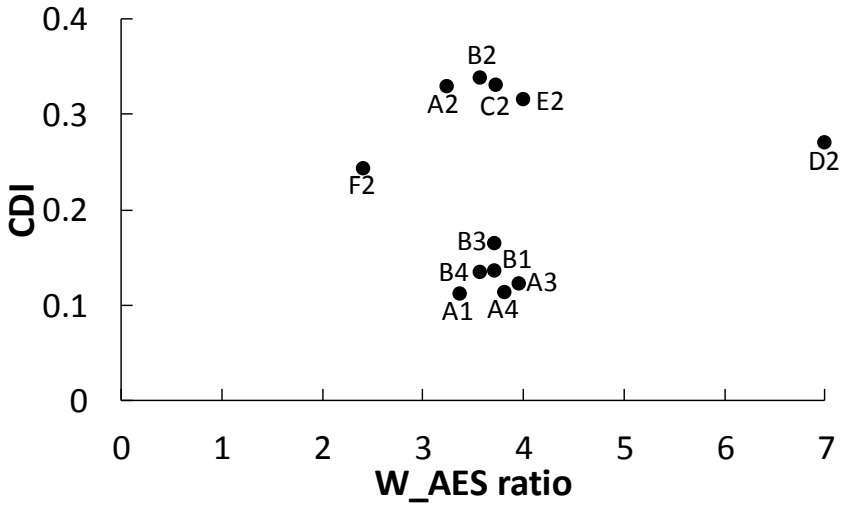

Figure D-5. Relation between co-adsorption index and W_AES ratio of all blends.

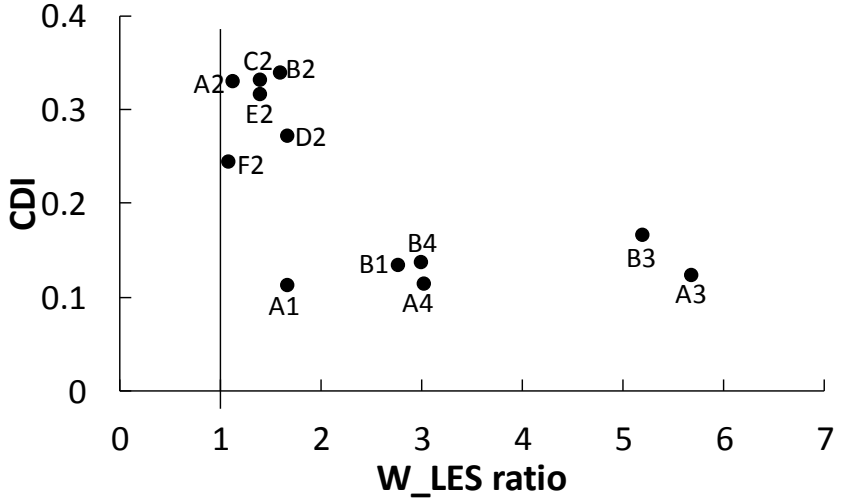

Figure D-6. Relation between co-adsorption index and W_LES ratio of all blends.

Furthermore, Figure D-6 lead to the same conclusion we reached in Figure 6-26. For a given comonomer content ratio, CDI will increase with increasing the W_LES ratio, indicating that

even we consider the weight averages of the longest ethylene sequences, the fractionation mechanism in HT-TGIC is not governed mainly by the adsorption of ethylene sequences on the support surface.

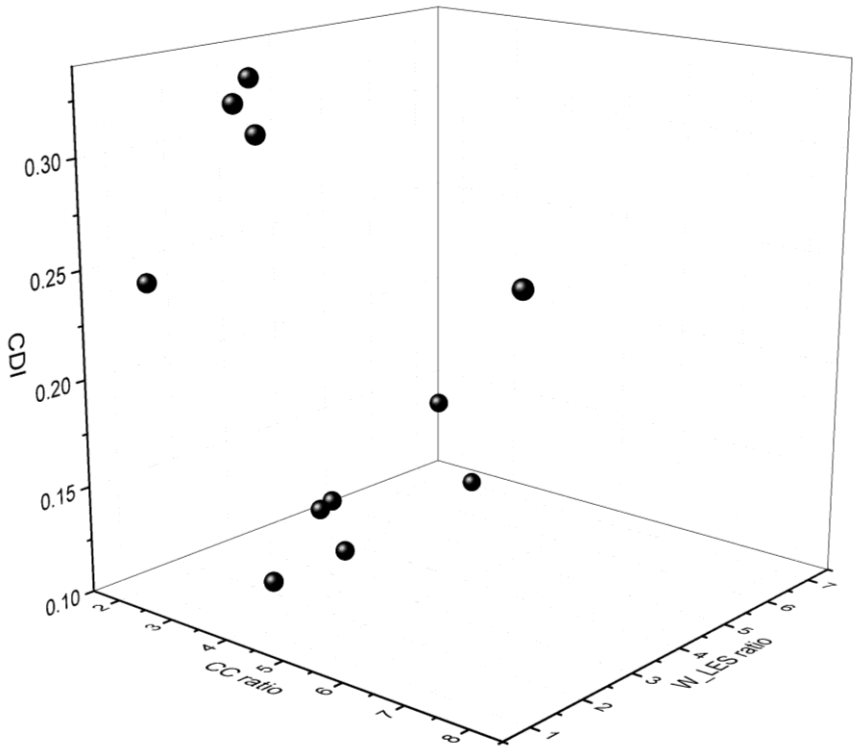

Figure D-4. 3D plot showing how the co-desorption index (CDI) varies with CC ratio and W_LES ratio.